The Distribution of Dissolved Cadmium in the Canadian Arctic Ocean

by

Sarah Jackson
BSc, from Victoria University of Wellington, 2011

A Thesis Submitted in Partial Fulfillment
of the Requirements for the Degree of

MASTER OF SCIENCE

in the School of Earth and Ocean Sciences

Supervisory Committee

The Distribution of Dissolved Cadmium in the Canadian Arctic Ocean

by

Sarah Jackson
BSc, from Victoria University of Wellington, 2011

Supervisory Committee

Dr. Jay T. Cullen, School of Earth and Ocean Sciences
Supervisor

Dr. Diana E. Varela, Department of Biology, and School of Earth and Ocean Sciences
Departmental Member

Dr. Roberta C. Hamme, School of Earth and Ocean Sciences
Departmental Member

Abstract

Supervisory Committee
Dr. Jay T. Cullen, School of Earth and Ocean Sciences
Supervisor
Dr. Diana E. Varela, Department of Biology, and School of Earth and Ocean Sciences
Departmental Member
Dr. Roberta C. Hamme, School of Earth and Ocean Sciences
Departmental Member

The biogeochemical cycling of oceanic dissolved cadmium (dCd) has been an active area of research for the past ~40 years, due in part to the close correlation with phosphate (PO_4). The global Cd:PO_4 relationship has led to the use of microfossil Cd/Ca as a paleoproxy for ocean circulation and nutrient utilization; however considerable spatial and temporal variability in the relationship - particularly in surface waters - limits the utility of the proxy. Understanding the global biogeochemical cycling of Cd is an active area of research; however the Arctic Ocean is largely omitted from global models due to lack of data. This work presents depth profiles of dCd and Cd/PO_4 ratios from 18 individual stations in the Canadian Arctic, collected during the Canadian GEOTRACES cruises GN02 and GN03, which connect the Arctic Ocean to the North Atlantic through the Canadian Arctic Archipelago (CAA). Salinity-driven water mass stratification exerts a primary control on the spatial distribution of Cd in the region, with elevated dCd and high Cd/PO_4 ratios (~0.37 pM/µM) associated with waters of Pacific-origin. The elevated dCd and Cd/PO_4 ratios are used as a tracer of Pacific-origin waters, identifying the presence of Pacific-origin water through the CAA and into Baffin Bay. High surface Cd/PO_4 ratios were observed across the transect, consistent with a general global increase in surface water Cd/PO_4 with increasing latitude.

The analysis of Cd and other bioactive trace metals (Mn, Fe, Ni, Cu, Zn and Pb) still presents considerable analytical challenges due to the high-risks of contamination, low concentrations and complex matrices. I present a novel multi-element analytical method, which combines the commercially-available seaFAST pico preconcentration system with ICP-MS/MS analysis. In this work, we demonstrate that ICP-MS/MS, which combines two mass-selecting quadrupoles separated by an octopole collision/reaction cell, effectively removes common interferences (ArO^+ on ^{56}Fe and MoO^+ on Cd) when pressurized with O_2 gas. Accurate and precise measurements of

the consensus references standards SAFe S and SAFe D and the certified reference material NASS-6 are presented as validation of the method. This thesis presents a novel method for the analysis of trace elements in seawater and discusses the biogeochemical cycling of Cd in the Arctic Ocean.

Table of Contents

List of Tables

List of Figures

Acknowledgments

Firstly, I would like to thank my supervisor, Jay Cullen, for making this project possible. Your constant kindness, support and wisdom have been invaluable to this process. Thank you for being a constant role model, both in science and in life.

Thank you to my committee members, Roberta Hamme and Diana Varela. I am forever thankful for your endless patience. A special thanks to Roberta for welcoming me into your lab group discussions as my group embarked on more exciting adventures.

Thank you to Jody Spence, for spending hours helping me to learn to use the ICP-MS/MS, and trusting me in my work.

Thank you to all the crew and scientists of the CCGS Amundsen for making the cruise such an enjoyable experience. A special mention to Kristin Orians and Maureen Soon, whose wisdom and experience were fundamental to ensuring my success on-board the vessel.

To Dave Janssen – it is no exaggeration to say that this thesis would not have been possible without you. You have been my mentor and my friend since I arrived here. Thank you for the encouragement pokes, for putting up with endless facts about NZ, and for providing me with a bottomless supply of beer. I look forward to a friendship that lasts a lifetime.

To Kathryn Purdon – thank you for being the best field assistant possible. You taught me far more than I taught you, and I couldn't have asked for a better person and friend to accompany me on my first research cruise.

To the Senior Lab Instructors – Duncan, David and Sarah – thank you for believing in and supporting me as an educator, and thank you for countless coffee conversations.

To my many other friends in SEOS and UVic. Thank you to all of you for making this experience so positive. Thank you for opening my eyes to the wonders this world holds – to mountain hikes, to kayak trips, to sailing adventures, to trail running escapades. I leave this island with a more fulfilling life then I could have hoped for, entirely thanks to all of you.

This work was supported by funding from the Natural Sciences and Engineering Research Council of Canada (NSERC) Discovery Grant and Climate Change and Atmospheric Research programs

Dedication

I dedicate this to my mother, for instilling in me a curiosity for the natural world. To my father, for fostering my sense of adventure. To my sister, for being wiser than I could ever hope to be. And to Joe, for making every day that little bit better.

Chapter 1: Introduction

1.1 Cadmium Geochemistry

Cadmium (Cd) is a soft, bluish-white metal located at the end of the 4d-transition series. It has an atomic number of 48, and is a Group 12 element, along with zinc (Zn) and mercury (Hg). Key physical and chemical properties of Cd are summarised in Table 1.1.

Table 1.1 Select chemical and physical properties of Cd[a]

Property	
Atomic number	48
Atomic weight (g mol^{-1})[b]	112.411
Atomic radius (pm)[c]	155
Ionic radius of Cd^{2+} (pm)[d]	95
Electron configuration	[Kr] $4d^{10}5s^2$
Melting point (°C)	320.9
Boiling point (°C)	767.3
Oxidation states	+2, +1 (rare)
Reduction potential (E^0) for $Cd^{2+} + 2e^- = Cd$ (V)	-0.402
First ionization energy (kJ mol^{-1})	867
Second ionization energy (kJ mol^{-1})	1,625
K_{sp} (25 ºC)[e]	$CdCO_3 = 1.0x10^{-12}$
	$Cd(OH)_2 = 7.2x10^{-15}$
	$Cd_3(PO_4)_2 = 2.5x10^{-33}$
	$CdS = 1x10^{-27}$

[a] Table modified from Rehkämper et al. 2012

[b] Wieser & Coplen 2010

[c] Slater 1964

[d] Shannon 1976

[e] Haynes, 2014

Table 1.2 Ionic index (Z^2/r) and covalent index ($X_m^2 r$) of select Group 12 elements. Data from Andersen, 1984.

Metal ion	Z^2/r	$X_m^2 r$
Zn^{2+}	5.40	2.20
Cd^{2+}	4.12	2.80
Hg^{2+}	3.63	4.10

It has a stable electron configuration ([Kr]$4d^{10}5s^2$). In nature, it is found predominantly in the +2 oxidation state, though a +1 oxidation state is also possible. It is classed as a soft metal, forming the most stable complexes with soft donor atoms (S>>N>O) (Andersen, 1984). The ionic index (Z^2/r) of Cd^{2+} is greater than that of Hg^{2+}, but smaller than Zn^{2+} (Zn^{2+}>Cd^{2+}>Hg^{2+}), while the covalent index ($X_m^2 r$) shows the opposite trend (Hg^{2+}>Cd^{2+}>Zn^{2+}) (Table 1.2). Cd has an atomic mass of 112.411 g mol^{-1}, from a combination eight naturally-occurring stable (or quasi-stable) isotopes, with atomic masses ranging from 106 to 116 (Table 1.3).

Table 1.3 Isotopic abundance of naturally occurring Cd-isotopes[a]

Mass Number	106	108	110	111	112	113	114	116
Isotope abundance (%)	1.25	0.89	12.48	12.80	24.11	12.23	28.74	7.52

[a] Data from Pritzkow et al. (2007)

Cadmium has a low crustal abundance; with a concentration of only ~0.1 ppm in average continental crust, it is ~750 fold less abundant than Zn (Rudnick & Gao, 2014). Several Cd minerals have been identified, with the most notable being greenockite, hawleyite (polymorphs of CdS), and otavite ($CdCO_3$), although no known deposits are commercially exploitable. Instead, Cd is primarily produced as a by-product of Zn processing as significant concentrations of Cd may be associated with Zn ore deposits. Cd is a chalcophile element, resulting in the bulk of Cd produced in association with zinc sulfide deposits (Butterman & Plachy, 2004).

1.2 Global Cadmium Emissions

Approximately 4,400 t of Cd is emitted each year, with almost $^{2}/_{3}$ of emissions coming from anthropogenic sources. Natural sources account for ~1,440 t/yr, and are dominated by volcanic emissions (~60%), with biogenic particles, wind-borne dust, terrestrial biomass burning and sea-salt spray being other important sources (Cullen & Maldonado, 2013). As for many element cycles, anthropogenic emissions have considerably perturbed the natural Cd cycle. Cd emissions began steadily increasing at the beginning of the 20th century; however increasing awareness over Cd toxicity has led to greater regulation, and anthropogenic emissions have decreased in recent decades (Butterman & Plachy, 2004). Due to the association of Cd with Zn (and to a lesser extent Cu and Pb) ores, Cd emissions occur primarily as a by-product of ore processing, with non-ferrous metal production contributing ~70% of the total anthropogenic Cd emissions (Cullen & Maldonado, 2013). Other anthropogenic sources include fossil fuel combustion, iron and steel production, cement production and waste disposal. The primary use of Cd is in Ni-Cd rechargeable batteries, with other important uses in pigments, as a coating or plating, and as a stabilizer in plastics (Butterman & Plachy, 2004).

1.3 Cadmium in Freshwaters

The anthropogenic perturbation to the natural Cd cycle has resulted in elevated concentrations in freshwater systems. Although there is considerable regional variability, the average concentration in world rivers is 0.08 μg L^{-1}, a 40-800 fold increase from pre-industrial concentrations (Gaillardet et al., 2014). Considerable regional variability in river concentrations exists which is likely related to local anthropogenic inputs, although variability in underlying bedrock also contributes to regional differences.

In aqueous systems, it is important to consider the speciation of Cd, as this controls the bioavailability and the partitioning between the dissolved or particulate phase. In freshwater systems, Cd complexation is dependent on pH, the concentration of other dissolved ions, and the binding characteristics of organic material. Organic complexation acts to reduce the free Cd ion concentrations ($[Cd^{2+}]$, and reduce the bioavailability or toxicity of Cd (Bewers et al., 1987). Although the organic ligands are poorly characterised, stability constants have been measured in a number of freshwater systems, with constants in the range of log K = 9.4-10.3 (Xue & Sigg, 1998). Organic complexation significantly reduces the concentration of $[Cd^{2+}]$ in eutrophic lakes, such that $[Cd^{2+}]/[Cd]_{Tot}$=0.01-0.03 (Cao et al., 2006; Xue & Sigg, 1998), with a much higher proportion of $[Cd^{2+}]$ observed in oligotrophic lakes ($[Cd^{2+}]/[Cd]_{Tot}$=0.8) (Xue & Sigg, 1998).

Partitioning of Cd between the dissolved and particulate phase in freshwater systems is in part controlled by the propensity of Cd to adsorb to particulate matter. The partitioning of Cd between the adsorbed phase and the dissolved phase has been measured for different substrates and is reported as K_d, where:

$$K_d = \frac{\text{amount sorbed per unit mass}}{\text{equilibrium dissolved concentration}}$$

with the highest K_d values observed for humic matter (18,000 +/- 3000 L kg^{-1}) and lower values observed in kaolinite clays (380 +/- 50 L kg^{-1}) (Gardiner 1974). K_d is influenced by pH, the oxidation status of the water, and the concentration of inorganic anions and metal cations. In general, higher pH acts to increase K_d, while higher ionic strength tends to decrease K_d (Bewers et al., 1987).

1.4 Cadmium in Ocean Waters

1.4.1 Cadmium Oceanic Distribution

Cadmium is delivered to the oceans either by rivers or through atmospheric deposition. Concentrations range from 1-1000pM (de Baar et al., 1994), with a residence time of ~10,000 years (Cullen & Maldonado, 2013). Constraints on sampling and analytical techniques meant that the first reliable measurements of Cd in seawater were not available until the 1970's (Boyle et al., 1976; Bruland et al., 1978). The vertical distribution of Cd is classified as a nutrient-type profile remarkably similar to the macronutrient PO_4^{3-} (de Baar et al., 1994), with a depletion in surface waters due to uptake by photosynthetic plankton and an increase in Cd concentrations through the thermocline as particulate matter regenerates (Fig. 1.1).

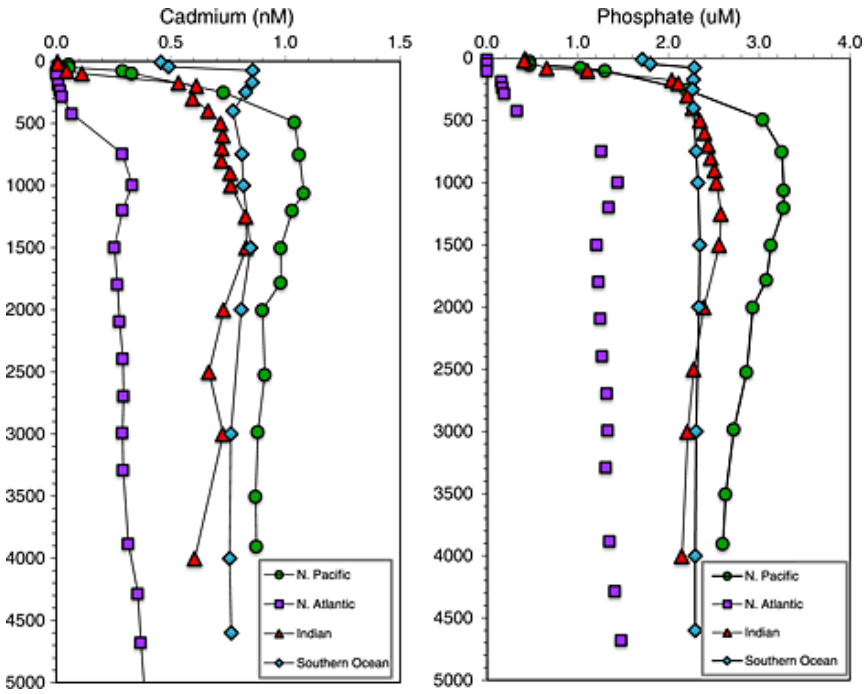

Figure 1.1 Depth profiles of dissolved Cd and PO_4 from the North Pacific (Bruland, 1980), North Atlantic (Quay & Wu, 2015), Indian (Saager et al, 1992), and Southern Ocean (Abouchami et al., 2011). Figure taken from Quay et al., 2015.

The global oceanic distribution of Cd is controlled by internal cycling mechanisms (biological uptake and regeneration) superimposed on global thermohaline circulation patterns. In general, deep-water forms in the North Atlantic and flows through the Southern Ocean and finally to the North Pacific, accumulating nutrients (including Cd) as it circulates (Broecker & Peng, 1982). The result is that North Atlantic deep-waters have low Cd concentrations (~320 pM), higher concentrations are seen in the Southern Ocean and the South Indian (~670-690 pM) and the highest in the North Pacific (~930 pM) (Quay et al., 2015). Coastal water also typically has higher concentrations of Cd, reflecting local terrestrial inputs from riverine and atmospheric sources and coastal upwelling (Bruland & Franks, 1983). Surface water Cd concentrations can be severely depleted in oligotrophic regions (<1 pM) and much higher in upwelling regions (~150 pM) (Bruland, 1992).

1.4.2 Speciation

As in freshwater systems, speciation controls the fate and cycling of Cd in seawater. In ocean waters, the majority of Cd is complexed with chloride ions or organic ligands. In surface waters, the majority of Cd is tightly bound to organic ligands with high stability constants ($K'_{cond,Cd'}$). The results from studies on organic speciation of Cd are shown in Table 1.4. In general, the degree of organic complexation is high in surface waters (~70%) although significant regional variability exists. Ellwood (2004) found up to 99% of Cd was organically complexed in surface waters off the coast of New Zealand. A lower degree of complexation was found in the North Pacific, with ~67% of Cd organically bound (Bruland, 1992). The degree of complexation typically decreases with depth, although again, regional variability exists which is likely related to upwelling conditions and water mass distributions (Baars et al., 2014). Bruland (1992) found no evidence of organic complexation below ~200m. In contrast, in the Atlantic sector of the Southern Ocean,

Baars et al. (2014) found relatively low organic complexation in surface waters south of the Antarctic Polar Front and no decrease with depth. They attribute this variability to upwelling conditions and the timing of the study (post-bloom). The organically-bound Cd is thought to be unavailable for biological uptake, although weak organic complexes may be bioavailable (Xu et al., 2012).

Table 1.4 Results from cadmium speciation studies[a]

Region	Depth (m)	$logK'_{Cd'}$	CdL (%)
Narragansett Bay (Rhode Island)[b]	Surface	9.0-9.2	73-83
North Pacific[c]	<200	10.0-10.8	11-80
North Pacific[c]	200-600	-	-
SAZ East Pacific[d]	<80	9.8-11.0	87-99
SAZ Atlantic Ocean	<80	9.9-10.4	86-96
SAZ Atlantic Ocean	200-500	10.3-10.5	93-97
SAZ Atlantic Ocean	4350	9.7	60
Antarctic Ocean	0-100	9.0-9.6	45-75
Antarctic Ocean	>100	9.0-9.7	35-62
Coastal Antarctica[e]	0-250	9.1-9.9	0-92

[a] Table modified from Baars et al. 2014. Data from Baars et al. 2014 unless otherwise specified.

[b] Kozelka & Bruland 1998

[c] Bruland 1992

[d] Ellwood 2004

[e] Capodaglio et al. 1998

In ocean waters, the remaining faction of Cd is primarily bound to chloride ions (Fig. 1.2). Approximately 36% is found as $CdCl^+$, 45% as $CdCl_2$, 16% as $CdCl_3^-$ and 3% as Cd^{2+} (Byrne, 2002; Byrne et al., 1988), with the distribution among the inorganic species changing as a function of salinity. The degree of organic speciation controls the concentration of inorganic Cd species ([Cd']), often reducing surface [Cd'] to sub-pM values and dramatically reducing the bioavailability of Cd (Cullen & Maldonado, 2013).

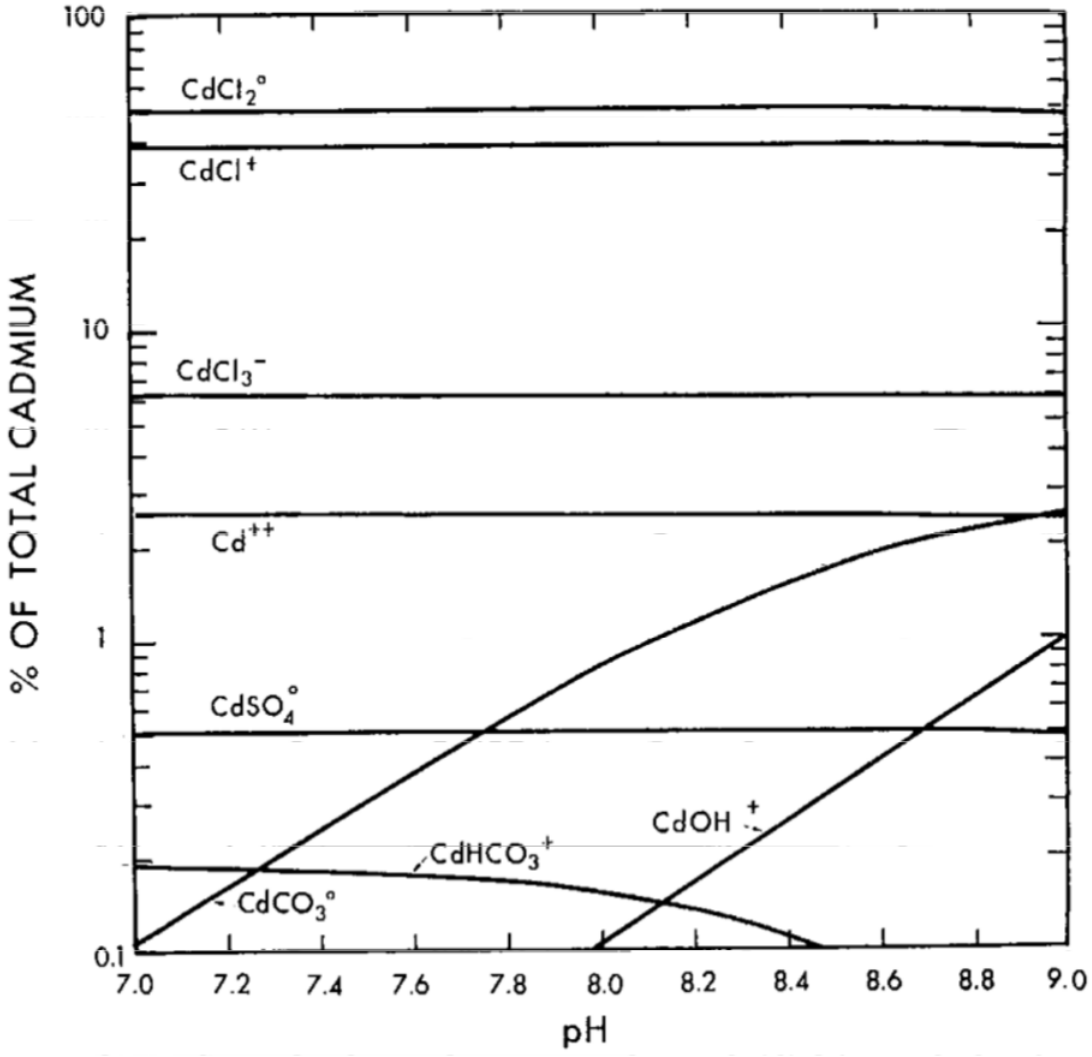

Figure 1.2 Calculated speciation of Cd in seawater at 25 ºC and 1 atm as a function of *p*H. Figure taken from Zirino & Yamamoto, 1972.

1.4.3 Biological Utilization of Cadmium

Despite the nutrient-type profile displayed by Cd, the biological role for Cd remained a mystery for over a decade after the first reliable measurements were made (Boyle et al.,1976; Bruland et al., 1978) . Evidence of biological utilization of Cd in phytoplankton was first observed in a marine diatom isolated in laboratory culture by Price and Morel (1990). The study showed that additions of Cd to Zn-limited cultures of the marine diatom *Thalassiosira weissflogii* increased

growth to 90% of the growth rate observed under Zn-replete conditions, leading the authors to suggest that Cd may substitute for Zn in a metalloenzyme. Further work showed that Cd was likely substituting for Zn in carbonic anhydrase (CA), an enzyme required by the carbon concentrating mechanism (CCM) to catalyze the conversion of HCO_3^- to CO_2 (Lee et al., 1995). Stimulation of growth rate by Cd supplementation under Zn-limiting conditions has since been demonstrated in several different phytoplankton species (Lee & Morel, 1995). A Cd-specific form of CA (CdCA), the only known Cd-specific protein, was discovered in *T. weissflogii*, with production of the enzyme modulated by pCO_2 conditions (Lane & Morel, 2000). Xu et al. (2008) showed that Cd can readily exchange with Zn as the catalytic centre in CA in diatoms, providing a competitive advantage for diatoms in metal-poor environments.

1.4.4 Cadmium Uptake by Phytoplankton

Cd uptake rates and intracellular Cd content of phytoplankton varies widely, driven by factors including species composition, trace metal availability, irradiance, and pCO_2. Culturing experiments have shown that uptake of Cd is directly proportional to [Cd'], and inversely proportional to [Zn'] and [Mn'] (where [M'] indicates the total inorganic species) (Lee et al., 1995; Sunda & Huntsman, 2000). Different biological mechanisms appear to drive the antagonistic relationships of Cd-Zn and Cd-Mn. The relationship with Mn appears to be driven by increased transport of Cd through the upregulation of an Mn transporter at low Mn concentrations. Conversely, transport of Cd at low Zn concentration is due to a high-affinity Cd/Co transporter which is likely upregulated to relieve Zn-stress by replacing Zn as the metal cofactor in CA (Lee et al., 1995; Lee & Morel, 1995; Price & Morel, 1990). Low pCO_2 has also been shown to increase Cd uptake, likely due to an increased requirement for CA in its role in the CCM, both in laboratory cultures (Lane & Morel, 2000) and in field studies (Cullen & Sherrell, 2005).

More recently, there is a growing body of work that suggests that Fe concentration exerts an important control on intracellular Cd:P ratios. Sunda and Huntsman (2000) suggested that Fe-limiting conditions lead to a Zn depletion, which in turn results in the upregulation of the Cd/Co transport system and higher intracellular Cd:P ratios, linking Fe-limited regions to higher Cd content. Subsequent shipboard incubations of Fe-limited cultures showed that additions of Fe decreased intracellular Cd:P ratios irrespective of Zn concentration, suggesting a direct control on Cd:P content by Fe (Cullen et al., 2003). The authors suggested that growth rate dilution may be the mechanism for the change in Cd content, with cellular uptake of P increasing when Fe-stress is alleviated while Cd uptake remains constant. More recent work has provided further evidence that Cd content increases under Fe-stress; however it was suggested that the upregulation of a non-selective divalent metal transporter in low-Fe conditions may explain the increase in cellular Cd (Lane et al., 2008). An extension of this work demonstrated that changes in cellular Cd under changing Fe condition cannot be explained by a single mechanism. Rather, it is a combination of changing species compositions, growth rate dilution and upregulation of transport systems that drives the observed increase in cellular Cd in Fe-limited conditions (Lane et al., 2009).

Cellular Cd quotas also appear to be strongly influenced by species composition, with Cd quotas varying by two orders of magnitude between 15 different marine eukaryotic phytoplankton species (Ho et al., 2003). Cd quotas are relatively high – almost 1/3 of the average Zn quota - given the only known biochemical use of Cd is in CA (Ho et al., 2003). The highest quotas are observed in coccolithophores, with lower ratios in diatoms followed by green algae. Variations in Cd:P in response to changes in irradiance and growth rate have also been shown to be controlled by phylogenetic groups (Finkel et al., 2007). The study found that while diatoms exhibit an increase in Cd:P in response to increases in irradiance, cyanobacteria Cd:P decrease, and no response is seen in prasinophyte and dinoflagellate species. Lane et al. (2009) found that Cd:C

ratios varied by 66-fold among 7 species of phytoplankton under Fe-replete conditions. When the species were cultured in Fe-limiting conditions, Cd:C increased for all species, although the magnitude of change was species dependent.

1.4.5 The Cd:PO_4 relationship

A striking similarity between dissolved Cd and PO_4 was observed when the earliest vertical profiles of Cd were measured in the North Pacific (Boyle et al. 1976; Bruland et al. 1978). As additional data became available from other ocean basins, it became apparent that while Cd and PO_4 are strongly correlated, there is a distinctive break in the slope at $PO_4 \approx 1.3$ μM (also known as the "kink") (Fig. 1.3). Below $PO_4 \approx 1.3$ μM, the relationship is defined by a slope of ~0.2 nM/μM, and is primarily North Atlantic data. Above $PO_4 \approx 1.3$ μM, the slope increases to ~0.4, and is primarily defined by data from the Indian, Southern and Pacific Oceans (Cullen, 2006; de Baar et al., 1994; Quay et al., 2015).

The linearity of the Cd-PO_4 relationship led to the use of Cd as a proxy for nutrient content and deep-water circulation of the paleocean (Boyle, 1988), which was extended by Elderfield and Rickaby (2000) to include the surface ocean and determine variability in the efficiency of the biological pump across glacial-interglacial timescales. The proxy, which uses the Cd/Ca ratio preserved in foraminifera tests to reconstruct paleo PO_4 concentrations, requires a robust mechanistic understanding of the Cd-PO_4 relationship, including the causes of temporal and spatial variability. The non-linearity of the Cd-PO_4 relationship ("the kink") complicates the utility of Cd as a paleoproxy, and a mechanistic understanding of the observed variability of the Cd-PO_4 relationship is necessary for meaningful use of the proxy. Several mechanisms have been proposed to explain the kink. Boyle (1988) suggested that different depths of remineralization of Cd and PO_4 could explain the kink; however the coincidence of the Cd and PO_4 peaks does not

support this theory. Conversely, Elderfield and Rickaby (2000) suggested that the kink is merely an artifact of preferential uptake of Cd relative to PO_4 in surface waters and that the Cd-PO_4 relationship can be described by a Rayleigh fractionation model with a constant fractionation factor.

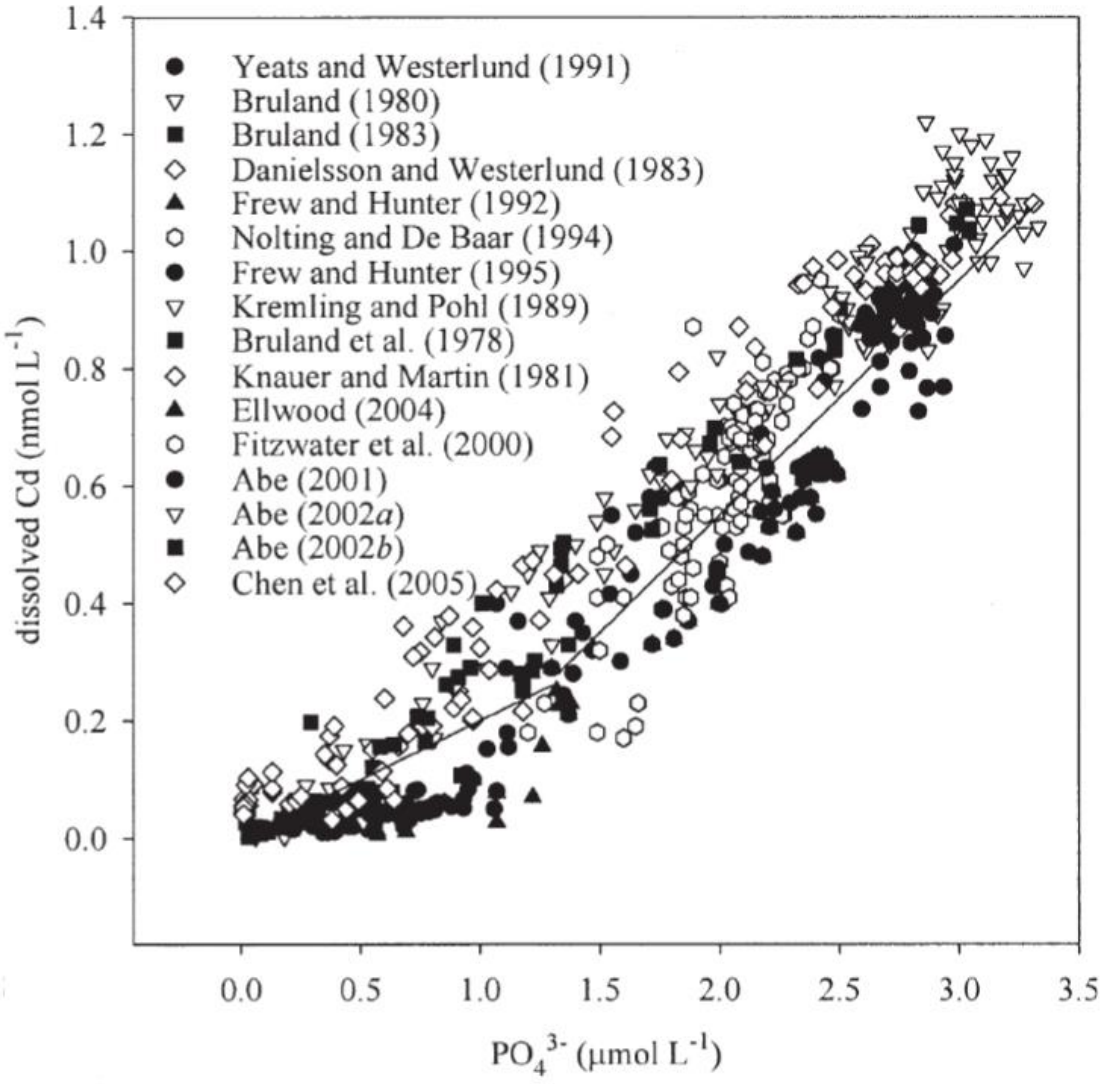

Figure 1.3 Compilation of dissolved Cd versus PO_4 from a global database. Lines represent the two distinct relationships, with [PO_4] <1.3 µmol L^{-1} primarily Atlantic waters and [PO_4] > 1.3 µmol L^{-1} primarily Indian-Southern-Pacific Ocean waters. Solid symbols represent stations in HNLC regions, while open symbols are from stations in which surface [PO_4] <0.3 µmol L^{-1}. Figure taken from (Cullen, 2006)

Significant evidence exists to suggest that the Cd:P content of phytoplankton is dependent on micronutrient concentrations (Cullen & Sherrell, 2005; Lane et al., 2008; Sunda & Huntsman, 2000) which led to the suggestion that chronic Fe-limitation in high-nutrient low-cholorphyll (HNLC) regions may be the cause of the "kink" (Cullen, 2006). Cullen (2006) suggested that a growth rate dilution effect, imposed by chronic Fe-limitation, results in phytoplankton with greater Cd:P ratios in HNLC regions, resulting in lower dissolved Cd/PO_4 ratios in surface waters and higher Cd/PO_4 ratios through the nutricline than in Fe-replete regions. As previously discussed, this idea was expanded upon to suggest that a combination of growth rate dilution and upregulation of metal transport systems in HNLC regions explains the observed differences between HNLC and Fe-replete regions (Lane et al., 2009).

An alternate explanation suggests that the kink is the result of mixing of water masses with different preformed Cd/PO_4 ratios (Frew & Hunter, 1992). The authors suggested that injections of subantarctic surface waters into intermediate depth could explain the kink, as these waters are depleted in Cd. Though this model helped explain the kink, it was not consistent with profiles from the eastern Atlantic Ocean (Yeats et al., 1995) and did not provide a mechanistic understanding. More recent work on Cd isotopes (Baars et al., 2014; Gault-Ringold et al., 2012) and Cd distributions (Baars et al., 2014; Xie et al., 2015) have presented evidence that injections of Subantarctic Mode Water (SAMW) play an important role in the global Cd-PO_4 relationship. These recent studies suggest that the low Cd/PO_4 ratios in SAMW may be a result of high Cd:P in phytoplankton due to HNLC conditions in the Southern Ocean (Baars et al., 2014).

More recently, models have been used to help understand the global variation in the Cd:PO_4 ratio. Quay et al. (2015) used a compilation of measurements of dissolved Cd and PO_4 from 182

stations and inferred particulate Cd:P ratios and fractionation factors (FF, where $FF=[Cd/P]_{particles}/[Cd/PO_4]_{seawater}$) to understand the impacts of thermohaline circulation and particle degradation on the global Cd-PO_4 relationship. Analysis of the large dataset showed that differences in Cd:P of exported particles was largely dependent on whether HNLC conditions existed, with higher Cd:P and FF in HNLC regions. The authors credited low Fe, Zn and Mn availability, reduced growth rates, and differences in species composition (a dominance of diatoms) in HNLC regions with the high particulate Cd:P ratios. The authors also ran a simple multibox model, which produced results consistent with the observed deepwater Cd/PO_4 values for different ocean basins, indicating that particulate Cd:P, dependent on HNLC conditions, exerted a strong control on deepwater ratios. The model also demonstrated that the deepwater Atlantic Cd/PO_4 was strongly influenced by particulate Cd:P ratios in the Southern Ocean, indicating that variability in HNLC conditions in the Southern Ocean during glacial-interglacial cycles and coincident variability in Cd:P ratio of exported particles could strongly influence Atlantic deepwater Cd/PO_4 and limits the utility of Cd as a paleoproxy. A modelling study by Wu and Roshan (2015) was used to understand the depth-dependent variability in the Cd/PO_4 ratio. The authors suggested that different groups of particulate organic carbon (POC) could explain both depth-dependent and interbasin variations in Cd/PO_4 ratios. The model indicates that differences in remineralization rates and depths of Cd-poor non-ballast POC ($[Cd/P]^{excess}$) and Cd-rich ballast-associated POC ($[Cd/P]^{protected}$) can explain the observed variability in the Cd/PO_4 ratio. A lower $[Cd/P]^{protected}$ ratio in the North Atlantic than in the North Pacific is required to accurately model measured Cd/PO_4 ratios, which the authors suggest may be linked to higher $[Cd/P]^{protected}$ ratios in POC associated with opal ballast, due to higher intracellular Cd:P for the diatom *Thallassiosira oceanica* than for the coccolithophore *Emiliana huxleyi* (Finkel et al., 2007; Ho et al., 2003; Lane et al., 2009). Roshan and Wu (2015) also used a regenerative mixing model (combining both conservative mixing and particle regeneration mechanisms in a multi-box

model) to examine the controls on the Cd distribution in the North Atlantic. They determined that at depths greater than 1000m, Cd distribution is mainly controlled by conservative mixing, while between 300-1000m regeneration of particulate material can contribute >50% of the measured Cd, complicating the utility of Cd as a paleoproxy for intermediate depths.

1.5 The Distribution of Cadmium in the Arctic

With a surface area of 9.5×10^{12} m^2, the Arctic Ocean only represents approximately 3% of the global ocean by area (Jakobsson et al., 2002). The enclosed ocean can be considered as two major basins – the Eurasian and the Amerasian (Canadian) – separated by Lomonosov Ridge. The Alpha-Mendeleyev ridge further subdivides the Amerasian basin into the Canada and Makarov basins, while the Nansen ridge separates the Eurasian basin into the Amundsen and Nansen basins. The Arctic Ocean also notably contains broad continental shelf regions, which account for ~53% of the total area (Jakobsson et al., 2002) and include the Barents, Kara, Laptev, East Siberian, Chukchi, White and Beaufort Seas, as well as the continental margins of the Canadian Arctic Archipelago (CAA) and Northern Greenland. The effects of climate change are exaggerated in the Arctic, with warming occurring at two to three times the global rate (Trenberth et al., 2007) and satellite observations indicating that summer sea ice extent has decreased by 9.4% - 13.6% per decade, combined with decreases in ice volume (Vaughan et al., 2013). Due primarily to unfavourable conditions and remoteness however, the Arctic Ocean remains one of the most under-studied oceanic regions, although there has been a considerable increase in scientific efforts in response to the rapidly changing conditions.

The Arctic Ocean plays an important role in the global ocean system, by providing exchange of heat and freshwater between the North Pacific and North Atlantic (Beszczynska-Möller et al., 2011). Water enters the Arctic Ocean from the North Pacific via Bering Strait and from the North

Atlantic via Fram Strait and the Barents Sea while export of water from the Arctic occurs through the CAA, Davis Strait and Fram Strait (Beszczynska-Möller et al., 2011). The Arctic is strongly stratified, owing largely to significant freshwater input from large Arctic rivers (Jakobsson et al., 2004). While there exist considerable regional differences in hydrography, the deepwater across the Arctic is supplied by dense, saline water from the North Atlantic Ocean, while the Pacific-origin water is largely restricted to the Canada Basin and forms a colder, fresher layer (McLaughlin et al., 1996). The surface layer, or Polar Mixed Layer (PML) is significantly altered by seasonal cycles, including sea ice formation and melt, river runoff and biological cycling (Jakobsson et al., 2004).

There are very few profiles of dissolved trace metals available for the Western Arctic. Moore (1981) presented a profile of Zn, Cd, Cu and Al from the LOREX ice station, located near the North Pole. Dissolved Cd (dCd) was high in surface waters ~0.30 nM, increasing to a maximum of 0.60 nM coinciding with the nutrient maximum, with the profile closely resembling profiles of PO_4 and SiO_2. Profiles were also obtained from the CESAR ice station in the Canada Basin (Yeats, 1988) and the Canadian Ice Island (Yeats & Westerlund, 1991) which closely resembled the LOREX profile, with a maximum in Cd that corresponds with the nutrient maximum. More recently, Cid et al. (2012) presented profiles of dissolved and total dissolved Al, Mn, Fe, Co, Ni, Cu, Zn, Cd and Pb in the Chukchi and Beaufort Seas. This work identified a maximum in the halocline for all the metals except Al, and found that Ni, Cu, Zn and Cd were found to be predominantly in the dissolved form. Kondo et al. (2016) recently published profiles for Mn, Fe, Ni, Zn and Cd in the Chukchi Sea and Canada Basin, which again showed a maximum in the halocline. Cd was shown to be strongly correlated with PO_4, suggesting that the primary control on Cd was internal biogeochemical cycling. There was little variability in either PO_4 or Cd in the upper halocline in the transect, suggesting that internal recycling in the Canada Basin was

negligible, and that Cd may be transported considerable distance in the halocline with little modification.

1.6 The Canadian GEOTRACES program

The GEOTRACES program was developed in collaboration with over 30 nations, to improve understanding of the global cycling of trace elements and isotopes (TEIs). TEIs play an important role as regulators or tracers of important biogeochemical cycles or physical processes, but a paucity of data has limited the current understanding of TEI cycling. GEOTRACES aims to improve the understanding of global TEI biogeochemical cycles by focusing on fluxes, internal cycling, and the development of proxies. The Canadian GEOTRACES program has played a prominent role in the development and deployment of a comprehensive Arctic sampling program. In 2015/2016 the USA, Germany and Canada completed cruise sections which spanned the Arctic Ocean. The results from the cruises will provide a synoptic picture of the biogeochemical cycling of TEIs in the Arctic Ocean. The focus of the Canadian program, which encompassed the Canada Basin, Canadian Arctic Archipelago and Baffin Bay, is to understand the connection between the Pacific and the Atlantic Ocean.

1.7 Thesis Focus

This thesis aims to provide a comprehensive understanding of the distribution of Cd through the Canadian High Arctic, covering the Canada Basin, the Canadian Arctic Archipelago, and Baffin Bay. Changing climatic conditions, which are forcing large-scale physical and biogeochemical changes in the Arctic Ocean, have highlighted the necessity for improved data coverage in the Arctic Ocean.

Chapter 2 presents a novel method for the analysis of Mn, Fe, Ni, Cu, Zn, Cd and Pb in seawater. The method uses an automated solid-phase extraction system, with Nobias PA1 ion exchange resin, to both preconcentrate and extract trace metals from seawater. The extracted samples are analysed by ICP-MS/MS, which consists of two mass-selecting quadrupoles separated by a collision/reaction cell, resulting in accurate and precise results. **Chapter 3** presents dissolved Cd data from the Arctic Ocean. The results show a clear influence of high-Cd Pacific-origin water throughout the Canada Basin and CAA, with evidence of mixing of Pacific-origin and Atlantic-origin waters in Baffin Bay.

Chapter 2: Determination of Mn, Fe, Ni, Cu, Zn, Cd and Pb in seawater using offline extraction and triple quadrupole ICP-MS/MS

2.1 Abstract

Highly resolved temporal and spatial distributions of trace elements in ocean water can provide insight into ocean processes but carry a significant analytical demand which require methods that combine accuracy and precision with high sample throughput. Here a multi-element method is presented which combines the commercially-available seaFAST preconcentration system with ICP-MS/MS for the analysis of Mn, Fe, Ni, Cu, Zn, Cd and Pb in seawater. Samples (20 mL or 40 mL) are loaded on to a chelation resin column and trace metals eluted into 2.5 mL of 1.6 N HNO_3. Analysis of the eluate was carried out by ICP-MS/MS, which combines two mass-selecting quadrupoles separated by an octopole collision/reaction cell. The collision/reaction cell was pressurized with O_2 gas for the analysis of Mn, Ni, Cu, Cd and Pb and H_2 gas for the analysis of Fe and Zn which removed common interferences (e.g ArO^+ on ^{56}Fe and MoO^+ on Cd) yet maintained the highest instrument sensitivity across the entire mass range. Measured blanks and detection limits were at ≤10 pmol L^{-1} levels, except for Fe (blank 0.14 nmol L^{-1}) and were suitable for open-ocean seawater analysis. We report results for the certified reference material NASS-6, consensus reference standards SAFe S and SAFe D and depth profiles of trace metals from the Arctic Ocean, collected as part of the Canadian GEOTRACES program.

2.2 Introduction

With approximately half of global autotrophic primary production occurring in our oceans (Falkowski, 1997), understanding the role trace metals play in biogeochemical cycling has become increasingly important (Morel & Price, 2003). The past few decades have improved the scientific understanding of the roles trace metals play as micronutrients, toxins, important tracers of anthropogenic input, and potential paleoproxies (Henderson et al., 2007). Historically, research has focussed on iron (Fe), as Fe complexes play an essential role in several key metabolic functions of phytoplankton, including as an essential component in photosynthetic electron transport and nitrogen fixation (Sunda & Huntsman, 1995). The low availability of Fe in surface waters means it limits primary productivity in up to 50% of the surface ocean (Moore et al., 2004) leading to intensive studies of Fe sources and sinks (Boyd & Ellwood, 2010; Tagliabue et al., 2017). Similarly Zn, which is the co-factor in carbonic anhydrase (CA), a catalytic enzyme involved in photosynthetic carbon concentrating mechanisms (Badger & Price, 2003), may limit or co-limit primary productivity in open ocean waters (Franck et al., 2003; Morel et al., 1994; Sunda & Huntsman, 2005; Varela et al., 2011). Cadmium (Cd) is known to substitute for Zn as the co-factor in CA and may exert controls on community composition and productivity (Lane & Morel, 2000; Price & Morel, 1990). Copper (Cu) can be toxic at elevated concentrations (Mann et al., 2002; Price & Morel, 1994); however it is still an important micronutrient in low-Fe waters, where Cu-containing enzymes can replace Fe-containing analogues (Peers & Price, 2006). Manganese (Mn) is useful as a tracer of redox cycling (Chester & Jickells, 2012) and riverine input (Landing & Bruland, 1980), while lead (Pb) is used as a tracer of anthropogenic aerosols deposited to the ocean surface (Boyle, 2001; Cullen & McAlister, 2017). Understanding the distribution and cycling of trace metals in the ocean is the principle objective of the

GEOTRACES program, launched in 2008 as an international collaboration between marine scientists from over 30 nations (Henderson et al., 2007).

In order to meet the analytical burden inherent in the stated goals of the GEOTRACES program, it was necessary to develop a high-precision, high-throughput method which allowed for the rapid multi-element determination of trace metals in seawater. Trace metals are typically found in pmol L^{-1} to nmol L^{-1} concentrations, leading to problematic interferences from the mmol L^{-1} concentrations of cations and anions present in the seawater matrix. To overcome this, methods have primarily focussed on the separation of single or multiple elements from the matrix, coupled with analysis on an inductively coupled plasma mass spectrometer (ICP-MS). The separation and preconcentration methods that have been used include solvent extraction (Bruland et al., 1979), co-precipitation with $Mg(OH)_2$ (Saito & Schneider, 2006; Wu & Boyle, 1997), and solid-phase extraction using a chelating resin. Resins containing a variety of functional groups have been successfully used in the extraction procedure, including 8-hydroxyquinoline (8-HQ) (Landing et al., 1986; Mclaren et al., 1985), iminodiacetate (IDA) (Beck et al., 2002; Milne, Landing et al., 2010), and nitrilotriacetic acid (NTA) (Lee et al., 2011; Lohan et al., 2005). Several recent studies have successfully used a resin containing both ethylenediaminetriacetate (EDTriA) and IDA functional groups for multi-element analyses (Biller & Bruland, 2012; Sohrin et al., 2008). The commercially available seawater preconcentration system, *seaFAST*-pico (Elemental Scientific, Omaha, NE, USA), couples this resin with an automated, trace metal clean, flow-injection system for successful determination of the biogeochemically important trace elements (Lagerström et al., 2013).

The majority of multi-element solid-phase extraction methods utilise an ICP-MS for analysis. Analysis on ICP-MS has many advantages, including a wide linear dynamic range, making it suitable for multi-element methods, and the possibility of obtaining isotopic information.

However, spectral interferences are problematic with ICP-MS and several strategies have been developed to overcome this. The use of sector-field ICP-MS (ICP-SFMS) has allowed for much higher mass resolution, allowing the separation of the peaks of analytes and interfering ions (Jakubowski et al., 2011). While ICP-SFMS has greatly improved the technical capabilities of ICP-MS, it is still not possible to resolve all interferences, and the high purchase cost of the instrument has led to the development of alternate instrumentation. Collison/reaction cell (CRC) technology has developed over the last ~20 years to aid in the suppression of interferences. The CRC is pressurized with either a non-reactive gas (e.g. He) and/or a reactive gas (e.g. H_2, O_2, NH_3), which are able to remove interferences either by non-reactive collisions in combination with kinetic energy discrimination or by reactions with the reactive-gases (Tanner et al., 2002). While the CRC is an effective tool for improving detection limits, it can be challenging to prevent the formation of new interferences within the CRC. Recently, ICP-tandem mass spectrometers (ICP-MS/MS, also called triple quadrupole ICP-MS) have become commercially available (Agilent Technologies 8800, 8900; Thermo Fisher iCap–tq). These newly developed ICP-MS/MS are able to overcome many of the problems faced by single quadrupole ICP-MS (a recent review article by Balcaen et al., 2015 describes the instrument and applications). The tandem MS configuration of these instruments consists of two quadrupole mass filters separated by a collision/reaction cell. This differs from conventional single quadrupole ICP-MS by the addition of the quadrupole mass filter between the ion source and the collision/reaction cell allowing for mass-selection of the ions that enter the CRC, leading to much improved control over the reactions occurring in the CRC. The ICP-MS/MS has already been successfully used to make direct measurements of Cd in seawater, through careful removal of the MoO^+ isobaric interference (Zhu & Itoh, 2016).

In this study we present a novel method for the rapid determination of Mn, Fe, Ni, Cu, Zn, Cd and Pb using the ICP-MS/MS, following offline matrix removal and pre-concentration with the *seaFAST*-pico preconcentration system. The precision and accuracy of the method was confirmed by the analysis of SAFe inter-comparison samples for which consensus values exist and certified reference material (NASS-6). The utility of the method is demonstrated through the presentation of depth profiles of trace metals obtained through analysis of Arctic Ocean seawater samples.

2.3 Experimental

2.3.1 Instrumentation

All of the analyses were carried out using an Agilent 8800 ICP-MS/MS instrument (Agilent Technologies). The instrument consists of two mass-selecting quadrupoles (Q1 and Q2) separated by a third generation octopole collision/reaction cell (CRC). For our work, the instrument was operated in two modes, single-quad mode and MS/MS mode. In single-quad mode, Q1 functioned only as an ion-guide, such that the instrument behaved like a traditional ICP-MS. In MS/MS mode, both Q1 and Q2 acted as mass filters. This allowed control over the species entering the CRC, and careful selection of the reaction gas ensured that interferences were effectively removed. The CRC was pressurized with He, H_2 and O_2 to evaluate which gas was most effective at removing spectral interferences. The instrument was run in single-quad mode for all gases, and MS/MS mode when pressurized with H_2 and O_2. In each case, the instrument parameters were optimized for maximum sensitivity across the mass range while minimizing the formation of molecular interferences. Eluted samples were transferred to an Agilent SPS 4 Autosampler connected to the ICP-MS/MS and were introduced using a 0.4mL/min concentric Micromist™ glass nebulizer. The instrument operating conditions are listed in Table 2.1.

Table 2.1 Typical operating conditions of the Agilent 8800 ICP-MS/MS

Instrument parameter	Operating conditions
RF applied power (W)	1600
Plasma sampling depth (mm)	10.0
Dilution gas flow rate (L min^{-1})	0.40
Carrier gas flow rate (L min^{-1})	0.88
Extract 1 (V)	0.0
Extract 2 (V)	-145.0
Omega bias (V)	-75
Omega lens (V)	8.8
Cell gas flow rate (mL min^{-1})	He: 5.0; H_2: 5.0; O_2: 0.35
Octopole bias (V)	No gas: -8.0; He: -18.0; H_2: -18.0; O_2: -5.0
KED (V)	No gas: 5.0; He: 5.0; H_2: -3.0; O_2: -7.0
Wait time offset (msec)	No gas: 0; He: 0; H_2: 0; O_2: 4
Nebulizer	Concentric glass nebulizer

2.3.2 Reagents

All reagents were prepared in a Class-100 laminar flow hood in a class-1000 space, using the highest grade reagents available. Ultra-pure deionized water (MQW) was generated using a Milli-Q Element system (>18 MΩ) (Millipore, Darmstadt, Germany) and used to prepare all reagents. Standards and ICP-MS/MS test solutions were all prepared by dilution of 10 $\mu g \cdot mL^{-1}$ single-element standards (High-Purity Standards, SC, USA). For the preconcentration procedure, the 1.6 M HNO_3 elution acid was prepared using ultrahigh-purity HNO_3 (SeaStar Chemicals, Sydney, BC, Canada) and spiked with 1$\mu g \cdot L^{-1}$ Indium (In) which served as an internal standard for instrument sensitivity (High-Purity Standards, North Charleston, SC, USA). For the buffer, a saturated ammonium acetate solution (19.2 M) was prepared by bubbling high-purity anhydrous ammonia gas through twice-distilled acetic acid. The concentrated solution was diluted to 2.3 M, and the pH was adjusted to pH = 6.0 ± 0.1 using concentrated, twice-distilled NH_3. A 0.012 M HCl rinse solution was prepared fresh each day from ultrahigh-purity HCl (SeaStar Chemicals, Sydney, BC, Canada).

2.3.3 Extraction Procedure

The commercially-available *seaFAST*-pico SC-4 DX system (ESI, Omaha, NE, USA) was used to remove the bulk seawater matrix and pre-concentrate the trace metals. The *seaFAST*-pico system uses solid phase extraction (SPE) by way of a column loaded with Nobias PA-1 resin functionalized with ethylenediaminetriacetic acid and iminodiacetic acid coordination groups that display high affinity for a variety of TMs across a broad range of pH. Details of the method are described in Lagerström et al, 2013. Briefly, samples are processed as follows:

1) *Fill loops*: The 10mL sample loop is overfilled, using an integrated vacuum pump and the buffer line is filled, using a syringe pump.
2) *Load column*: Syringe pumps mix buffer and sample online, and the buffered sample is pushed across the analytical column where metal ions are selectively bound.
3) *Wash matrix*: Buffer and MQW are mixed online and rinse the column, removing unchelated matrix ions.
4) *Elute column*: 2.5mL of elution acid spiked with internal standard was used to elute trace metals from the column into pre-cleaned, metal-free centrifuge tubes (VWR, Radnor, PA, USA)
5) *Condition column*: Buffer and MQW are mixed online and pushed across the column, to raise pH and condition the column for the next sample.

Steps 1-3 were repeated 2 times or 4 times prior to elution, for an 8-fold or 16-fold preconcentration factor respectively.

2.3.4 Shipboard Procedures

Open-ocean seawater samples were collected on two cruises in the Arctic Ocean aboard the CCGS Amundsen, GEOTRACES sections GN02 (10 Jul 2015 – 20 Aug 2015, from 56°N to 75°N and from 53°W to 98°W) and GN03 (4 Sept 2015 – 1 Oct 2015, from 74°N to 77°N and from 96°W to 150°W). Seawater was collected using a modified trace-metal rosette sampling system (Measures et al., 2008), consisting of a powder-coated aluminium frame equipped with twelve 12 L Teflon-coated GO-FLO bottles (General Oceanics, FL USA) attached to a 4000 m 4-member conducting Vectran cable encased in polyurethane (Cortland Cable Co., Cortland NY USA). GO-FLO bottles were deployed in the open position and lowered to below the deepest desired depth. Bottles were closed at the desired depth on the ascent to reduce the potential for contamination from the rosette and instrument payload. On deck, GO-FLO bottles were relocated to a HEPA-filtered clean container for sample collection. Seawater was gravity-filtered through 0.2 µm Acropak filters (Pall Corporation) and acidified on-board to pH = 1.7 with 12 M high-purity HCl (SeaStar Chemical) for storage. 500 mL LDPE bottles (Nalgene) were acid-washed according to GEOTRACES protocols (Cutter et al., 2010) and used for sample collection and storage.

2.4 Results and Discussion

2.4.1 Effect of reaction cell gas on signal intensity

By running the instrument in MS/MS mode, it is possible to effectively decompose polyatomic interferences in the CRC. However, using a reaction cell gas can dramatically reduce the signal intensity on certain elements. We compared the signal intensity of a solution containing 1 µg L^{-1} each of Mn, Fe, Ni, Cu, Zn, Cd and Pb run in no-gas mode with the signal intensity observed

using three different CRC gases: He, H_2 and O_2 (Fig. 2.1). For Fe, relative signal intensity was determined relative to the signal using O_2 gas, as large interferences from $^{40}Ar^{16}O^+$ in no-gas mode made relative difference in the signal intensity between CRC gases unresolvable. With He as the CRC gas, the instrument was run in single quad (SQ) mode, with Q1 set as a non-selective ion guide. With H_2 and O_2 as the CRC gas, the instrument was run in MS/MS mode, with Q1 and Q2 set to the *m/z* of the selected ion. Helium was found to cause a substantial decrease in signal intensity for all elements except for ^{208}Pb: signal intensity was <10% of the signal intensity in no-gas mode for Mn and Zn, and <25% for Ni, Cu and Cd. With H_2 and O_2 as the CRC gases, the signal sensitivity was greater than 40% of the signal in no-gas mode for all elements, except in the case of Ni and Cu in H_2 mode where signal sensitivity was <20% of signal in no-gas mode.

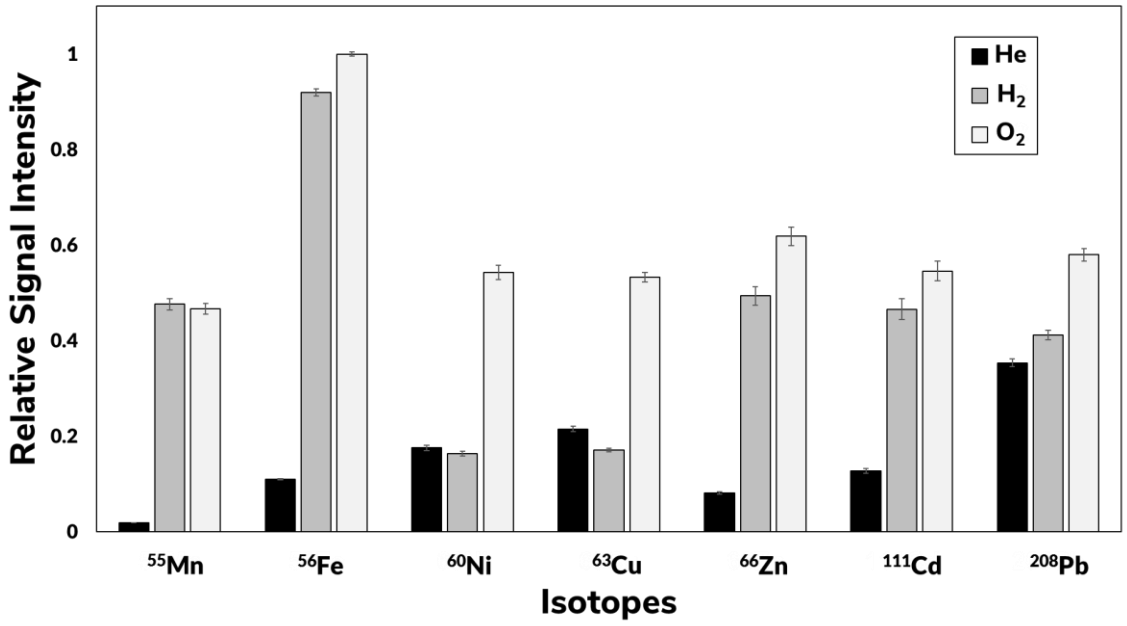

Figure 2.1 Effect of the collision/reaction cell gas on signal intensity. Signal intensities were determined in a solution containing 1 µg L^{-1} of Mn, Fe, Ni, Cu, Zn, Cd and Pb. Relative signal intensities were calculated as the measured signal intensity in each gas mode (He, H_2, and O_2) relative to vented mode for Mn, Ni, Cu, Zn, Cd and Pb. For Fe, relative signal intensity was determined relative to O_2.

2.4.2 Effect of reaction cell gas on polyatomic interferences

In order to accurately measure the concentration of Fe and Cd in seawater, it is necessary to remove or correct for polyatomic interferences from $^{40}Ar^{16}O^{+}$ and $Mo^{16}O^{+}$ respectively. To test the effectiveness of the gases at removing interferences, we measured the background equivalent concentration (BEC) and the signal intensity in single-quad mode (SQ) for all gases (no gas, He, H_2 and O_2) , and in MS/MS mode for H_2 and O_2 reaction gases (Fig. 2.2). For Fe, our background solution was 0.8 mol L^{-1} HNO_3, and the signal solution was 1 µg L^{-1} Fe in 0.8 mol L^{-1} HNO_3. For Cd, the background solution was 100 µg L^{-1} Mo in 0.8 mol L^{-1} HNO_3 and the signal solution contained 1 µg L^{-1} Cd and 100 µg L^{-1} Mo in 0.8 mol L^{-1} HNO_3.

For Fe, there was a dramatic decrease in both signal intensity and BEC when a CRC gas was used. The BEC was >50 µg kg^{-1} in no-gas mode, which we infer to be derived primarily from the $^{40}Ar^{16}O^{+}$ interference, while this diminished to 60 ng kg^{-1} with He as the reaction gas and ~20 ng kg^{-1} with both H_2 and O_2 as the reaction gas in MS/MS mode. The BEC was reduced in MS/MS mode when compared to SQ mode for both H_2 and O_2 gases. While the BEC, which we attribute primarily to $^{40}Ar^{16}O^{+}$ interference, still contributed to the observed Fe signal, the BEC was stable throughout the ICP-MS/MS run (± 7% variability in BEC throughout run) and could be considered a baseline blank signal which was corrected for by subtraction from the sample signal.

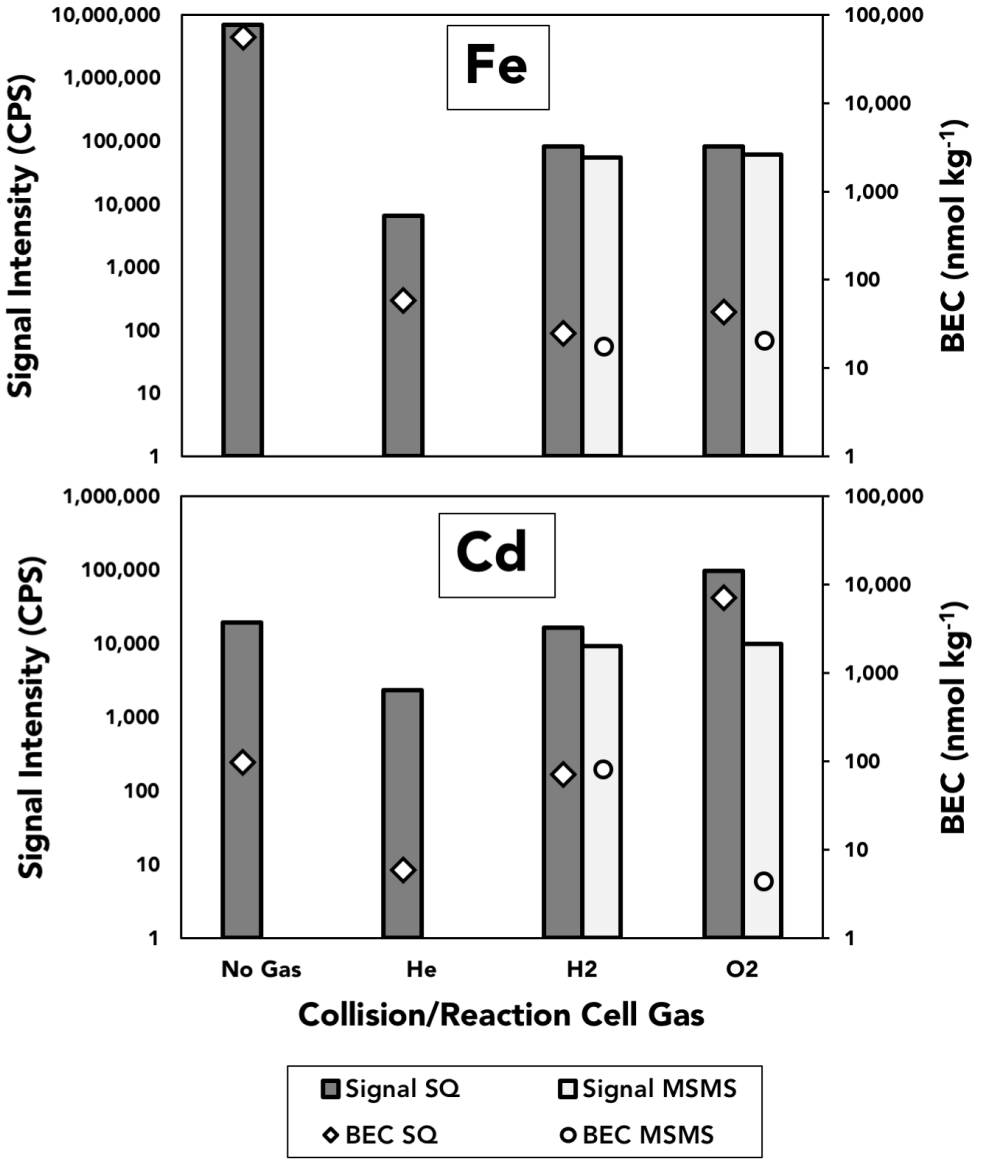

Figure 2.2 Effect of reaction/collision cell gases (no gas, He, H_2 and O_2) on instrument sensitivity (bars) and BEC (symbols) for Fe and Cd. In SQ mode, Q1 acted as an ion guide. When H_2 and O_2 were used as reaction gases, the system was also run in MS/MS mode with Q1 and Q2 both set to the same *m/z* (on-mass mode). The signal intensity was obtained from a signal solution (1 µg L^{-1} Fe in 0.8 mol L^{-1} HNO_3 for Fe and 1 µg L^{-1} Cd and 100 µg L^{-1} Mo in 0.8 mol L^{-1} HNO_3 for Cd) and the BEC was determined from a blank solution (0.8 mol L^{-1} HNO_3 for Fe and 100 µg L^{-1} Mo in 0.8 mol L^{-1} HNO_3 for Cd).

For Cd, the BEC (which we attribute primarily to an interference from $MoO^{+)}$ contributed 96 ng kg^{-1} signal in no-gas mode, which was reduced to 6, 80 and 4 ng kg^{-1} with He, H_2 and O_2 as the reaction gases, respectively (with H_2 and O_2 in MS/MS operating mode). The BEC was similar in SQ and MS/MS mode when H_2 gas was used, but dramatically decreased in MS/MS mode when O_2 gas was used, demonstrating the advantage of including a second mass-selecting quadrupole prior to the collision/reaction cell. For both Fe and Cd, there was a notable decrease in the background contribution when the reaction cell gases were used. For Fe, both H_2 and O_2 produced similar signal intensities and BEC. For Cd, O_2 was the most effective gas at decreasing the BEC while maintaining high sensitivity when run in MS/MS mode. Based on their effects on signal sensitivity and BEC, both H_2 and O_2 run in MS/MS mode were investigated further for use in the CRC.

2.4.3 Effect of gas flow rate on instrument sensitivity and interference removal

Using a reaction gas in the CRC has the advantage of decreasing the effect of polyatomic interferences, however it can also reduce the sensitivity of the analytes and increase the BEC. As this is a multi-element method, it was necessary to optimize the gas flow rate such that sensitivity across all analytes was maximised, while polyatomic interferences were minimised.

To examine the impact of the reaction gas on sensitivity, we first looked at the effect of H_2 and O_2 flow rate on the most interference prone elements, Fe and Cd (Fig. 2.3). We used the same signal and background solutions for Fe and Cd as were used in the previous test, but systematically varied the gas flow rates of H_2 and O_2. Both raw CPS and BEC were measured at H_2 flow rates of 3, 4, 4.5, 5, 5.5, 6 and 7 mL min^{-1} and O_2 flow rates of 0.10, 0.20, 0.25, 0.30, 0.35, 0.40 and 0.50 mL min^{-1} for Fe and Cd. For Fe, sensitivity was similar for most flow rates in both gases (~50,000 CPS/ µg kg^{-1}), while the minimum BEC was observed with H_2 gas (17 ng kg^{-1} at a flow rate of

5.5 mL min^{-1} H_2 versus 22 ng kg^{-1} at a flow rate of 0.35 mL min^{-1} O_2. For Cd, the sensitivity was similar for both reaction gases (~90,000 CPS/µg kg^{-1}), however the BEC was at a minimum when O_2 was used as a reaction gas, at flow rates greater than 0.35 mL min^{-1} (BEC < 5 ng kg^{-1}) compared to BEC >10 ng kg^{-1} for all flow rates with H_2 as the reaction gas.

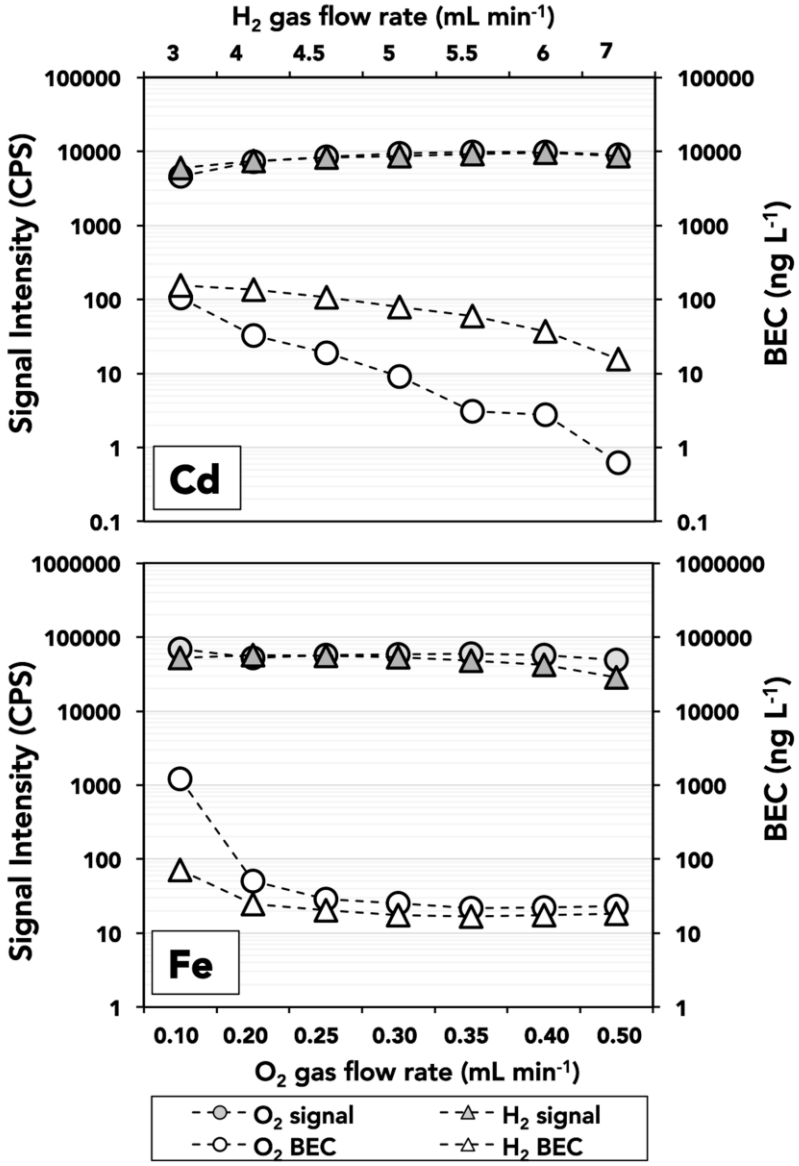

Figure 2.3 Effect of H_2 and O_2 gas flow rate on signal intensity and BEC for Fe and Cd. The signal intensity was obtained from a signal solution (1 µg L^{-1} Fe in 0.8 mol L^{-1} HNO_3 for Fe and 1 µg L^{-1} Cd and 100 µg L^{-1} Mo in 0.8 mol L^{-1} HNO_3 for Cd) and the BEC was determined from a blank solution (0.8 mol L^{-1} HNO_3 for Fe and 100 µg L^{-1} Mo in 0.8 mol L^{-1} HNO_3 for Cd).

For Cd, we found that the contribution of MoO^+ to the observed signal decreased as we increased the O_2 flow rate. A maximum BEC of 105 ng kg^{-1} was observed at an O_2 flow rate of 0.10 mL min^{-1}, which continuously decreased as the flow rate was increased, to a minimum of 1 ng kg^{-1} at 0.50 mL min^{-1}. The assumed mechanism of the removal of the MoO^+ interference in O_2 mode is by the formation of MoO_2^+ through reaction with O_2 gas, shown by Eq 1.

$$\mathbf{MoO^+ + O_2 \rightarrow MoO_2{}^+ + O} \qquad \mathbf{\Delta H = -0.46\ eV} \qquad \mathbf{(1)}$$

(Agilent Technologies, Inc., 2012)

The reaction is dependent on the pressure of O_2 in the CRC. At higher pressures, determined by higher O_2 flow rates, we expect a greater formation of MoO_2^+, shifting the *m/z* of the interfering ion from 111 to 127, which was reflected in our results (Fig. 2.3).

The effect of H_2 and O_2 gas flow rates on signal sensitivity and BEC were also investigated for Mn, Ni, Cu, Zn and Pb (Fig. 2.4). For Ni and Cu, sensitivity was maximised and BEC minimised with O_2 as the CRC gas. For Mn and Pb, both sensitivity and BEC were comparable with H_2 and O_2 as reaction gases. For Zn, sensitivity was greater with O_2 gas, however the BEC was lower with H_2 gas. For optimum sensitivity with minimum BEC, we opted to analyse Mn, Ni, Cu, Cd and Pb with O_2 as the reaction gas, at a flow rate of 0.35 mL min^{-1} and Fe and Zn with H_2 as the reaction gas, at a flow rate of 5.5 mL min^{-1}.

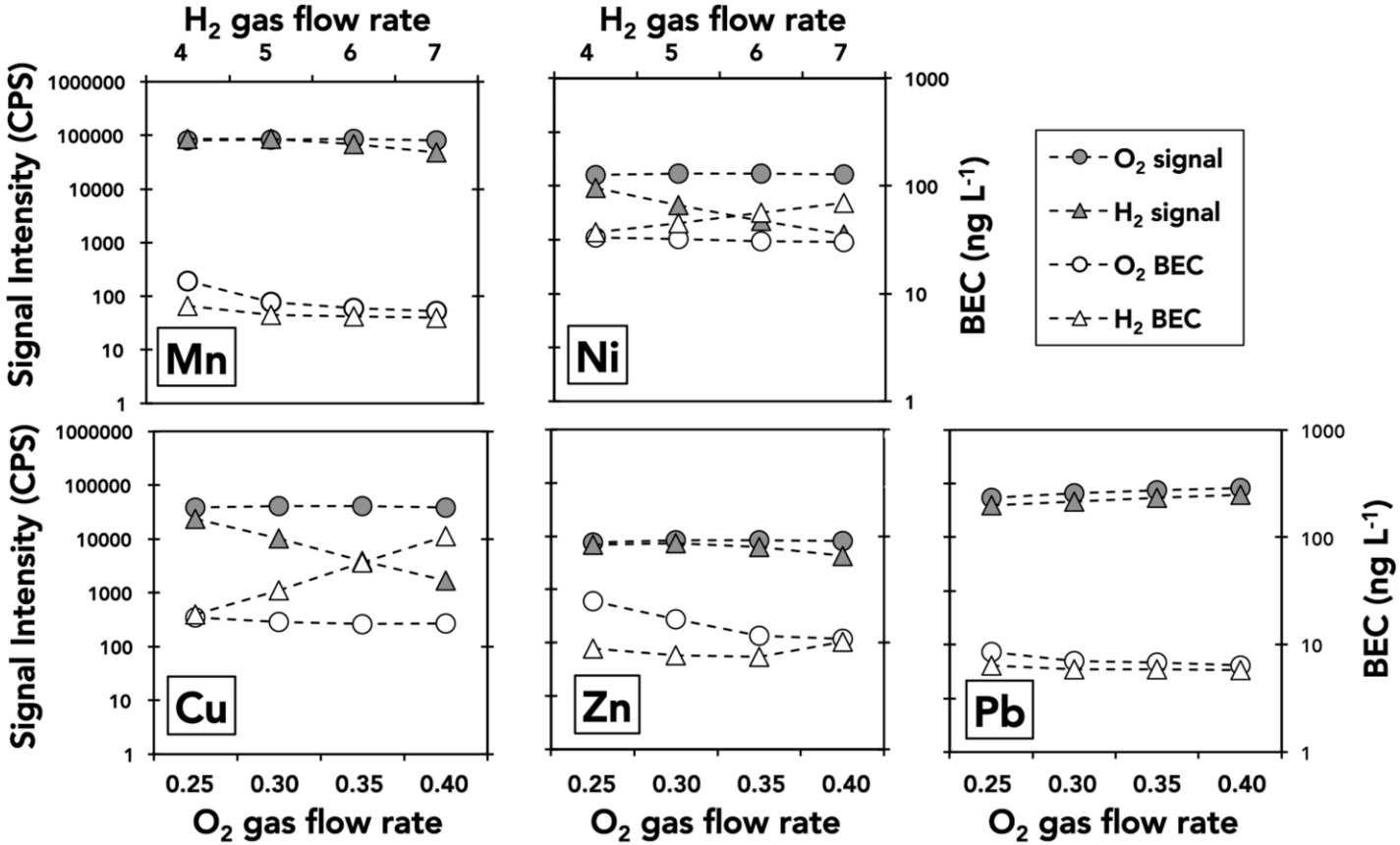

Figure 2.4 Effect of H_2 (triangles) and O_2 (circles) gas flow rate on the signal intensity and BEC of Mn, Ni, Cu, Zn, Pb. The signal intensity was measured in a solution containing 1 µg L^{-1} each of Mn, Fe, Ni, Cu, Zn, Cd and Pb in 0.8 mol L^{-1} HNO_3**.** The BEC was determined from a blank solution of 0.8 mol L^{-1} HNO_3.

Table 2.2 Average blanks and detection limits of this method from 10 extractions, compared to other recent studies. Detection limits are 3 times the standard deviation of the blank. NA indicates metal not analysed. Results were obtained in O_2 mode unless otherwise indicated. * indicates a 16-fold preconcentration factor, † indicates results obtained in H_2 mode.

	Blanks				Detection Limits			
	This study	Quéroué et al., (2014)	Lagerström et al., (2013)	Biller & Bruland, (2012)	This study	Quéroué et al., (2014)	Lagerström et al., (2013)	Biller & Bruland, (2012)
Mn (nmol L^{-1})	0.006	0.004	0.008	0.0056	0.002	0.002	0.002	0.002
Fe (nmol L^{-1})	0.14*†	0.26	0.067	0.03	0.029*†	0.092	0.014	0.014
Ni (nmol L^{-1})	0.053	0.013	0.027	0.2	0.03	0.003	0.013	0.089
Cu (nmol L^{-1})	0.03	0.054	0.013	0.034	0.008	0.03	0.003	0.054
Zn (nmol L^{-1})	0.025†	NA	0.118	0.80	0.017*†	NA	0.016	0.90
Cd (pmol L^{-1})	0.34*	0.19	NA	1.013	0.6*	0.12	NA	0.58
Pb (pmol L^{-1})	0.46	0.74	NA	0.027	0.3	0.21	NA	NA

2.4.4 Blanks and detection limit

To determine blanks associated with the method, we ran a solution containing 125 mL MQW with 250 µL HCl (SeaStar Chemicals, Sydney, BC, Canada) and 125 µL of Pacific open-ocean surface seawater for matrix-matching as has been previously reported in Lagerström et al, 2013. Our blank was preconcentrated by the same method as our samples, with 20 mL or 40 mL of blank loaded onto the column, which was eluted with 2.5 mL of elution acid. This ensures that any volume-dependant blanks were correctly accounted for (i.e. blanks from the buffer or elution acid). Other potential sources for blanks included the autosampler bottles, elution vials, the preconcentration manifold (pumps, tubing and valves) and from the ICP-MS/MS. The observed blanks were all at picomolar or sub-picomolar levels, except for Fe (0.14 nmol L^{-1}). Fe and Pb blanks were comparable to Quéroué *et al.* (2013), but significantly greater than other studies. Mn, Ni, Cu, Zn and Pb blanks and detection limits for all elements were comparable to blanks reported in previously published studies (Table 2.2).

The high blanks calculated for Fe (0.14 nmol L^{-1}) are likely due to the interference from ArO^+ even under optimized conditions and are subtracted from all results. To determine the contribution of ArO^+ to the Fe blank compared to the contribution from the extraction procedure, several aliquots of the 1.6 M HNO_3 elution acid were run on each day of analysis on the ICP-MS/MS and the counts in the elution acid and the extracted blanks were compared. While the elution acid itself could contain some concentration of Fe, we attribute the majority of the elution acid blank to the ArO^+ interference. We found the ArO^+ contributed between 60-85 % of the observed blank signal each run, with the percentage contribution from ArO^+ internally consistent on each day of analysis. Our detection limits were calculated on each day of analysis, as three times the standard deviation of the blanks. As blanks varied from day to day depending on

individual reagents and fluctuations in instrument baseline, we have presented the average of the detection limits observed over multiple instrumental runs. We found that our detection limits were again comparable to other recent studies, and were all less than the expected concentrations of metals in our samples. The detection limits for Mn, Ni, Cu, Zn and Cd were all less than 1% of the concentration of SAFe D, while the detection limits of Pb and Fe were ~1% and ~9%. For SAFe S, the detection limits for Mn, Ni, Cu and Pb were all ~1% of the consensus concentration. Fe, Zn and Cd are all in very low concentrations in SAFe S hence 40mL loads were used to achieve a 16-fold preconcentration factor to both improve the detection limits and sensitivity. Detection limits were ~25 % of the concentration of SAFe S for Fe and Zn, and ~50 % for Cd.

2.4.5 Reference material

The accuracy of the method was evaluated through the analysis of three reference samples: the certified reference material NASS-6 (National Research Council, Canada) and two consensus standards from the Sampling and Analysis of Fe (SAFe) intercalibration cruise, SAFe S (surface) and SAFe D2 (deep). Results are reported in Table 2.3.

Our results for NASS-6 agree with the certified values for all elements, within analytical uncertainty. Concentrations in SAFe S are representative of open Pacific Ocean surface water levels and are therefore very low for some metals; however all metals were found to agree with the consensus values within analytical uncertainty, except Mn. In SAFe D, we had good agreement between the measured and consensus values for all metals, except for Mn. Our measured values for Mn in both SAFe S and SAFe D are higher than the reported consensus values; however several other groups have reported similarly elevated values for Mn (Biller & Bruland, 2012; Quéroué et al., 2014).

Table 2.3 Results of the repeated analysis of consensus reference material, SAFe S and SAFe D and certified reference material, NASS-6. Consensus values for SAFe S and D were updated May 2013. Uncertainties represent the standard deviation of repeat measurements. Results were obtained in O_2 mode unless otherwise indicated. * indicates a 16-fold preconcentration factor, † indicates results obtained in H_2 mode.

	SAFe S O_2, n = 9 H_2, n = 6		SAFe D2 O_2, n = 13 H_2, n = 9		NASS-6 (n = 4)	
	Measured	Consensus	Measured	Consensus	Measured	Certified
Mn (nmol L^{-1})	0.94 ±- 0.02	0.81 ± 0.06	0.46 ± 0.03	0.36 ± 0.05	9.46 ± 0.06	9.65 ± 0.91
Fe (nmol L^{-1})	0.081 ± 0.018*†	0.095 ± 0.008	0.972 ± 0.038†	0.956 ± 0.024	9.22 ± 0.10	8.86 ± 0.82
Ni (nmol L^{-1})	2.43 ± 0.05	2.34 ± 0.09	9.05 ± 0.12	8.85 ± 0.26	5.22 ± 0.01	5.13 ± 0.43
Cu (nmol L^{-1})	0.49 ± 0.01	0.53 ± 0.05	2.27 ± 0.03	2.34 ± 0.15	3.64 ± 0.05	3.90 ± 0.39
Zn (nmol L^{-1})	0.065 ± 0.005*†	0.071 ± 0.010	7.83 ± 0.08†	7.62 ± 0.26	3.60 ± 0.05	3.93 ± 0.31
Cd (pmol L^{-1})	0.8 ± 0.3*[a]	1.1 ± 0.3	1034 ±16	1011 ± 24	272 ± 21	277 ± 17
Pb (pmol L^{-1})	51.3 ± 0.7	49.2 ± 2.3	29.0 ± 2.4	28.4 ± 1.5	21.2 ± 0.2	29.0 ± 9.7

2.4.6 Application of the method to open ocean profiles

This method was used to analyse ~300 samples from GEOTRACES section GN02 and GN03 in the Arctic Ocean. We present vertical profiles for each of the elements from a single station, CB2 (75° 49'N, -129° 08'E) in the central Canada Basin (Fig. 2.5). The profiles for all elements are oceanographically consistent and similar to those reported by previous studies in the region (Cid et al., 2012; Moore, 1981). Mn has a scavenged-type profile, with a surface water maximum concentration that diminishes with depth. Ni, Cu, Zn and Cd all show mid-depth maxima, at ~150m, that is associated with nutrient- and trace metal-enriched Pacific-origin water at this depth in this region of the Beaufort Sea. Fe displays a more uniform profile, with a sub-surface minimum observed at ~50m. Pb also displays a fairly uniform profile, though with some variability which could be due to contamination during sampling or analysis.

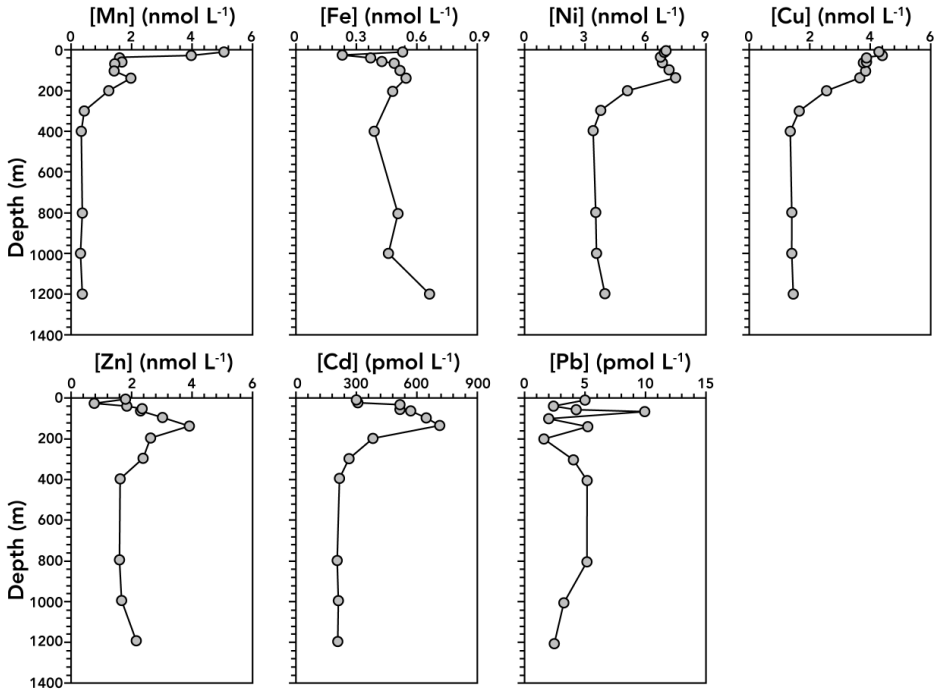

Figure 2.5 Vertical depth profiles of Mn, Fe, Ni, Cu, Zn, Cd and Pb collected during GEOTRACES GN02 at station CB2 (75° 49'N, -129° 08'E) in the Arctic Ocean.

2.5 Conclusions

I developed an accurate and precise method for the analysis of Mn, Fe, Ni, Cu, Zn, Cd and Pb at oceanographically relevant levels in filtered seawater. Combining solid-phase extraction (SPE) using the seaFAST pico (ESI, Omaha, NE, USA) preconcentration system with ICP-MS/MS obtained low blanks and detection limits, with high sample throughput. The additional mass-selector in the ICP-MS/MS prior to the collision/reaction cell provides the user with more control over the suppression of interferences.

Oxygen gas was found to be an effective reaction gas in the CRC for the analysis of Mn, Ni, Cu, Cd and Pb, and hydrogen gas was found to be effective for the analysis of Fe and Zn, removing polyatomic interferences on Cd and Fe and allowing for the accurate quantification of metals across the mass range. Consistently low blanks and detection limits were observed which were suitable for the analysis of most open ocean seawater samples.

The determined blanks and detection limits are comparable to those achieved in studies using sector-field ICP-MS providing a cost-effective alternative method for the analysis of trace metals in seawater. The SAFe consensus standards, SAFe S and SAFe D and the certified reference seawater, NASS-6, were analysed and showed agreement with consensus values, confirming the validity of this method. The automation of the method, coupled with the lower purchase-cost of the ICP-MS/MS makes this a useful method for laboratories aiming to expand their analytical capabilities and is necessary with an increase in global participation in large oceanographic programs, such as GEOTRACES.

Chapter 3: Dissolved Cadmium in the Canadian Arctic Ocean

3.1 Introduction

Early research into the distribution of dissolved cadmium (Cd) concentrations in seawater found depletions in surface waters and increased concentrations with depth remarkably similar to the macronutrients, in particular phosphate (PO_4) (Boyle et al., 1976; Bruland et al., 1978; de Baar et al., 1994). Cd and PO_4 are closely correlated throughout global oceans, with a "kink" in the relationship at PO_4~1.3µmol L^{-1} (Boyle, 1988; de Baar et al., 1994), with North Atlantic and surface water primarily defining the slope below the kink and Indian, Pacific and Southern Ocean waters defining a steeper slope above the kink (de Baar et al., 1994; Löscher et al., 1997). The correlation between Cd and PO_4 has led to the use of preserved Cd/Ca ratios in microfossils as paleoproxies, both for deep-water circulation (Boyle, 1988) and surface-water nutrient-utilization (Elderfield & Rickaby, 2000a). However, an incomplete mechanistic understanding of what drives the "kink" in the Cd:PO_4 relationship, as well as meridional and inter-basin variations in Cd/PO_4 ratios have limited the use of Cd as a paleoproxy (Cullen, 2006; Saager & de Baar, 1993). Several explanations for the kink have been proposed; Cullen (2006) proposed that chronic Fe-limitation in High-Nutrient Low-Chlorophyll (HNLC) regions leads to lower surface Cd/PO_4 ratios and may drive the "kink" in the Cd:PO_4 relationship. Another mechanism suggests that injections of Cd-depleted waters into intermediate depths leads to the kink (Frew & Hunter, 1992), with stable isotopes providing evidence for the importance of the Cd-depleted Sub-Antarctic Mode Water (SAMW) in Cd cycling (Abouchami et al., 2014; Baars et al., 2014; Gault-Ringold et al., 2012). Despite incomplete understanding of the drivers behind the global Cd:PO_4 relationship, deep waters (>1000m) appear to show constant basin-dependent Cd/PO_4 ratios. The deep-water Cd/PO_4 ratio increases with the age of the waters, from ~0.23 nM/µM in the North

Atlantic (Danielsson et al., 1985; Quay & Wu, 2015) to ~0.30 nM/µM in the Southern Ocean and South Indian Ocean (Frew & Hunter, 1992; Saager et al., 1992) to ~0.35 nM/µM in the North Pacific (Bruland, 1980).

Variations in phytoplankton uptake of Cd and cellular Cd:P ratios, which drive the biological cycling of Cd, have been observed in experiments with both laboratory isolates and field studies with natural algal assemblages. Cd has been shown to restore growth of Zn-limited phytoplankton (Price & Morel, 1990) by substituting for Zn in carbonic anhydrase (CA) (Lee et al., 1995) or as a Cd-specific CA (Lane & Morel, 2000). Laboratory studies have found that Cd uptake rates are directly related to free ion concentration of Cd [Cd'] and inversely proportional to [Zn'] and [Mn'] (where [M'] indicates the total inorganic species) (Lee et al., 1995; Sunda & Huntsman, 2000), while decreasing partial pressure of carbon dioxide (pCO_2) increases Cd uptake (Cullen & Sherrell, 2005; Lane & Morel, 2000). Decreasing Fe concentrations also affects phytoplankton Cd:P, with additions of Fe to Fe-limited cultures causing a decrease in Cd:P ratios in phytoplankton cultures (Cullen & Sherrell, 2005; Lane et al., 2009; Sunda & Huntsman, 2000). Community composition may also exert a strong influence on surface dissolved Cd/PO_4, owing to variations of cellular Cd:P across phytoplankton taxa (Ho et al. 2003). Changing irradiance and hence growth rate also exerts an influence on Cd:P; however phylogenetic groups appear to control whether this leads to increases or decreases in cellular Cd:P (Finkel et al., 2007).

More recently, modelling studies have been used to understand the global relationship between Cd and PO_4, with respect to surface water variations, basin-dependant changes in deepwater ratios, and changes in the Cd/PO_4 ratio with depth. Quay et al (2015) analysed a global dataset from 182 stations, and found that the Cd:P ratios of exported particles were primarily dependant on whether HNLC conditions existed. In HNLC regions particles tend to have higher Cd:P and a

greater fractionation factor (FF, where FF=$[Cd:P]_{particles}/[Cd/PO_4]_{seawater}$). The authors also used a multibox model to investigate the impacts of thermohaline circulation and particle degradation on deepwater Cd/PO_4 ratios, which further illustrated that deep-water Cd/PO_4 ratios are strongly affected by the Cd:P of degrading particles, which in turn are impacted by whether HNLC conditions exists or not. Wu and Roshan (2015) also used a model to help understand the depth-dependent variation in the Cd/PO_4 ratio and differences in the ratio between the North Pacific and the North Atlantic, which demonstrated that a difference in regeneration depths between Cd-poor non-ballast particulate organic carbon (POC) and Cd-rich ballast-associated POC could explain both interbasin and depth-dependent differences in Cd/PO_4.

Although considerable advances have been made to understand the controls on the global distribution of Cd, the Arctic Ocean is largely omitted from models primarily due to a lack of available data. The Arctic Ocean represents only 3% of the total area of the world's ocean, but it provides the only natural pathway for direct communication between the North Pacific and North Atlantic making it an important region oceanographically. Water enters the Arctic from the Atlantic via Fram Strait and Barents Sea, and from the Pacific via Bering Strait, and exits via Fram Strait or the Canadian Arctic Archipelago (CAA) (Carmack & McLaughlin 2011). Pacific-origin water carries a distinct high-nutrient signal, allowing it to be traced through the Arctic (Jones et al., 2003). Early trace metal studies in the Arctic Ocean discovered a peak in Cd coincident with the nutrient maximum observed in the Pacific-origin waters (Moore, 1981; Yeats, 1988; Yeats & Westerlund, 1991). More recent work in the Chukchi Sea and western Canada Basin has again shown that a peak in Cd is found in the high-nutrient Pacific-origin waters, with likely transport of these Cd-enriched waters across the Canada Basin (Cid et al., 2012; Kondo et al., 2016)

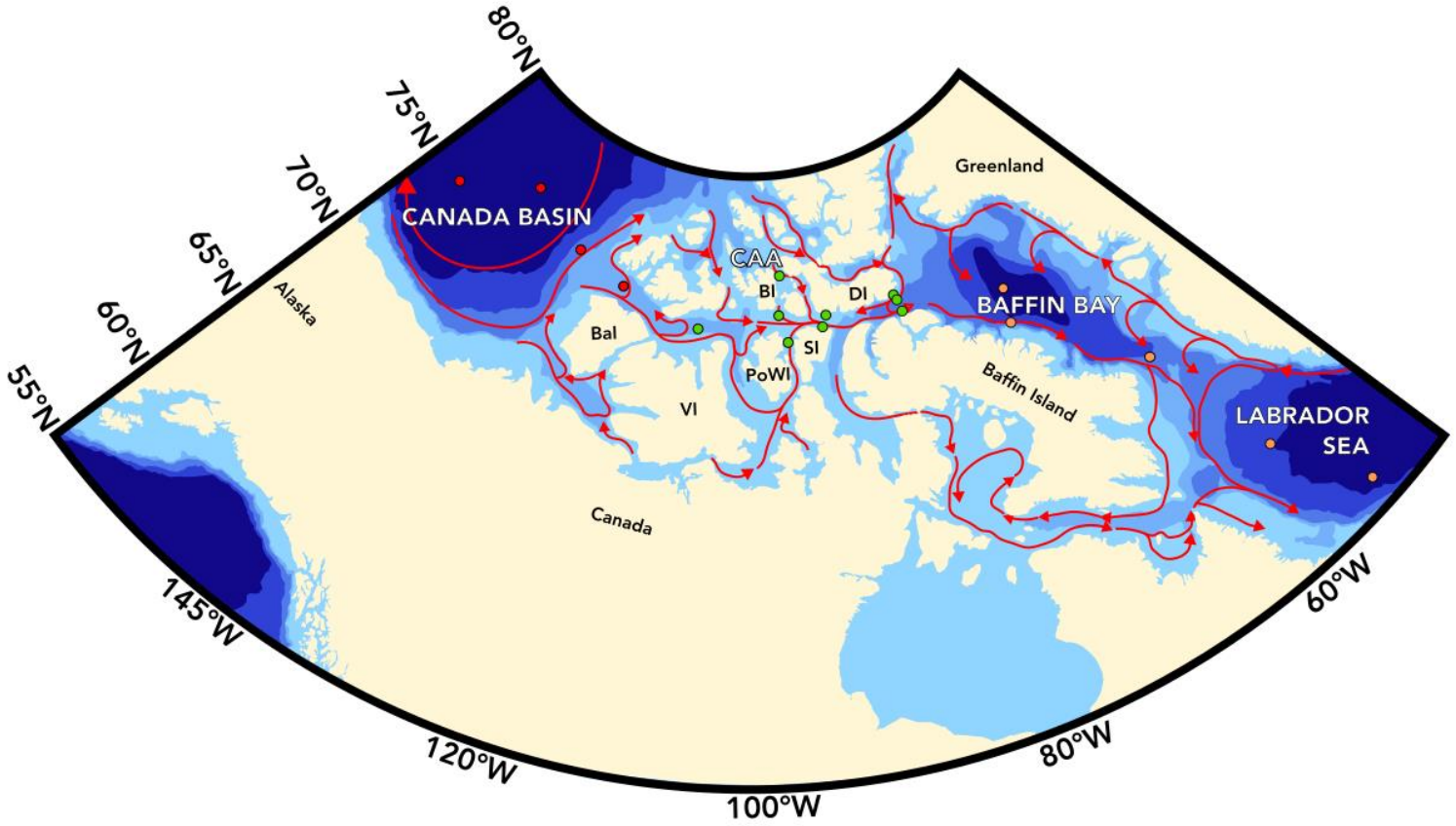

Figure 3.1 Sampling locations for CCGS Amundsen GN02 and GN03 (Red circles: Canada Basin, green circles: Canadian Arctic Archipelago, orange circles: Baffin Bay and the Labrador Sea). Surface currents shown with red arrows (Canada Basin modified from Steele et al, 2004; CAA modified from Michel et al, 2006 and Wang et al, 2011; Baffin Bay modified from Curry et al, 2011). BaI: Banks Island, VI: Victoria Island, PoWI: Prince of Wales Island, SI: Somerset Island, DI: Devon Island, BI: Bathurst Island.

This study was part of the GEOTRACES Canadian sections GN02 and GN03 which collected samples from Baffin Bay, the Canadian Arctic Archipelago and the Canada Basin in Summer and Fall 2015. Here we present profiles of dissolved Cd and Cd/PO_4 ratios from GN02 and GN03, contributing to the sparse datasets currently available for the Arctic Ocean.

3.2 Methods

3.2.1 Sampling locations and collection

Samples were collected on the CCGS Amundsen as part of GEOTRACES sections GN02 (10 Jul 2015 – 20 Aug 2015) and GN03 (4 Sept 2015 – 1 Oct 2015) which covered an area from 56°N to 77°N and 53°W to 150°W in the Canadian Arctic Ocean (Fig. 3.1). Vertical profiles of 8 to 25 discrete depths were obtained at 18 stations: four in the Canada Basin, nine in the Canadian Arctic Archipelago, three in Baffin Bay and two in the Labrador Sea (Fig. 3.2). A trace-metal clean sampling system consisting of a powder-coated aluminium frame which held twelve 12L Teflon-coated GO-FLO bottles attached by a 4000m 4-member conducting Vectran cable encased in polyurethane (Cortland Cable Co., Cortland NY USA) (Measures et al., 2008) was used to collect seawater samples. The rosette was fitted with a Conductivity-Temperature-Depth Sensor (SeaBird SBE 911plus) equipped with a dissolved oxygen sensor (SBE 43) which obtained oceanographic parameters. On-board the ship, samples were gravity-filtered through 0.2 µm Acropak filters (Pall Corporation) into 500mL LDPE bottles (Nalgene) in a HEPA filtered air environment. The sample bottles were pre-cleaned according to GEOTRACES protocols (Cutter et al., 2010; Appendix A). After collection, samples were acidified to pH=1.7 using SeaStar Baseline HCl and kept at room temperature until analysis (SeaStar Chemicals, Sidney, BC).

3.2.2 Sample Analysis

Samples were analysed in a Class-1000 clean room at the University of Victoria, BC. Trace-metal extraction and preconcentration was performed using the *seaFAST*-pico SC-4 DX system (ESI, Omaha, NE, USA). The automated seaFAST system preconcentrated samples by a factor of 8 while removing the bulk seawater matrix through solid phase extraction (Lagerström et al., 2013). For each sample 20mL of seawater was loaded onto a column which contained Nobias PA-1 resin (containing the functional groups ethylenediaminetriacetic acid and iminodiacetic acid). The column was then rinsed with an ammonium acetate buffer solution (pH=6.0) prepared by bubbling high-purity anhydrous ammonia gas through twice-distilled acetic acid with the pH adjusted by additions of NH_3 to remove the matrix. Samples were eluted in 2.5 mL of 1.6 M SeaStar Baseline HNO_3 (SeaStar Chemicals, Sidney, BC, Canada). The preconcentrated samples were analysed using the Agilent 8800 ICP-MS/MS. The ICP-MS/MS consists of two mass-selecting quadrupoles (Q1 and Q2) separated by a collision/reaction cell (CRC). MoO^+ causes a problematic interference on Cd analysis and effective removal is necessary for accurate and precise Cd analysis. To remove the interference and accurately analyse Cd concentrations, Q1 and Q2 were both set at *m/z* of 111, and the CRC was pressurized with O_2. O_2 gas reacted with MoO^+ to form MoO_2^+, shifting the *m/z* of the interference from 111->127. The efficiency of this removal was monitored by running a Cd-free Mo calibration curve, which allowed for the removal of any residual interference on Cd. SAFe reference material was analysed to confirm the accuracy of the measurements. The consensus value for Cd for SAFe D2 is 1011 ± 24 pM, and we measured a value of 1034 ± 16 pM. Our detection limit was 0.5pM.

3.3 Hydrography and General Circulation

GEOTRACES GN02 and GN03 traverses a wide expanse of the Arctic Ocean, which can be considered as three distinct geographic regions: the Canada Basin, the Canadian Arctic Archipelago, and Baffin Bay and the Labrador Sea. These regions have distinct hydrographic structure, which will be discussed individually below.

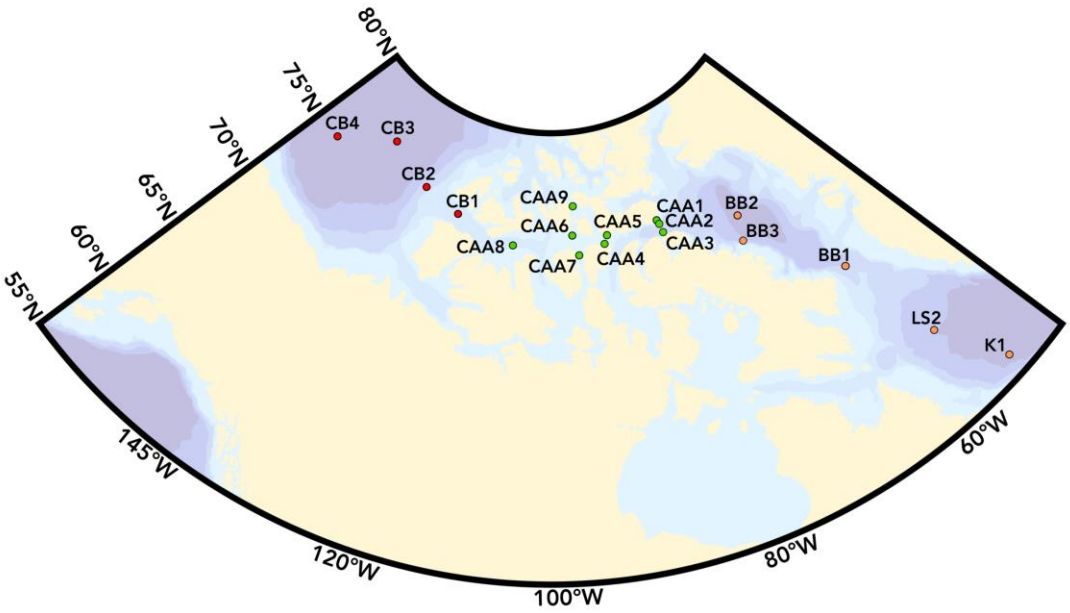

Figure 3.2 Station locations for GN02 and GN03 in the Canada Basin (red symbols), Canadian Arctic Archipelago (green symbols) and Baffin Bay and the Labrador Sea (orange symbols).

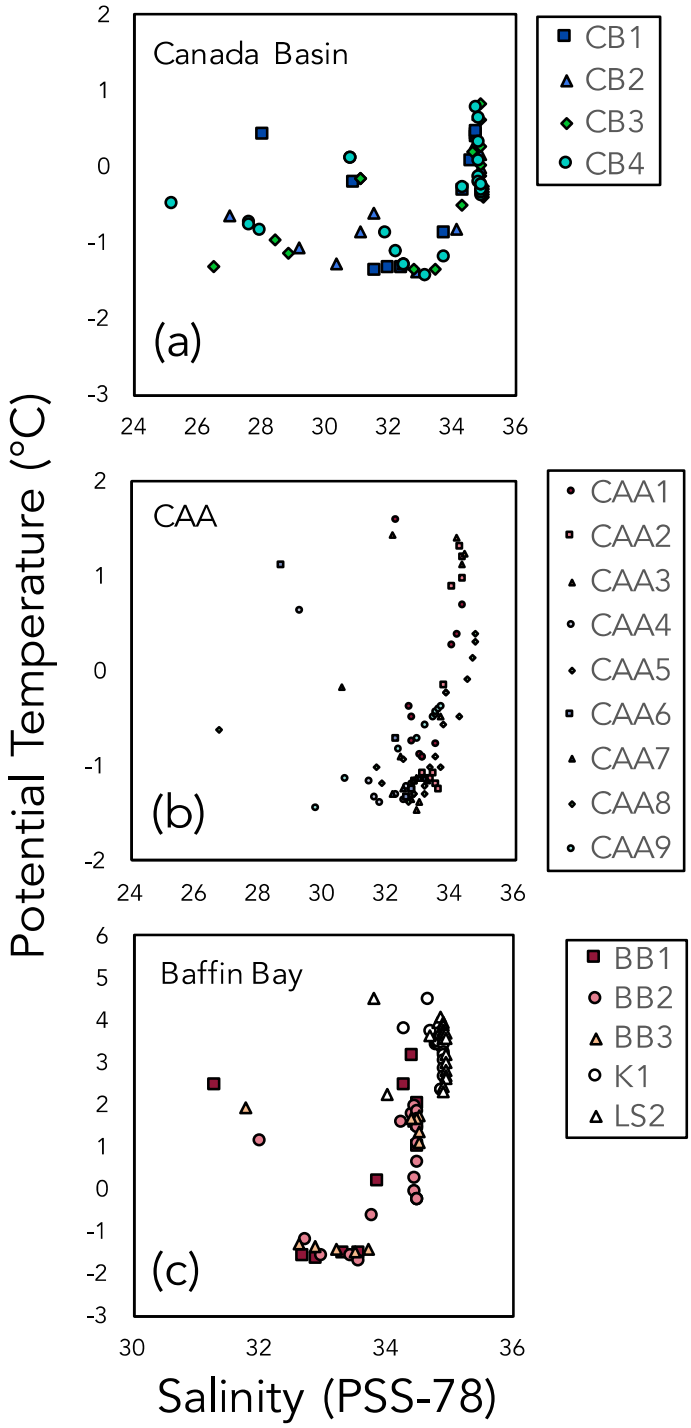

Figure 3.3 Potential Temperature-Salinity diagrams for (a) Canada Basin, (b) Canadian Arctic Archipelago, and (c) Baffin Bay.

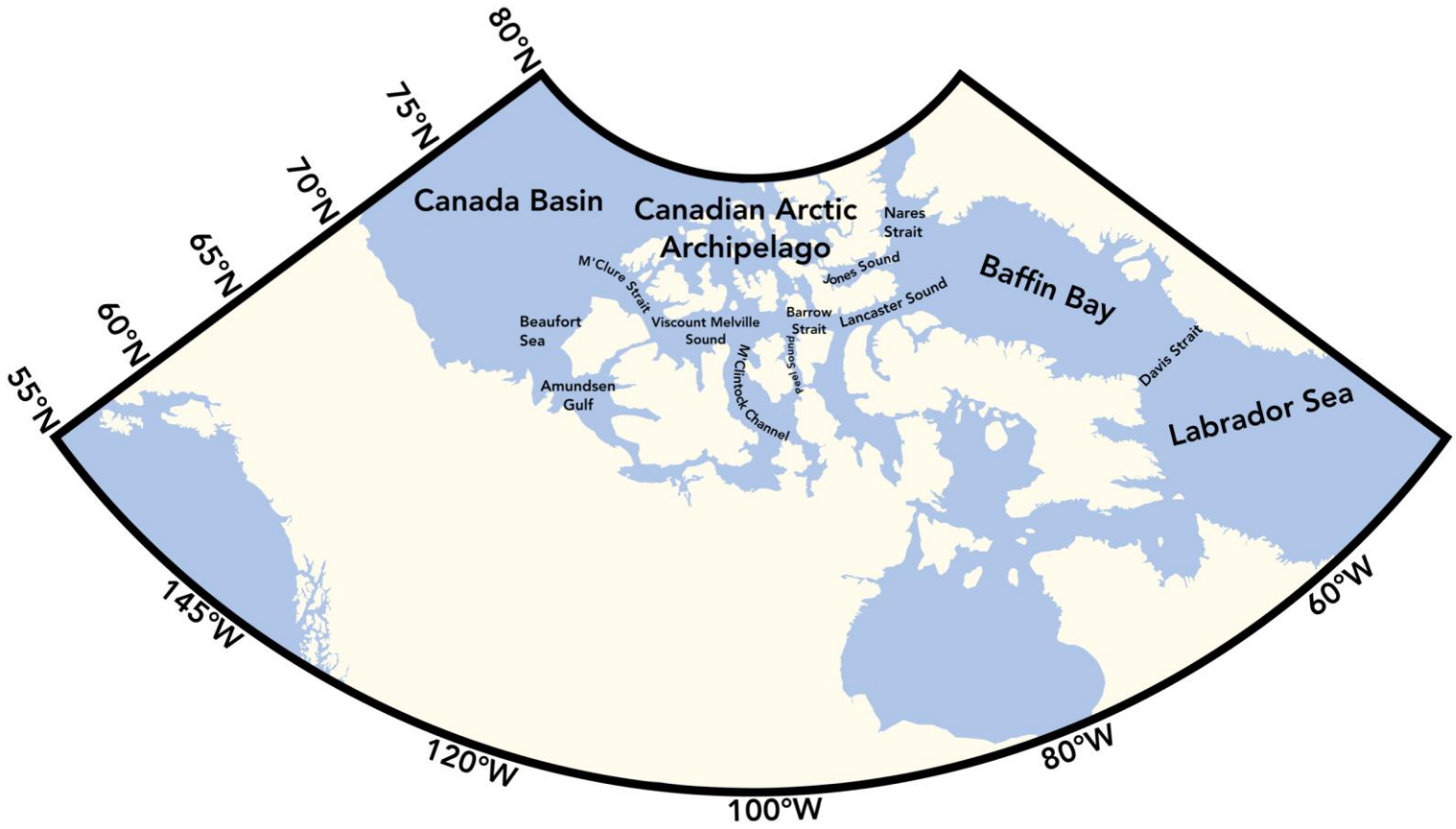

Figure 3.4 Geographical features of the Canada Basin, Canadian Arctic Archipelago, Baffin Bay and the Labrador Sea**.**

3.3.1 Canada Basin

The Canada Basin is a sub-basin of the Arctic Amerasian Basin, separated from the Makarov Basin by the Mendeleev-Alpha Ridge, reaching depths of ~3500m. The Canada Basin receives water from both the North Atlantic and the North Pacific. Pacific waters enter via the shallow Bering Strait (~50m), with a net annual transport of ~0.8 Sv, undergoing significant modification as it transits the Chukchi Shelf (Coachman & Aagaard, 1988). Atlantic waters enter via Fram Strait and the Barents Sea, undergoing significant modification as they transit the Barents Sea Shelf and the shelf of the Eurasian Sea (McLaughlin et al., 1996).

Five distinctive water masses were identified in the Canada Basin, shown on a temperature-salinity diagram (Fig. 3.3a) which were characterized in a manner consistent with previous studies in the region (e.g. McLaughlin et al. 2005; Cid et al. 2012; Kondo et al. 2016). These water masses are: (1) Surface water layer (SWL), which extends to a depth of 40-70m. This layer has variable temperatures (between -1.4˚C and 0.4˚C) and salinity (25-32), thanks to inputs of freshwater from sea ice melt and Mackenzie River runoff. (2) The upper halocline layer (UHL), with temperatures between -1.5˚C and -0.9˚C and salinities between 32.0 and 33.7 and extends to a depth of 150-250m. The UHL, also referred to as the Pacific Halocline, is derived of water which enters the Arctic Ocean from the North Pacific via Bering Strait. As the waters transit 700km across the Chukchi shelf the water is modified by shelf processes, including ice formation and melting, biological activity, and sediment resuspension and interactions (McLaughlin et al., 2005). (3) The lower halocline water (LHL) from ~200m to ~300m, with a temperature between -0.3˚C and -0.9˚C and salinities between 33.8 and 34.4. (4) the Atlantic Layer (AL) extends to a depth of ~1000m, and is relatively warm (T>0˚C) with salinities between 34.6 and 34.9. (5) The Canada Basin Deep Water (CBDW) is found below ~1000m, and has temperature <0˚C and salinity >34.9.

3.3.2 Canadian Arctic Archipelago

The Canadian Arctic Archipelago (CAA) represents one of two major flow pathways for water from the Arctic Ocean to the North Atlantic, the other being the Fram Strait. Flow through the CAA is complex, and water masses undergo significant modification through physical and biogeochemical processes during transit. The mean flow is eastwards, from the Pacific, to the Arctic, into the North Atlantic, due to higher steric sea level in the North Pacific relative to the North Atlantic. The CAA consists of a number of interconnected channels, with deep basins separated by shallow sills. Water enters the CAA from the Canada Basin via M'Clure Strait, the Amundsen Gulf or through complex pathways through the Queen Elizabeth Islands. A shallow sill (125m) at Barrow Strait separates the CAA into western and eastern part (McLaughlin et al., 2004; Michel et al., 2006).

At the west end of the transect, Canada Basin waters enter the CAA via M'Clure Strait, restricted by a sill of ~375m depth (Fig. 3.1; Fig. 3.4). Both Pacific and Atlantic water masses can be identified in the M'Clure Basin and Viscount Melville Basin, with Atlantic waters below a depth of ~135m. The Atlantic Water can be identified by an increase in temperature with depth and a change in the salinity slope (Fig. 3.3b). East of the Barrow Strait, complex flow dynamics and mixing make identification of Pacific and Atlantic origin water masses more complex.

The flow of water eastwards is restricted by the 125m deep sill at Barrow Strait. East of the sill, there is evidence of continued eastward flow of water from the Canada Basin on the southern edge of the channel. At the northern edge, waters flow westwards into the channel from Baffin Bay, as part of a southwards flow from Nares Strait or a northwards flow from the North Atlantic along the western coast of Greenland (Jones & Coote, 1980).

3.3.3 Baffin Bay

The final region, Baffin Bay, lies between Baffin Island and Greenland, forming a mediterranean sea with an area of approximately 1400km by 55km. Baffin Bay is connected to the Arctic Ocean via complex pathways through the Canadian Arctic Archipelago (Fig. 3.4). Jones Sound, Lancaster Sound and Nares Strait connect Baffin Bay to the Arctic, while Davis Strait (~600m deep sill) connects it to the Labrador Sea (Tang et al., 2004).

In Baffin Bay, we identified 3 water masses based on the classification from Tang et al (2004)**:** Arctic Water, West Greenland Intermediate Water (WGIW), and Baffin Bay Deep Water (BBDW) (Fig 3.3c). The Arctic Water constitutes a cold, low-salinity layer which occupies the upper 150-200m of water column. The Arctic Water is formed from the confluence of multiple pathways, entering Baffin Bay from the CAA via Lancaster Sound, Jones Sound and Nares Strait, as well as from the West Greenland Current which flows northward along the western edge of Greenland. The Arctic Water is identified by salinities <34 and T>0 °C.

The WGIW forms a warm, salty layer at a depth between 250m and 1000m. It is identified by salinities >34 and T>0 °C. This water enters Baffin Bay through the eastern Davis Strait and circulates through Baffin Bay. Below depth of ~1000m lies the BBDW. This water mass is cooler and saltier than the overlying WGIW, with T ~-0.5°C and S <34.5. The origins of this water mass are still debated, with authors variously suggesting that the water mass originates from Nares Strait subsurface water (Bailey, 1956; Collin, 1965), a mixture of Labrador Sea deep water and brine enriched surface water (Sverdrup et al., 1942; Tan & Strain, 1980), or from the formation and later migration of cold and saline water in the North Winter polynya in winter (Bourke & Paquette, 1991; Bourke et al., 1989).

3.4 Results and Discussion

3.4.1 Distribution of Cd and PO_4 in the Canada Basin

The distribution of Cd in the Canada Basin is strongly affected by water mass structure. In the surface water layer (SWL), dissolved Cd (dCd – the fraction of Cd <0.2 µM) is ~270 pM at CB4 and CB3, and increases to ~300 pM at the shallower shelf break and shelf stations CB2 and CB1 (Fig. 3.5). Concentrations increased rapidly through the surface layer, reaching a maximum in dCd in the UHL, between 600-740 pM. The dCd maximum is deepest at CB4, at 220m and increasingly shallower towards the coast, decreasing to 150m at CB2 and CB3, and 75m at CB1, but is consistently found on the σ_θ=26.5 isopycnal surface. There is a rapid decrease in dCd with depth through the LHL to the AL. Below ~400m at CB2, CB3 and CB4, dCd is 207± 2 pM and remains constant with depth toward the seafloor.

Depth profiles of PO_4 are very similar to dCd and are strongly influenced by the water mass structure, with a clear nutrient maximum in the UHL. The nutrient-rich UHL layer is of Pacific-origin and undergoes significant transformation during transit across the highly productive Chukchi Sea (Grebmeier et al., 2006). A number of biological and physical processes affect the chemical signature of the Pacific-origin water, including biological production and subsequent remineralization, interaction with sediments, sea-ice formation and melt, and riverine inputs (Carmack & McLaughlin, 2011; Mathis et al., 2007). Recent studies of trace metals in the Western Arctic (Chukchi Shelf to the Canada Basin) found elevated concentrations of dFe and dMn in Chukchi Shelf bottom waters (Cid et al., 2012; Hioki et al., 2015; Kondo et al., 2016), indicating that interactions with shelf sediments are a source of trace metals to the halocline. Both Kondo et al (2016) and Cid et al (2012) also found that concentrations of other trace metals (Mn, Fe, Ni, Zn and Cd) were elevated across the Chukchi Shelf and slope region within the UHL waters. While those studies were limited to the extent of the Chukchi shelf break, the close

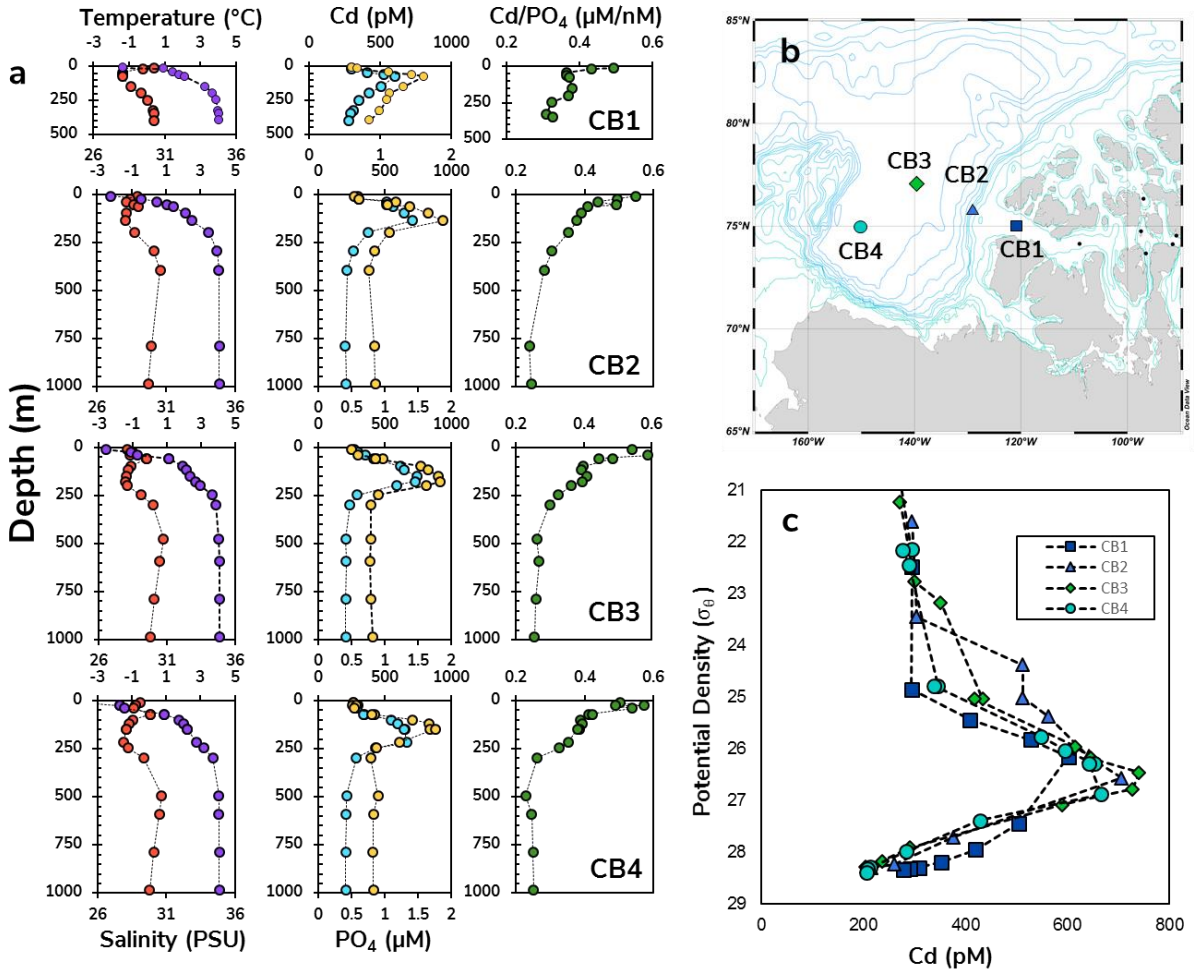

Figure 3.5 (a) Vertical distributions of temperature (red circles) and salinity (purple circles), dCd (blue circles) and [PO_4] (yellow circles), and Cd/PO_4 (greencircles) for stations CB1, CB2, CB3, and CB4. (b) Sampling locations in the Canada Basin. (c) Potential density vs dCd for CB1, CB2, CB3, and CB4.

correlation observed between PO_4 and dCd (Cid et al., 2012; Kondo et al., 2016) led the researchers to suggest that it was likely that elevated dCd would be found throughout the Canada Basin in the UHL, as elevated PO_4 concentrations have been measured throughout the Canada Basin in the UHL. The coincidence of both elevated PO_4 and dCd in the UHL suggests a common source for both parameters, likely due to interactions with shelf sediments. We observe subsurface Cd maxima in the UHL at all stations in the Canada Basin, coincident with the PO_4 maxima.

Spatial variations in dissolved Cd/PO_4 ratios also appear to be controlled by the water mass structure. High Cd/PO_4 ratios are seen in surface waters at all stations, at 0.47±0.05 nM/uM. Note that from here on, Cd/PO_4 refers to the ratio of dissolved Cd to PO_4 in a discrete water sample in nM/µM, $Cd:PO_4$ refers to the slope of Cd to PO_4 in nM/µM, and Cd:P refers to the ratio of particulate Cd to P in nmol/µmol. All ratios will be presented without units. The ratio decreases to 0.37±0.03 in the UHL and further decreases through the LHL to 0.25±0.02 in the AIW.

Quay et al. (2015) and Elderfield and Rickaby (2000) both observed a meridional trend in surface water Cd/PO_4 ratios – with minimum values observed between 30°N-30°S (Cd/PO_4=0.10±0.09) and a general poleward increase, with a ratio of Cd/PO_4=0.26±0.07 above 50°. This poleward increase is attributed to variations in particulate Cd:P reflected in the Rayleigh fractionation factor ($[Cd:P]_{particles}/[Cd/PO_4]_{seawater}$). The surface Cd/PO_4 ratio observed in the Canada Basin was high – at 0.47±0.05 it is one of the higher Cd/PO_4 surface ratios observed globally. The high ratio is likely due to a number of factors including advection of Pacific-origin waters with a high Cd/PO_4 ratio, additional input of Cd relative to PO_4 from riverine input or sea ice melt, or by a biological fractionation and export of particles with low Cd:P ratio. The Cd:P of exported particulate matter is strongly influenced by Cd/P cellular ratios of the phytoplankton community,

which can vary by orders of magnitude thanks to inter-species differences in Cd quotas (Ho et al., 2003). A previous study found that picoeukaryotes (the green algae Prasinophyceae *Micromonas*) dominated the late summer phytoplankton bloom (Blais et al., 2017; Tremblay et al., 2009). Studies on the Cd quota of different marine phytoplankton found that green algae typically have lower Cd quotas than coccolithophores and diatoms (Ho et al., 2003), and export of green algae with low Cd:P quotas could contribute to the elevated Cd/PO_4 we observe in surface waters in the Canada Basin. The cellular quotas are also influenced by external factors, such as [Fe'], [Mn'], [Zn'] and *p*CO2 (Cullen et al., 1999). Uptake of Cd has been found to be enhanced under Fe-limited conditions, either due to biodilution (where Cd uptake remains constant, but growth rate increases with increasing Fe-availability, resulting in higher Cd:P quotas in Fe-lmited phytoplankton) (Cullen, 2006; Cullen et al., 2003) or by upregulation of metal non-specific metal transporters (Lane et al., 2008)**.** Cd uptake has also been shown to be inversely proportional to [Zn'] and [Mn'] (Sunda & Huntsman, 1998). Kondo et al. (2016) quantified the degree of Fe-limitation in the Canada Basin using the index Fe* (Fe* = $dFe-0.47PO_4$), where positive values generally indicate sufficient dFe. All samples had positive Fe* values, indicating that the Canada Basin is replete in Fe, so we might expect lower Cd:P ratios in exported particles, which would contribute to the high surface Cd/PO_4 ratio we observed.

Deepwater global Cd/PO_4 ratios have clear interbasin trends, with an increase in the ratio related to deep water age (de Baar et al., 1994). In the North Atlantic, deep water has a Cd/PO_4 ratio of 0.25±0.02, increasing to 0.35 in the North Pacific (Quay et al., 2015). We found that the Pacific-origin UHL water in our study region has a Cd/PO_4 ratio of 0.37±0.02 while the Atlantic-origin AIW has a ratio of 0.25±0.02, both of which are very similar to the global average deep water values indicating the strong influence that source waters exert on the Cd/PO_4 ratios in the Arctic interior.

3.4.2 Distribution through the Canadian Arctic Archipelago

The complex physics and water flow pathways in the CAA exert a strong control on the distribution of dCd in the region. As discussed earlier, flow through the CAA in our transect is predominately eastward, entering the CAA from the Canada Basin at M'Clure Strait, and into Baffin Bay via Lancaster Sound. A shallow (125m) sill at Barrow Strait is a natural barrier that separates the transect into eastern and western sections. To the west of Barrow Strait, at CAA8, the distribution of dCd is very similar to what was observed in the upper ~400m of the Canada Basin. There is a concentration maximum of ~650 pM at 90m depth, on the $\sigma_\theta \approx 26.5$ isopycnal, both at CAA8 and CB1, which coincides with the UHL waters. Below ~300m depth is Atlantic-origin water, with a lower nutrient signature, and diminished dCd of ~320 nM (Fig. 3.6).

CAA9, CAA6 and CAA7 are located close (50-150km) to the shallow Barrow Strait sill, and here we see differences in the dCd distribution consistent with previously observed circulation patterns and Coriolis forcing (e.g Wang et al. 2012; Michel et al. 2006; McLaughlin et al. 2004). As at CAA8, a peak of 600 pM in dCd is observed at CAA7, though at 160m it is deeper than at CAA8. Despite the greater depth, both peaks are found on the $\sigma_\theta \approx 26.5$ isopycnal. The shallow sill at Barrow Strait is a barrier to eastward flow from Viscount Melville Sound, and approximately half of the flow is deflected south into M'Clintock Channel (Wang et al., 2012), with the Coriolis force causing the flow to hug the southern edge of the channel. This water deflects north through Peel Sound before rejoining the eastward flowing water through Lancaster Sound, at approximately the location of CAA7 (Wang et al., 2012). The coincidence of both dCd peaks at $\sigma_\theta \approx 26.5$ is consistent with the circulation models, suggesting that water arriving at CAA7 has flowed south through M'Clintock before returning north through Peel Sound.

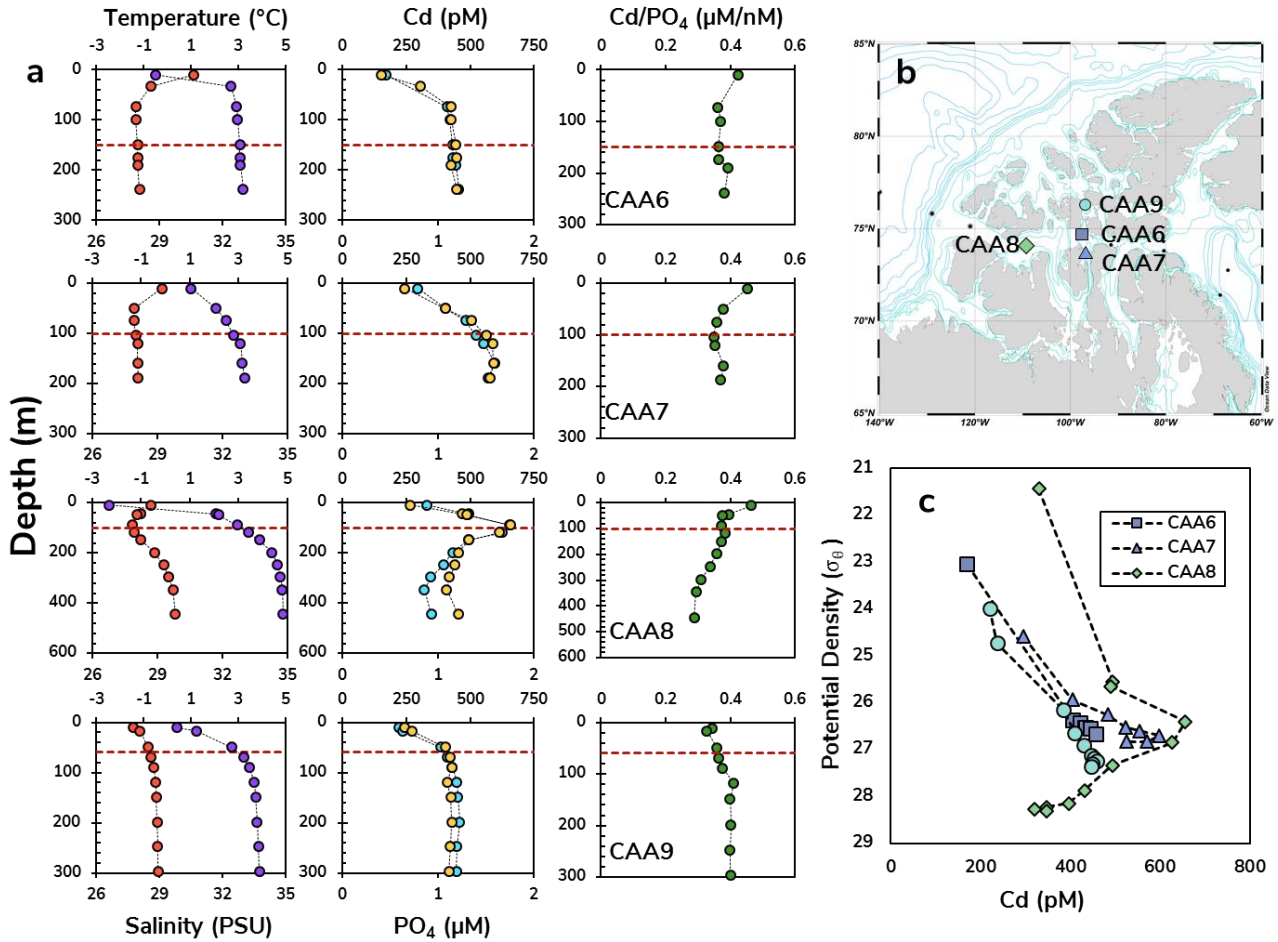

Figure 3.6 (a) Vertical distributions of temperature (red circles) and salinity (purple circles), dCd (blue circles) and [PO_4] (yellow circles), and Cd/PO_4 (green circles) for stations CAA6, CAA7, CAA8, and CAA9. Red dashed lines indicate the $\sigma_\theta \approx 26.5$ isopycnal. (b) Sampling locations in western Canadian Arctic Archipelago. (c) Potential density vs dCd for CAA6, CAA7, CAA8, and CAA9.

Though we see clear evidence of high-Cd Pacific-origin water at CAA7, there is no evidence of the low-Cd Atlantic-origin water present at CAA8 below 300m. A shallow sill at M'Clintock Channel restricts the flow of deeper waters through Peel Sound and may act as a barrier to this Atlantic-origin water.

Depth profiles of dCd at stations CAA6 and CAA9 are markedly different from the distributions observed at CAA8 and CAA7. Both are depleted in dCd in the surface waters and increase to ~450 pM through the upper ~120m and then remain constant with increasing depth. Water enters the CAA from many different pathways, including southward flowing pathways through the Queen Elizabeth Islands (Fig. 3.1). Though the depth profile at CAA6 appears different to those at CAA7 and CAA8, the peak in dCd is found along the same isopycnal as at the other stations ($\sigma_\theta \approx 26.5$). In contrast, CAA9 has no peak at $\sigma_\theta \approx 26.5$, instead peak dCd concentrations are found at $> \sigma_\theta = 27$. This provides evidence that water arriving at CAA9 has followed a different pathway and has a different source to that at CAA8 and CAA7. The coincidence of the peak at CAA6 with CAA7 and CAA8 suggest the water may have the same source, though the reduction in the dCd peak concentrations (from ~600 pM at CAA8 to ~450 pM at CAA6) implies the water mass has been modified. CAA6 likely contains a considerable contribution from the eastward flowing water masses observed at stations CAA7 and CAA8, however there may also be a contribution from westward flowing water flowing from Baffin Bay, with less of a Pacific component.

Stations CAA5 and CAA4 form a N-S transect in western Lancaster Sound while CAA3, CAA2 and CAA1 form a N-S transect at the eastern edge of Lancaster Sound, at the entrance to Baffin Bay (Fig. 3.7b). Both CAA5 and CAA4 have a peak in dCd of ~500 pM at $\sigma_\theta = 26.5$, at a depth of ~160m for CAA4 and ~140m for CAA5. Again, these peaks are located along the same isopycnal ($\sigma_\theta \approx 26.5$) as at CAA8 and CAA7. Near CAA4 and CAA5, previous work has shown that flow is

predominantly eastwards, both from direct observations (Prinsenberg & Bennett, 1987) and from models (Wang et al., 2012). Cd/PO_4 ratios throughout the water column at both stations are high: >0.34 at all depth at CAA4, and >0.39 below 45m at CAA5. The high Cd/PO_4 ratios suggest a significant proportion of Pacific-origin water is found at the stations. Jones et al. (2003) have previously used variations in the nitrate-phosphate relationship between Atlantic-origin and Pacific-origin water in the Arctic to determine the contribution of Pacific-origin water in each region. They found that water flowing through Barrow Strait was essentially all Pacific-origin. Our samples are collected slightly to the east of Barrow Strait, but the high Cd/PO_4 ratios suggest that this region still has a very high fraction of Pacific-origin water.

At the eastern end of Lancaster Sound, the Baffin Current penetrates westward into the northern edge of Lancaster Sound due to Coriolis forcing before looping south and returning eastward along the southern edge. At CAA1, we still see a peak in both dCd and PO_4, however this peak is no longer at σ_θ=26.5, and is instead found at a higher density, at $\sigma_\theta \approx 27$. The westward flow along the northern edge of Lancaster Sound is part of the Baffin Current, part of which originates in the Arctic. The Arctic water arrives via Nares Strait and Jones Sound (Fissel et al., 1982) and so the water masses are different to those arriving through Barrow Strait. The peak observed at CAA1, although associated with a different water mass to other stations in the CAA, has a similar Cd/PO_4 ratio (0.40) suggesting that it is similarly Pacific-origin water, although it has arrived via a different pathway. At CAA3, on the southern edge of the channel, we once again observe evidence of Pacific-origin water from the Canada Basin, with a clear peak in dCd and PO_4 at σ_θ=26.5 and an associated Cd/PO_4 of 0.41. Circulation models indicate that this is Pacific-origin water which has been advected along the southern edge of Lancaster Sound (Wang et al., 2012), and is the same water mass we observed at CAA8, CAA7 and CAA5. CAA2, in the central channel, has a different profile.

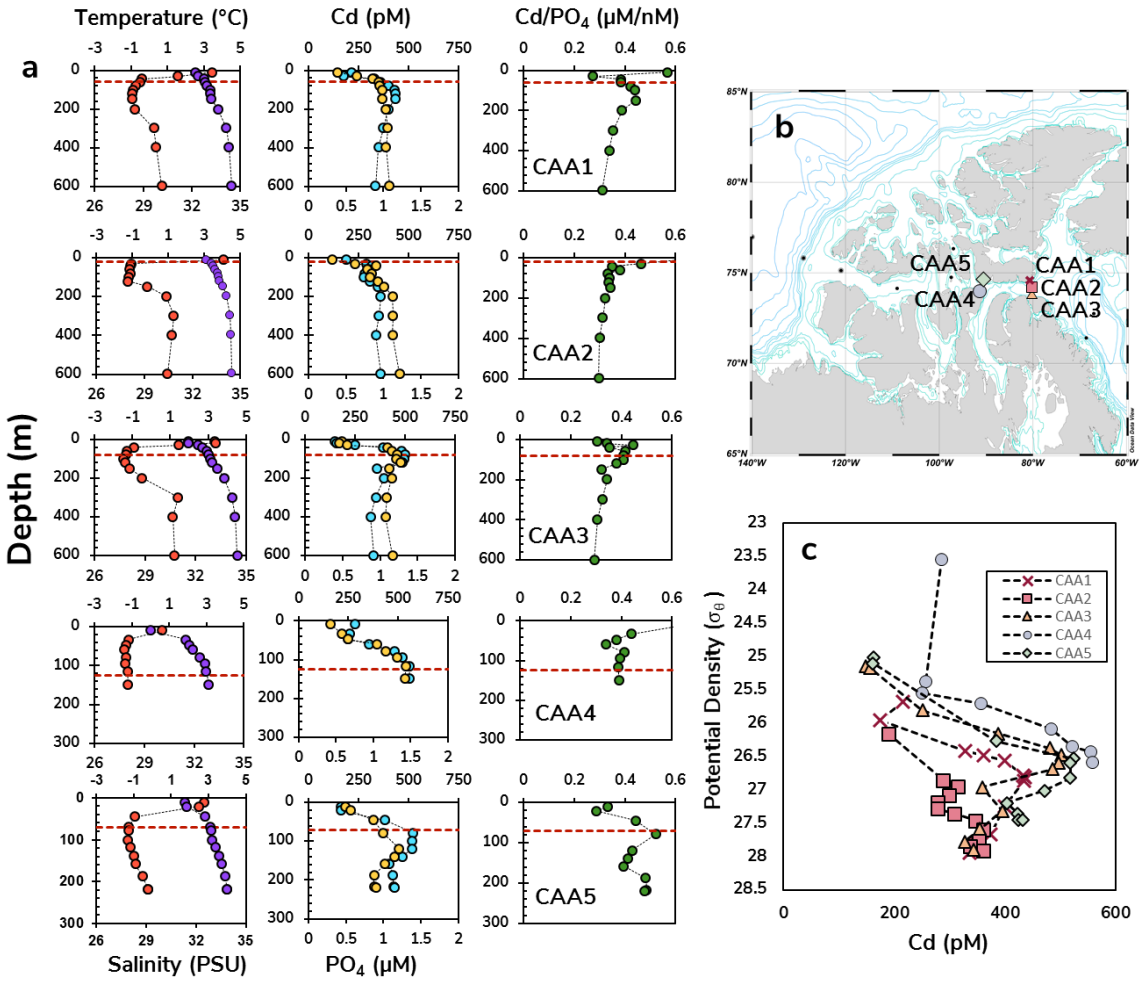

Figure 3.7 (a) Vertical distributions of temperature (red circles) and salinity (purple circles), dCd (blue circles) and [PO_4] (yellow circles), and Cd/PO_4 (green circles) for stations CAA1, CAA2, CAA3, CAA4, and CAA5. Red dashed lines indicate the $\sigma_\theta \approx 26.5$ isopycnal. (b) Sampling locations in eastern Canadian Arctic Archipelago. (c) Potential density vs dCd for CAA1, CAA2, CAA3, CAA4, and CAA5.

There is a decrease in temperature between 50m and 120m, which is associated with a peak in dCd and PO_4 at 60m, however this peak is much less pronounced than at other stations (315 pM). It has been previously suggested that Baffin Bay waters may penetrate into central Lancaster Sound (Fissel et al., 1982). There is a mid-depth maxima in dCd at $\sigma_\theta \approx 27.5$ which is coincident with mid-depth maxima at both stations BB2 and BB1 suggesting a similar source for these water

masses, although a similar mid-depth maxima is not observed at either CAA1 or CAA2 (Fig. 3.8). This suggests that CAA2 has a different source to both the northern and southern edges of the channel, and may indicate the flow of Baffin Bay waters separate from the Baffin Current into the channel.

3.4.3 Distribution in Baffin Bay and the Labrador Sea

Baffin Bay provides a link between outflowing water from the Arctic (via Jones Sound, Lancaster Sound and Nares Strait) to the North Atlantic (via Davis Strait) (Fig. 3.1). The three stations in Baffin Bay in our study are located in deep central Baffin Bay (BB2), on the western edge (BB3) and in Davis Strait (BB1). The Arctic Water can be observed as a distinctive cold layer (~-1.5°C) that extends to a depth of 150m in central Baffin Bay (BB2) and Davis Strait (BB1) and to 200m in western Baffin Bay (BB3) (Fig. 3.3c). A local maximum in dCd of 320-400 pM can be seen in this layer, at a depth of between 30-50m (Fig 3.8a). A weaker PO_4 maxima can be seen at the same depth. Carmack and McLaughlin (2011) also identified a weak nutrient maximum in this layer, which they associated with advection of Pacific-origin waters through Baffin Bay. The high dCd we observed, which has been associated with the advection of Pacific-origin water throughout the transect indicates the continued presence of Pacific-origin water at a depth of ~30-50m in Baffin Bay. Furthermore, we measured a Cd/PO_4 ratio of 0.36-0.39 in the nutrient maximum, which is consistent with the Cd/PO_4 ratio observed in Pacific-origin water in both the CAA and the Canada Basin.

In the central Baffin Basin (BB2), Baffin Bay Deep Water is found below a depth of ~1200m, and is identified by lower temperatures (~-0.5°C) than the overlying WGIW. In the BBDW, nutrient regeneration is observed as a decrease in O_2 (not shown) and an increase in PO_4 with

depth. dCd also increases with depth, however the Cd:PO_4 slope through the BBDW is much lower than the global Cd:PO_4 slope. In the BBDW, the Cd:PO_4 slope is only 0.08, while a slope of 0.2 is typical for the North Atlantic (de Baar et al., 1994; Wu & Roshan, 2015). There is also a decrease in the dissolved Cd/PO_4 ratio in the BBDW, from 0.28 ± 0.02 in the WGIW to 0.23 ± 0.01 in the BBDW. The low Cd:PO_4 slope and decrease in dissolved Cd/PO_4 ratio suggests either that particulate matter being regenerated in the BBDW has a low Cd:P ratio, or that there is a loss of Cd or source of PO_4 in the deepwaters that is not currently accounted for.

A 600m deep sill seperates the Labrador Sea from Baffin Bay at Davis Strait. We sampled two stations in the Labrador Sea, K1 and LS2 (Fig. 3.9). At both stations dCd and PO_4 display much more typical nutrient-type profiles than elsewhere in the Canadian Arctic Ocean, with depletions in the surface waters and higher concentrations in the deep waters. dCd in the surface waters in the Labrador Sea are the lowest observed in the study region, with surface concentrations of only 25 pM at K1 and 17 pM at LS2. Below ~100 m at both stations, dCd is constant at ~255 ± 7 pM. PO_4 was similarly distributed, with surface water PO_4 below the detection limit at LS2 and 0.10 µM at K1. Below ~100m, concentrations of PO_4 were constant at 1.03 ± 0.03 µM.

The Labrador Sea is characterized by strong seasonal cycles, and highly productive summer months (Harrison & Li, 2008). During the winter, strong vertical mixing and deep convection supply nutrients to the surface waters, which can support high biological production when light conditions are favourable. In the summer months, increases in stratification and high-rates of biological productivity can result in depletions in surface water nutrients, such that phytoplankton growth is nutrient-limited (Harrison & Li, 2008) . Sampling was conducted in the Labrador Sea in July, which likely coincided with the spring bloom. The distributions of both dCd and PO_4 are consistent with high rates of productivity. We see a strong decrease in both dCd and PO_4 in the surface waters, and increases in concentration at depth as the organic matter is respired.

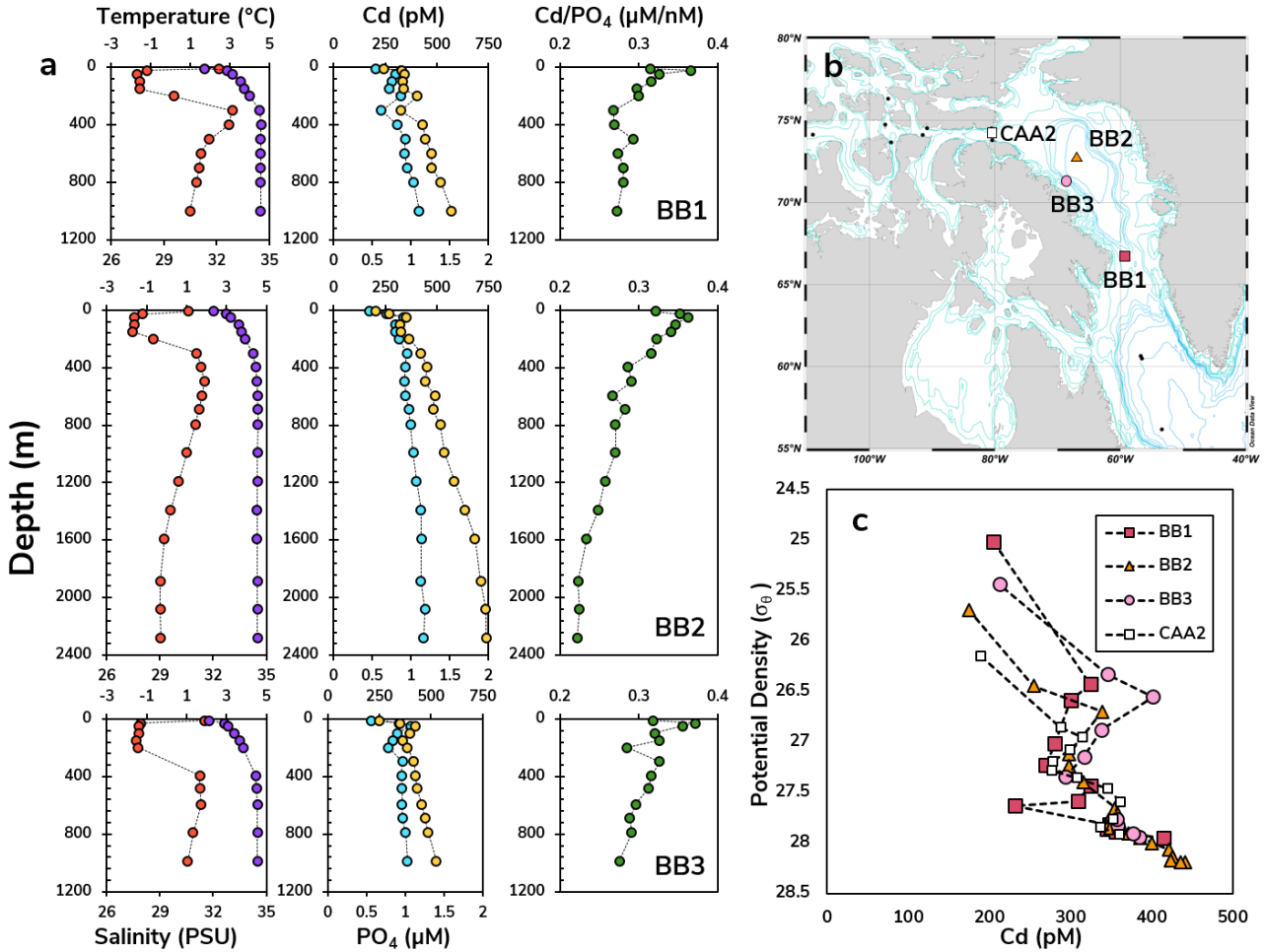

Figure 3.8 (a) Vertical distributions of temperature (red circles) and salinity (purple circles), dCd (blue circles) and [PO_4] (yellow circles), and Cd/PO_4 (green circles) for stations BB1, BB2, and BB3. (b) Sampling locations in Baffin Bay. (c) Potential density vs dCd for BB1, BB2, BB3 and CAA2.

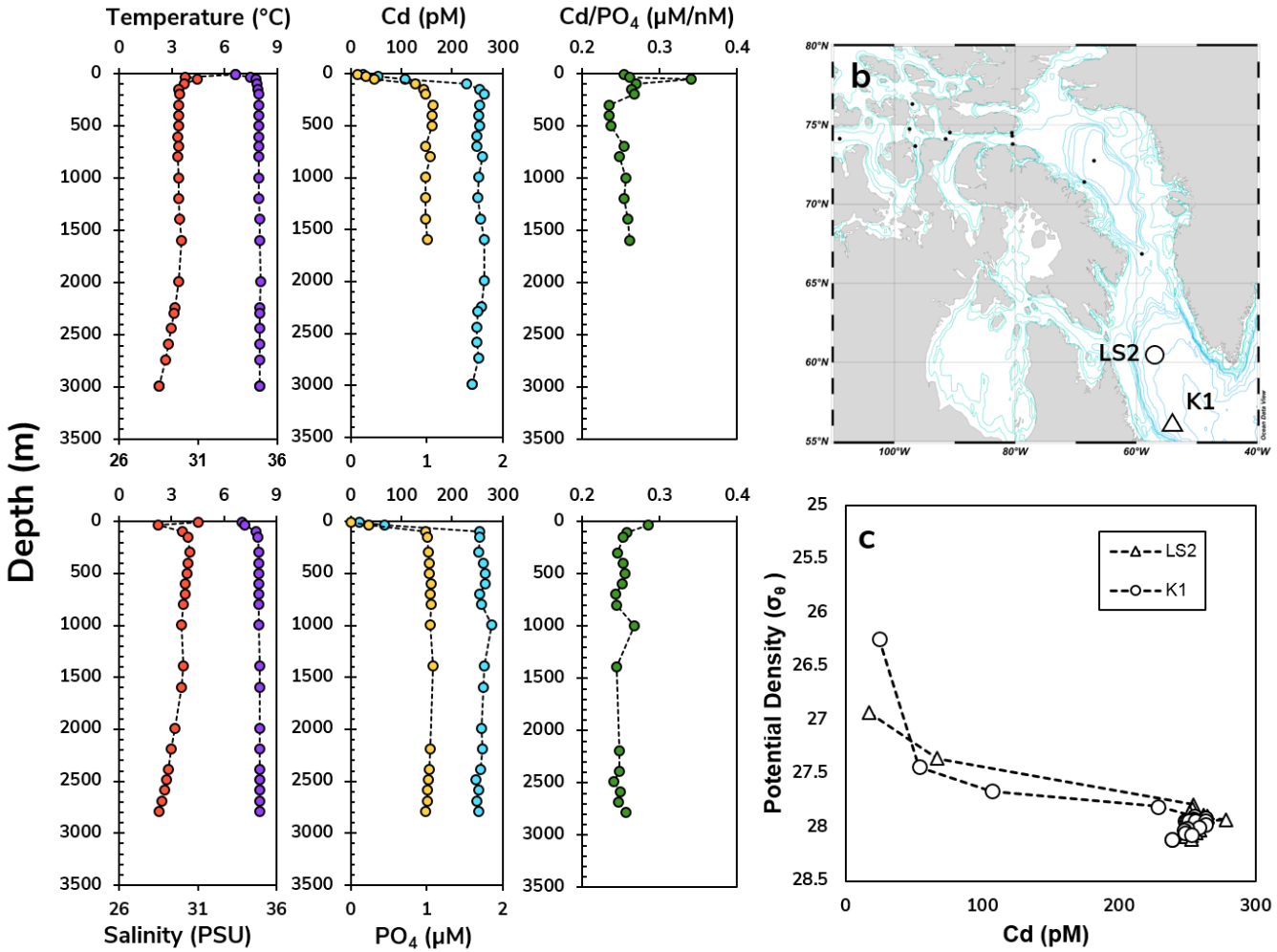

Figure 3.9 (a) Vertical distributions of temperature (red circles) and salinity (purple circles), dCd (blue circles) and [PO_4] (yellow circles), and Cd/PO_4 (green circles) for stations LS2 and K1. (b) Sampling locations in the Labrador Sea. (c) Potential density vs dCd for LS2 and K1.

Concentrations of dCd and Cd/PO_4 ratios in waters below ~200 m are consistent with previous studies and modelled results, which have shown that North Atlantic Deep Water (NADW) is characterized by Cd/PO_4 ratios of ~0.23 (Quay et al., 2015). In this study, Cd/PO_4 was 0.25 ± 0.01 below 200 m, which is very similar to previous measurements of NADW. Both the low concentrations of dCd and low Cd/PO_4 ratios were considered to be indicative of North Atlantic-origin water throughout this study, and measurements taken in the Labrador Sea were considered to be representative of end-member North Atlantic-origin water.

3.4.4 The Global Cadmium-Phosphate Relationship

The North Pacific and North Atlantic have distinctive and different $Cd:PO_4$ slopes (Fig. 3.10). The $Cd:PO_4$ slope for the North Pacific is ~0.35, but is only 0.25 for the North Atlantic (de Baar et al., 1994; Quay et al., 2015). As our transect has both Pacific-origin and Atlantic-origin waters, a single Cd:PO4 slope cannot be applied to our data, with region-specific and water-mass specific trends adding complexity to the relationship. In the Canada Basin, water-mass effects are clearly seen. The deep waters all have a concentration of ~200pM Cd and 0.9µM PO_4, with a Cd/PO_4 ratio of 0.27, and sit very close to the global North Atlantic average $Cd:PO_4$ slope. Water from the upper ~300m of the water column, however, shows a slope much more consistent with the North Pacific $Cd:PO_4$ slope. Conversely, all of the Labrador Sea data sits along the North Atlantic $Cd:PO_4$ slope, reflecting the origins of the water masses. The CAA shows some scatter in the $Cd:PO_4$ relationship, but shows a slope similar to the North Pacific slope. The scatter is likely from the removal or addition of Cd relative to PO_4 due to physical processes, such as riverine input and sea ice melt and formation.

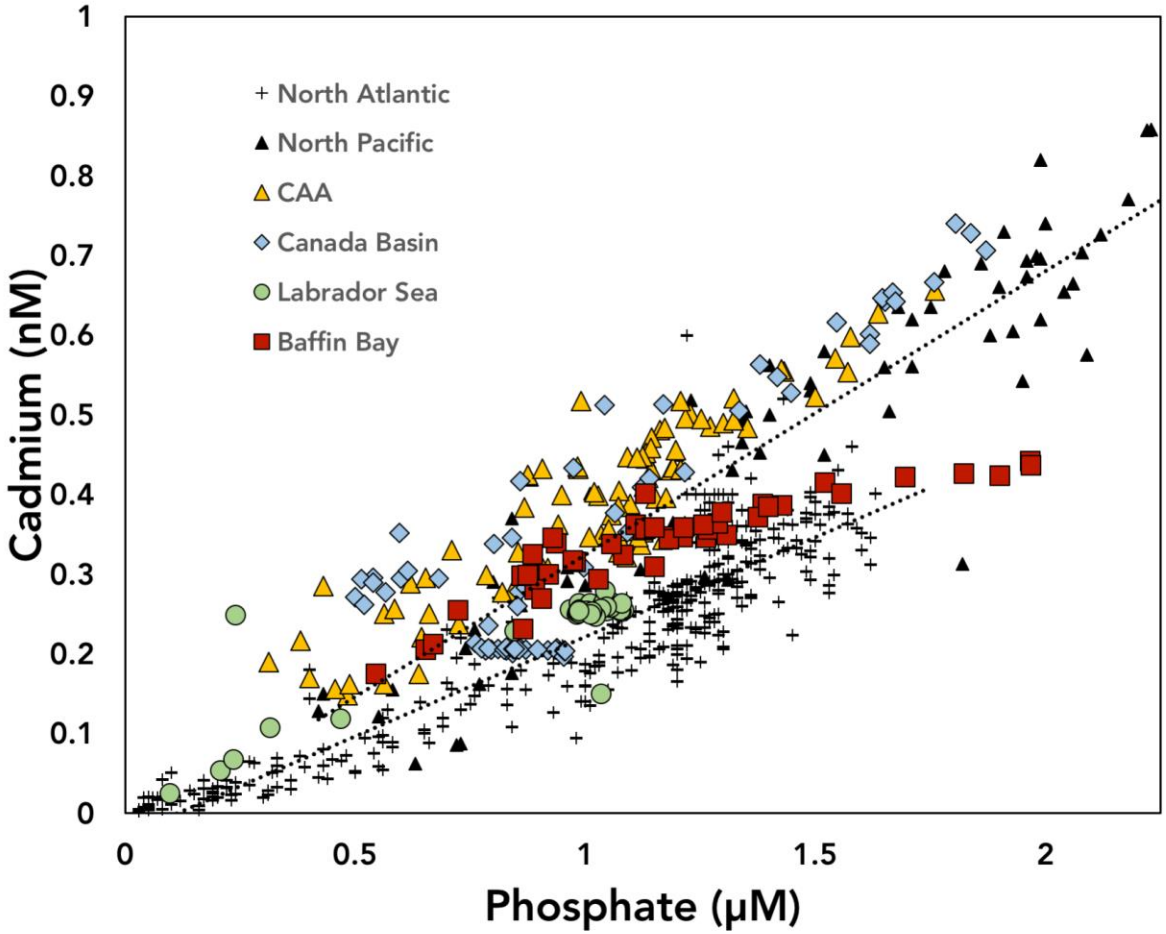

Figure 3.10 dCd versus PO_4 in the Canada Basin (blue diamond), CAA (yellow triangle), Baffin Bay (red square), and the Labrador Sea (green circles). Global relationships for the North Atlantic (grey diamonds) and North Pacific (grey circles) also shown. North Pacific and North Atlantic data from Quay et al., 2015 and references therein.

While the Cd:PO_4 slope in most regions of our transect shows direct influence from the source region, the Cd:PO_4 slope in Baffin Bay is distinct from either the North Pacific or the North Atlantic. The surface waters have a Cd:PO_4 slope very similar to the North Pacific, suggesting significant influence of North Pacific waters even in Baffin Bay. The WGIW samples lie between the Cd-PO_4 slopes characteristic of North Pacific and North Atlantic values, indicating that they may be representative of mixing between the Pacific and Atlantic end-members. The BBDW have a Cd-PO_4 slope which is much lower than either the Pacific or Atlantic slope, at only 0.08 nM/µM. This implies the regeneration of particles with a very low Cd:P ratio, or suggests that there is another process removing Cd relative to PO_4 or adding P relative to Cd in the deep waters. A potential water-column sink for Cd is sulfide precipitation in low-oxygen waters (Janssen et al., 2014). While O_2 is depleted in deep Baffin Bay waters, it is still well above the suggested threshold for sulfide precipitation (75µM in the North Atlantic, while O_2 is > 100µM in deep Baffin Bay) and so is an unlikely cause of the low Cd:PO_4 slope. The BBDW is unlikely to have formed from mixing between Atlantic and Pacific water masses, as the concentrations of Cd and PO_4 in the BBDW are considerably higher than North Atlantic deepwater values (Fig. 3.10). This suggests that the most likely cause for the low concentrations of Cd relative to PO_4 in deep Baffin Bay is the regeneration of low Cd:P particulate matter.

3.5 Conclusions

This study demonstrates that the distribution of Cd across the Canadian Arctic is strongly influenced by the local water masses. Cadmium is enriched in Pacific-origin UHL waters throughout all regions of our study area, with a distinctive Cd/PO_4 ratio. A clear maximum can be

seen in the UHL in the Canada Basin, which can be traced through the Canadian Arctic Archipelago and into Baffin Bay and Davis Strait. Beyond Davis Strait, in the Labrador Sea, the high Cd signal is lost. Across the entire transect, Pacific-origin waters have a Cd/PO_4 ratio of ~0.37, while in the Labrador Sea the highest ratio observed was 0.28. The similar distribution and close correlation of Cd and PO_4 across the transect implies that the distributions of both are largely controlled by internal biogeochemical cycling. Although the concentrations of Cd and PO_4 vary across the transect, from maximum dCd of ~740 pM in the Canada Basin to only ~320 pM in the sub-surface maxima in Baffin Bay, the Cd/PO_4 ratio in these Pacific-origin waters remains constant and is a useful marker for tracing the transit of this water mass through the Canadian Arctic.

Water masses across the entire transect show $Cd:PO_4$ relationships consistent with the relationships observed in both the North Pacific and North Atlantic, except for Baffin Bay Deep Waters. The mechanisms driving the deviation from the global $Cd:PO_4$ relationship in BBDW warrant further investigation, and additional research into other biogeochemical properties of the water mass may help to elucidate the processes controlling the curious $Cd:PO_4$ signal we observed.

Chapter 4: Conclusions

This thesis presents some of the only measurements of dissolved cadmium (dCd) in the Canadian Arctic Ocean, and the first geochemical section of dCd through the Canadian Arctic Archipelago which connects the Arctic Ocean to the North Atlantic. This chapter presents a summary of the major findings and a discussion of the implications for the biogeochemical cycling of Cd as well as suggestions for future work.

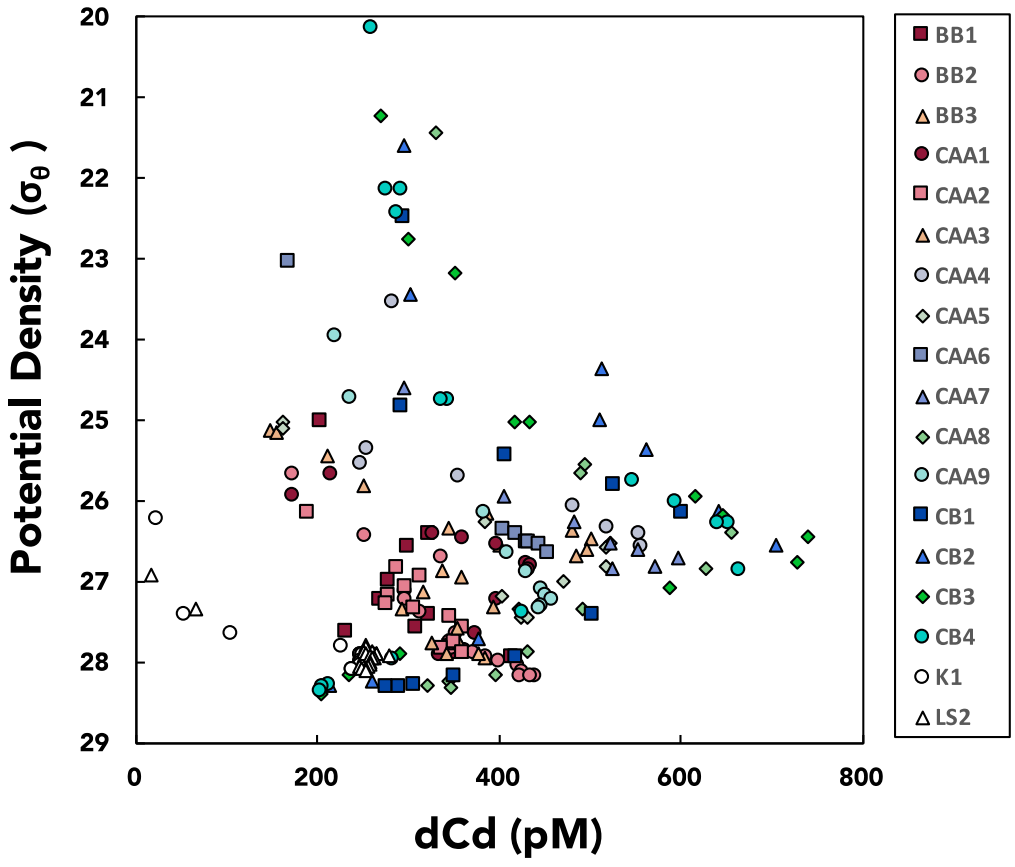

Figure 4.1 Potential density vs dCd for all stations on GEOTRACES sections GN02 and GN03.

This work confirmed that salinity driven water mass stratification in the Arctic Ocean exerts a primary control on the spatial distribution of Cd. In the Canada Basin, the Pacific-origin UHL layer is clearly identifiable by high dCd concentrations (600-740 pM) relative to the underlying Atlantic-origin water (~200 pM). The Pacific-origin waters are found on the σ_θ=26.5 isopycnal throughout most of the transect, and this isopycnal was associated with maximum dCd concentrations at most stations (Fig. 4.1).

The association of elevated dCd with waters of Pacific-origin allows the use of dCd to track the movement of this feature in response to transport and mixing in the Arctic. Understanding how Arctic waters are transported and modified from the Canada Basin into the Atlantic via the CAA is a key research objective of the Canadian GEOTRACES program. The CAA represents a crucial connection between the Pacific and Atlantic Oceans, with the transport of Arctic water into Baffin Bay and the Labrador Sea exerting a significant influence on biological productivity and the thermohaline circulation (Yamamoto-Kawai et al., 2006). The Canadian GEOTRACES program aims to provide a geochemical tracer baseline for future change, improve the understanding of the sensitivity of the region to climatic and anthropogenic perturbations, and improve the ability to quantify the response to these changes. Although several geochemical properties have already been identified as tracers of the Pacific-inflow, notably barium and nutrient-relationships (Cooper et al., 1997), the large difference in dCd between Pacific and Atlantic-origin water makes it a useful additional tracer. The use of dCd as a tracer is advantageous as it is unaffected by water column processes that may influence traditional tracers like N*. Furthermore, Cd/PO_4 ratios are distinct between Atlantic and Pacific-origin water masses, providing an additional means for identifying the presence of Pacific-origin water throughout the transect. dCd and Cd/PO_4 are valuable as tracers as they are less susceptible to in

situ water-column modification processes than traditional tracers of Pacific-origin water (such as N*). Both dCd and Cd/PO_4 ratios showed that Pacific-origin water penetrates into the central Baffin Bay basin.

Understanding global trends and regional variability in the $Cd:PO_4$ relationship has been a primary focus since dissolved Cd could be reliably measured in the ocean in the 1970's (Boyle et al., 1976; Bruland et al., 1978), due largely to the potential of Cd as a paleoproxy. Cd/Ca ratios in benthic foraminifera microfossils are routinely used to reconstruct past deep water PO_4 concentrations and as a tracer of past ocean circulation (Boyle, 1988; Marchitto & Broecker, 2006; Rosenthal et al., 1997). Planktonic Cd/Ca ratios have also been used to infer paleo nutrient utilization in surface waters (Elderfield & Rickaby, 2000); however significant spatial and temporal variability in surface water Cd/PO_4 ratios coupled with a limited mechanistic understanding of the causes of the variability have limited the utility of the paleoproxy. Although considerable scatter still exists, previous researchers identified a general increase in Cd/PO_4 ratios in surface waters with increasing latitude (Elderfield & Rickaby, 2000; Quay & Wu, 2015). The data presented in this work is consistent with the trend, with high surface water Cd/PO_4 ratios observed across the transect, which we attribute to the export of low Cd:P particles or the physical modification of the water mass. The Arctic Ocean has previously been omitted from any global models of Cd cycling due to lack of data, but the GEOTRACES Arctic program, of which this work is a component, will allow for integration of Arctic data into global models.

This dataset provides insights into the Cd biogeochemical cycles for only a portion of the Arctic Ocean. Collaboration with both the US (GN01) and German GEOTRACES (GN04 and GN05) cruises will provide a more complete understanding of the biogeochemical cycling of Cd through the Arctic Ocean, including a clearer understanding of the key sources and sinks. Although high

dCd concentrations are observed in the Pacific-origin waters in this study, understanding the sources of the high-dCd are beyond the scope of this work. The US GEOTRACES transect, which transits the Chukchi Shelf regions, will provide insight into the source of the high Cd concentrations. The US GEOTRACES cruise transect spans the Chukchi shelf, where the Pacific-inflow undergoes modification before entering the Canada Basin. These data will provide information about the sources and sinks for trace metals, notably how the water mass is transformed during interaction with shelf sediments and sea-ice melt and formation.

Although only dissolved Cd data are discussed in this work, data was generated for 6 other key trace metals (Mn, Ni, Fe, Cu, Zn and Pb). The trace metals respond differently to key processes, such as scavenging, biological uptake, sea ice melt or anthropogenic input. A multi-faceted approach to Arctic biogeochemical cycling, which incorporates all seven trace metals measured in this work, may help to untangle some of the physical and biological processes which modify the water masses during the transit through the Arctic. In the future, it would be beneficial for the data from all the metals measured to be considered together to provide a more comprehensive understanding of the different process affecting trace metals throughout the Arctic Ocean.

The results from this work showed anomalous results for the Cd:PO_4 slope in deep Baffin Bay, which warrant further investigation. The sources contributing to Baffin Bay Deep Water are still debated, and may help to explain the curious results we observed. Source waters with a surprisingly low Cd/PO_4 ratio, or re-dissolution of particles with low Cd:P ratios are the most likely explanations for the decrease in Cd/PO_4 with depth in Baffin Bay, but further work is required to fully explain the observed feature. Preliminary data from the Canadian GEOTRACES program has indicated that there are unusual results for multiple chemical properties in deep Baffin Bay.

Recently, investigations into Cd isotopic ratios have provided additional insights into the global Cd biogeochemical cycles, with ratios presented in per mil (‰) using δ^{114}Cd notation, where:

$$\delta^{114}\text{Cd}\ (‰) = \left[\left(\frac{\frac{114Cd}{110Cd}_{sample}}{\frac{114Cd}{110Cd}_{standard}}\right) - 1\right] \times\ 1000$$

Values are reported relative to the standard NIST SRM 3108. A higher δ^{114}Cd reflects an enrichment in heavier isotopes, while a lower value reflects an enrichment of light isotopes (hereafter referred to as heavy and light δ^{114}Cd). In general, biological uptake of Cd in surface waters leads to heavier dissolved δ^{114}Cd and a decrease in dCd, as phytoplankton preferentially assimilate lighter Cd isotopes. As the lighter Cd particulate matter is remineralized, dissolved δ^{114}Cd becomes lighter and dCd increases, resulting in an inverse correlation between dCd and δ^{114}Cd (Conway & John, 2015; Lacan, et al., 2006; Ripperger et al., 2007). The deepwater Cd isotopic composition is homogenous between the North Pacific, Southern Ocean and South China Sea (+0.3‰) (Abouchami et al., 2014; Ripperger et al., 2007; Xue et al., 2013; Yang et al., 2012), with a heavier isotopic signature in the North Atlantic (+0.23‰ to +0.5‰). Although Cd isotopes in seawater are a relatively new area of research, they have already provided insights into the biogeochemical cycling of Cd which cannot be discerned by Cd dissolved concentrations alone. Isotopically heavy dissolved Cd was measured in the Mauritanian oxygen minimum zone (OMZ), which may be caused by the precipitation of isotopically light Cd sulphides (Conway & John, 2015; Janssen et al., 2014). Cd isotopic stratification and meridional trends in the Southern Ocean have also helped to understand the combined influences of biological cycling and ocean-circulation on Cd biogeochemical cycling in the region (Abouchami et al., 2011, 2014; Gault-Ringold et al., 2012; Xue et al., 2013). Investigations into Cd isotopes in the Arctic Ocean may help in understanding the biogeochemical cycling of Cd in the region. A single depth profile of

$\delta^{114}Cd$ exists for the Canada Basin, with 5 discrete depths measured (Ripperger et al., 2007). Both the Pacific-origin water and Atlantic-origin water masses were sampled in the profile, identified by high dCd in the Pacific water (696.2 pM) and lower dCd in Atlantic water (220-204 pM). The water masses do not show resolvable differences in $\delta^{114}Cd$ (+0.39±0.10‰ in the Pacific-origin and +0.42±0.10‰ to +0.44±0.10‰ in the Atlantic-origin water); however improvements in analytical methods with concurrent reductions in errors may make these differences resolvable in future studies. Moderate levels of fractionation were observed in surface waters (+0.58±0.10‰ to 0.66±0.16‰). Future investigations into Cd isotopic ratios in Arctic Ocean may help to understand the sources and sinks of Cd in the Arctic Ocean. In particular, Cd isotopes may help to understand the modification of Pacific-origin water during transit over the Chukchi shelf, as input from biogenic shelf sediments would likely impart a different isotopic signal than either sea-ice melt or river input.

This work contributes a significant amount of new dCd data for the Arctic Ocean and provides insight into the biogeochemical cycling of Cd in the region. Further contributions from the GEOTRACES Arctic program will provide a more complete view of the cycling of Cd throughout the Arctic and contribute to the understanding of the global Cd cycle.

Bibliography

Abouchami, W., Galer, S. J. G., de Baar, H. J. W., Alderkamp, A. C., Middag, R., Laan, P., Feldmann, H., & Andreae, M. O. (2011). Modulation of the Southern Ocean cadmium isotope signature by ocean circulation and primary productivity. *Earth and Planetary Science Letters*, *305*(1–2), 83–91. https://doi.org/10.1016/j.epsl.2011.02.044

Abouchami, W., Galer, S. J. G., de Baar, H. J. W., Middag, R., Vance, D., Zhao, Y., Klunder, M., Mezger, K., Feldman, H., & Andreae, M. O. (2014). Biogeochemical cycling of cadmium isotopes in the Southern Ocean along the Zero Meridian. *Geochimica et Cosmochimica Acta*, *127*, 348–367. https://doi.org/10.1016/j.gca.2013.10.022

Agilent 8800 Triple Quadrupole ICP-MS: Understanding oxygen reaction mode in ICP-MS/MS. (2012). Agilent Technologies, Inc. Retrieved from http://www.agilent.com/cs/library/technicaloverviews/Public/5991-1708EN_TechOverview_ICP-MS_8800_ORS_mode.pdf

Andersen, O. (1984). Chelation of cadmium. *Environmental Health Perspectives*, *54*, 249–66. Retrieved from http://www.ncbi.nlm.nih.gov/pubmed/6734560

Baars, O., Abouchami, W., Galer, S. J. G., Boye, M., & Croot, P. L. (2014). Dissolved cadmium in the Southern Ocean: Distribution, speciation, and relation to phosphate. *Limnology and Oceanography*, *59*(2), 385–399. https://doi.org/10.4319/lo.2014.59.2.0385

Badger, M. R., & Price, G. D. (2003). CO_2 concentrating mechanisms in cyanobacteria: molecular components, their diversity and evolution. *Journal of Experimental Botany*, *54*(383), 609–22.

Bailey, W. B. (1956). On the Origin of Deep Baffin Bay Water. *Journal of the Fisheries Research Board of Canada*, *13*(3), 303–308. https://doi.org/10.1139/f56-020

Balcaen, L., Bolea-Fernandez, E., Resano, M., & Vanhaecke, F. (2015). Inductively coupled plasma – Tandem mass spectrometry (ICP-MS/MS): A powerful and universal tool for the interference-free determination of (ultra)trace elements – A tutorial review. *Analytica Chimica Acta*, *894*, 7–19. https://doi.org/10.1016/j.aca.2015.08.053

Beck, N. G., Franks, R. P., & Bruland, K. W. (2002). Analysis for Cd, Cu, Ni, Zn, and Mn in estuarine water by inductively coupled plasma mass spectrometry coupled with an automated flow injection system. *Analytica Chimica Acta*, *455*(1), 11–22. https://doi.org/10.1016/S0003-2670(01)01561-6

Beszczynska-Möller, A., Woodgate, R., Lee, C., Melling, H., & Karcher, M. (2011). A Synthesis of Exchanges Through the Main Oceanic Gateways to the Arctic Ocean. *Oceanography*, *24*(3), 82–99. https://doi.org/10.5670/oceanog.2011.59

Bewers, J. M., Barry, P. J., & MacGregor, D. J. (1987). Distribution and cycling of cadmium in the environment. In J. O. Nriagu & J. B. Sprague (Eds.), *Cadmium in the Aquatic Environment* (pp. 1–18). New York: John Wiley.

Biller, D. V., & Bruland, K. W. (2012). Analysis of Mn, Fe, Co, Ni, Cu, Zn, Cd, and Pb in seawater using the Nobias-chelate PA1 resin and magnetic sector inductively coupled plasma mass spectrometry (ICP-MS). *Marine Chemistry*, *130*, 12–20. https://doi.org/10.1016/j.marchem.2011.12.001

Blais, M., Ardyna, M., Gosselin, M., Dumont, D., Elanger, S. B., Tremblay, J.-E., Gratton, Y., Marchese, C., & Poulin, M. (2017). Contrasting interannual changes in phytoplankton productivity and community structure in the coastal Canadian Arctic Ocean. *Limnology and Oceanography*. https://doi.org/10.1002/lno.10581

Bourke, R. H., Addison, V. G., & Paquette, R. G. (1989). Oceanography of Nares Strait and northern Baffin Bay in 1986 with emphasis on deep and bottom water formation. *Journal of Geophysical Research*, *94*(C6), 8289. https://doi.org/10.1029/JC094iC06p08289

Bourke, R. H., & Paquette, R. G. (1991). Formation of Baffin Bay Bottom and Deep Waters (pp. 135–155). https://doi.org/10.1016/S0422-9894(08)70065-5

Boyd, P. W., & Ellwood, M. J. (2010). The biogeochemical cycle of iron in the ocean. *Nature Geoscience*, *3*(10), 675–682. https://doi.org/10.1038/ngeo964

Boyle, E. A. (1988). Cadmium: Chemical tracer of deepwater paleoceanography. *Paleoceanography*, *3*(4), 471–489. https://doi.org/10.1029/PA003i004p00471

Boyle, E. A. (2001). Anthropogenic Trace Elements In The Ocean. In *Encyclopedia of Ocean Sciences* (pp. 162–169). Elsevier. https://doi.org/10.1006/rwos.2001.0282

Boyle, E. A., Sclater, F., & Edmond, J. M. (1976). On the marine geochemistry of cadmium. *Nature*, *263*(5572), 42–44. https://doi.org/10.1038/263042a0

Broecker, W. S., & Peng, T. (1982). *Tracers in the sea*. Palisades, NY: Lamont-Doherty Geological Observatory, Columbia University.

Bruland, K. W. (1980). Oceanographic distributions of cadmium, zinc, nickel, and copper in the North Pacific. *Earth and Planetary Science Letters*, *47*(2), 176–198. https://doi.org/10.1016/0012-821X(80)90035-7

Bruland, K. W. (1992). Complexation of cadmium by natural organic ligands in the central North Pacific. *Limnology and Oceanography*, *37*(5), 1008–1017. https://doi.org/10.4319/lo.1992.37.5.1008

Bruland, K. W., & Franks, R. P. (1983). Mn, Ni, Cu, Zn and Cd in the Western North Atlantic. In *Trace Metals in Sea Water* (pp. 395–414). Boston, MA: Springer US. https://doi.org/10.1007/978-1-4757-6864-0_23

Bruland, K. W., Franks, R. P., Knauer, G. A., & Martin, J. H. (1979). Sampling and analytical methods for the determination of copper, cadmium, zinc, and nickel at the nanogram per liter level in sea water. *Analytica Chimica Acta*, *105*, 233–245. https://doi.org/10.1016/S0003-2670(01)83754-5

Bruland, K. W., Knauer, G. A., & Martin, J. H. (1978). Cadmium in northeast Pacific waters. *Limnology and Oceanography*, *23*(4), 618–625. https://doi.org/10.4319/lo.1978.23.4.0618

Butterman, W. C., & Plachy, J. (2004). *Mineral Commodity Profiles: Cadmium*. Retrieved from https://pubs.usgs.gov/of/2002/of02-238/

Byrne, R. H. (2002). Speciation in Seawater. In A. M. Ure & C. M. Davidson (Eds.), *Chemical Speciation in the Environment* (pp. 322–357). Oxford, UK: Blackwell Science Ltd. https://doi.org/10.1002/9780470988312.ch12

Byrne, R. H., Kump, L. R., & Cantrell, K. J. (1988). The influence of temperature and pH on trace metal speciation in seawater. *Marine Chemistry*, *25*(2), 163–181. https://doi.org/10.1016/0304-4203(88)90062-X

Cao, J., Xue, H., & Sigg, L. (2006). Effects of pH and Ca competition on complexation of cadmium by fulvic acids and by natural organic ligands from a river and a lake. *Aquatic Geochemistry*, *12*(4), 375–387. https://doi.org/10.1007/s10498-006-9004-6

Capodaglio, G., Turetta, C., Toscano, G., Gambaro, A., Scarponi, G., & Cescon, P. (1998). Cadmium, Lead and Copper Complexation in Antarctic Coastal Seawater. Evolution during the Austral Summer. *International Journal of Environmental Analytical Chemistry*, *71*(3–4), 195–226. https://doi.org/10.1080/03067319808032628

Carmack, E., & McLaughlin, F. (2011). Towards recognition of physical and geochemical change in Subarctic and Arctic Seas. *Progress in Oceanography*, *90*(1–4), 90–104. https://doi.org/10.1016/j.pocean.2011.02.007

Chester, R., & Jickells, T. (2012). The Transport of Material to the Oceans: Relative Flux Magnitudes. In *Marine Geochemistry* (pp. 92–124). Chichester, UK: John Wiley & Sons, Ltd. https://doi.org/10.1002/9781118349083.ch6

Cid, A. P., Nakatsuka, S., & Sohrin, Y. (2012). Stoichiometry among bioactive trace metals in the Chukchi and Beaufort Seas. *Journal of Oceanography*, *68*(6), 985–1001.

Coachman, L. K., & Aagaard, K. (1988). Transports through Bering Strait: Annual and interannual variability. *Journal of Geophysical Research*, *93*(C12), 15535. https://doi.org/10.1029/JC093iC12p15535

Collin, A. E. (1965). *Oceanographic observations in Nares Strait, northern Baffin Bay 1963*. Dartmouth, NS.

Conway, T. M., & John, S. G. (2015). Biogeochemical cycling of cadmium isotopes along a high-resolution section through the North Atlantic Ocean. *Geochimica et Cosmochimica Acta*, *148*, 269–283. https://doi.org/10.1016/j.gca.2014.09.032

Cooper, L. W., Cota, G. F., Pomeroy, L. R., Grebmeier, J. M., & Whitledge, T. E. (1999). Modification of NO, PO, and NO/PO during flow across the Bering and Chukchi shelves: Implications for use as Arctic water mass tracers. *Journal of Geophysical Research: Oceans*, *104*(C4), 7827–7836. https://doi.org/10.1029/1999JC900010

Cullen, J. T. (2006). On the nonlinear relationship between dissolved cadmium and phosphate in the modern global ocean: Could chronic iron limitation of phytoplankton growth cause the kink? *Limnology and Oceanography*.

Cullen, J. T., Chase, Z., Coale, K. H., Fitzwater, S. E., & Sherrell, R. M. (2003). Effect of iron limitation on the cadmium to phosphorus ratio of natural phytoplankton assemblages from the Southern Ocean. *Limnology and Oceanography*, *48*(3), 1079–1087. https://doi.org/10.4319/lo.2003.48.3.1079

Cullen, J. T., Lane, T. W., Morel, F. M. M., & Sherrell, R. M. (1999). Modulation of cadmium uptake in phytoplankton by seawater CO2 concentration. *Nature*, *402*(6758), 165–167. https://doi.org/10.1038/46007

Cullen, J. T., & Maldonado, M. T. (2013). Biogeochemistry of cadmium and its release to the environment. *Metal Ions in Life Sciences*.

Cullen, J. T., & McAlister, J. (2017). Biogeochemistry of Lead. Its Release to the Environment and Chemical Speciation. In A. Sigel, H. Sigel, & R. K. O. Sigel (Eds.), *Lead: Its Effects on Environment and Health*. Berlin, Boston: De Gruyter. https://doi.org/10.1515/9783110434330-002

Cullen, J. T., & Sherrell, R. M. (2005). Effects of dissolved carbon dioxide, zinc, and manganese on the cadmium to phosphorus ratio in natural phytoplankton assemblages. *Limnology and Oceanography*, *50*(4), 1193–1204. https://doi.org/10.4319/lo.2005.50.4.1193

Cutter, G., Andersson, P., Codispoti, L., Croot, P., François, R., Lohan, M. C., Obata, H., & Rutgers v. d. Loeff, M. (2010). Sampling and Sample-handling Protocols for GEOTRACES Cruises, (December). Retrieved from http://epic.awi.de/34484/

Danielsson, L.-G., Magnusson, B., & Westerlund, S. (1985). Cadmium, copper, iron, nickel and zinc in the north-east Atlantic Ocean. *Marine Chemistry*, *17*(1), 23–41. https://doi.org/10.1016/0304-4203(85)90034-9

de Baar, H. J. W., Saager, P. M., Nolting, R. F., & van der Meer, J. (1994). Cadmium versus phosphate in the world ocean. *Marine Chemistry*, *46*(3), 261–281. https://doi.org/10.1016/0304-4203(94)90082-5

Elderfield, H., & Rickaby, R. (2000). Oceanic Cd/P ratio and nutrient utilization in the glacial Southern Ocean. *Nature*, *405*(6784), 305–10. https://doi.org/10.1038/35012507

Ellwood, M. J. (2004). Zinc and cadmium speciation in subantarctic waters east of New Zealand. *Marine Chemistry*, *87*(1–2), 37–58. https://doi.org/10.1016/j.marchem.2004.01.005

Falkowski, P. G. (1997). Evolution of the nitrogen cycle and its influence on the biological sequestration of CO2 in the ocean. *Nature*, *387*(6630), 272–275. https://doi.org/10.1038/387272a0

Finkel, Z. V., Quigg, A. S., Chiampi, R. K., Schofield, O. E., & Falkowski, P. G. (2007). Phylogenetic diversity in cadmium : phosphorus ratio regulation by marine phytoplankton. *Limnology and Oceanography*, *52*(3), 1131–1138. https://doi.org/10.4319/lo.2007.52.3.1131

Fissel, D. B., Lemon ', D. D., & Birch ', J. R. (1982). Major Features of the Summer Near-Surface Circulation of Western Baffin Bay, 1978 and 1979, *35*(1), 180–200.

Franck, V., Bruland, K., Hutchins, D., & Brzezinski, M. (2003). Iron and zinc effects on silicic acid and nitrate uptake kinetics in three high-nutrient, low-chlorophyll (HNLC) regions. *Marine Ecology Progress Series*, *252*, 15–33. https://doi.org/10.3354/meps252015

Frew, R. D., & Hunter, K. A. (1992). Influence of Southern Ocean waters on the cadmium-phosphate properties of the global ocean. *Nature*, *360*, 144–146.

Gaillardet, J., Viers, J., & Dupré, B. (2014). Trace Elements in River Waters. In *Treatise on Geochemistry* (pp. 195–235). https://doi.org/10.1016/B978-0-08-095975-7.00507-6

Gardiner, J. (1974). The chemistry of cadmium in natural water—II. The adsorption of cadmium on river muds and naturally occurring solids. *Water Research*, *8*(3), 157–164. https://doi.org/10.1016/0043-1354(74)90038-4

Gault-Ringold, M., Adu, T., Stirling, C. H., Frew, R. D., & Hunter, K. A. (2012). Anomalous biogeochemical behavior of cadmium in subantarctic surface waters: Mechanistic constraints from cadmium isotopes. *Earth and Planetary Science Letters*, *341–344*, 94–103. https://doi.org/10.1016/j.epsl.2012.06.005

Grebmeier, J. M., Cooper, L. W., Feder, H. M., & Sirenko, B. I. (2006). Ecosystem dynamics of the Pacific-influenced Northern Bering and Chukchi Seas in the Amerasian Arctic. *Progress in Oceanography*, *71*(2–4), 331–361. https://doi.org/10.1016/j.pocean.2006.10.001

Guay, C. K., & Falkner, K. K. (1997). Barium as a tracer of Arctic halocline and river waters. *Deep Sea Research Part II: Topical Studies in Oceanography*, *44*(8), 1543–1569. https://doi.org/10.1016/S0967-0645(97)00066-0

Harrison, W. G., & Li, W. K. W. (2008). Phytoplankton Growth and Regulation in the Labrador Sea: Light and Nutrient Limitation. *Fish. Sci. J. Northw. Atl. Fish. Sci*, *39*(39), 71–82. https://doi.org/10.2960/J.v39.m592

Haynes, W. M. (2014). *CRC Handbook of Chemistry and Physics, 95th Edition*. CRC Press.

Henderson, G. M., Anderson, R. F., Adkins, J., Andersson, P., Boyle, E. A., Cutter, G., de Baar, H., Eisenhauer, A., Frank, M., Francois, R., Orians, K., Gamo, T., German, C., Jenkins, W., Moffett, J., Jeandel, C., Jickells, T., Krishnaswami, S., Mackey, D., Masque, P., Measures, C. I., Moore, J. K., Oschilles, A., Pollar, R., Rutgers van der Loeff, M., Schlitzer, R., Sharma, M., von Damm, K., & Zhang, J. (2007). GEOTRACES - An international study of the global marine biogeochemical cycles of trace elements and their isotopes. *Chemie Der Erde - Geochemistry*, *67*(2), 85–131. https://doi.org/10.1016/j.chemer.2007.02.001

Hioki, N., Kuma, K., Morita, Y., Sasayama, R., Ooki, A., Kondo, Y., Obata, H., Nishioka, J., Yamashita, Y., Nishino, S., Kikuchi, T., & Aoyama, M. (2015). Laterally spreading iron, humic-like dissolved organic matter and nutrients in cold, dense subsurface water of the Arctic Ocean. *Scientific Reports*, *4*(1), 6775. https://doi.org/10.1038/srep06775

Ho, T.-Y., Quigg, A., Finkel, Z. V., Milligan, A. J., Wyman, K., Falkowski, P. G., & Morel, F. M. M. (2003). The elemental composition of some marine phytoplankton. *Journal of Phycology*, *39*(6), 1145–1159. https://doi.org/10.1111/j.0022-3646.2003.03-090.x

Jakobsson, M., Grantz, A., Kristoffersen, Y., & Macnab, R. (2002). *Bathymetry and physiography of the Arctic Ocean and its constituent seas*. *The Organic Carbon Cycle in the Arctic Ocean*.

Jakobsson, M., Grantz, A., Kristoffersen, Y., Macnab, R., MacDonald, R. W., Sakshaug, E., Steain, R., & Jokat, W. (2004). The Arctic Ocean: Boundary Conditions and Background Information. In *The Organic Carbon Cycle in the Arctic Ocean* (pp. 1–32). Berlin, Heidelberg: Springer Berlin Heidelberg. https://doi.org/10.1007/978-3-642-18912-8_1

Jakubowski, N., Prohaska, T., Rottmann, L., & Vanhaecke, F. (2011). Inductively coupled plasma- and glow discharge plasma-sector field mass spectrometry : Part I. Tutorial: Fundamentals and instrumentation. *Journal of Analytical Atomic Spectrometry*, *26*(4), 693. https://doi.org/10.1039/c0ja00161a

Janssen, D. J., Conway, T. M., John, S. G., Christian, J. R., Kramer, D. I., Pedersen, T. F., & Cullen, J. T. (2014). Undocumented water column sink for cadmium in open ocean oxygen-deficient zones. *Proceedings of the National Academy of Sciences of the United States of America*, *111*(19), 6888–93. https://doi.org/10.1073/pnas.1402388111

Jones, E. P., & Coote, A. R. (1980). Nutrient Distributions in the Canadian Archipelago: Indicators of Summer Water Mass and Flow Characteristics. *Canadian Journal of Fisheries and Aquatic Sciences*, *37*(4), 589–599. https://doi.org/10.1139/f80-075

Jones, E. P., Swift, J. H., Anderson, L. G., Lipizer, M., Civitarese, G., Falkner, K. K., Kattner, G., & McLaughlin, F. (2003). Tracing Pacific water in the North Atlantic Ocean. *Journal of Geophysical Research*, *108*(C4), 3116. https://doi.org/10.1029/2001JC001141

Kondo, Y., Obata, H., Hioki, N., Ooki, A., Nishino, S., Kikuchi, T., & Kuma, K. (2016). Transport of trace metals (Mn, Fe, Ni, Zn and Cd) in the western Arctic Ocean (Chukchi Sea and Canada Basin) in late summer 2012. *Deep Sea Research Part I: Oceanographic Research Papers*, *116*, 236–252. https://doi.org/10.1016/j.dsr.2016.08.010

Kozelka, P. B., & Bruland, K. W. (1998). Chemical speciation of dissolved Cu, Zn, Cd, Pb in Narragansett Bay, Rhode Island. *Marine Chemistry*, *60*(3), 267–282. https://doi.org/10.1016/S0304-4203(97)00107-2

Lacan, F., Francois, R., Ji, Y., & Sherrell, R. M. (2006). Cadmium isotopic composition in the ocean. *Geochimica et Cosmochimica Acta*, *70*(20), 5104–5118. https://doi.org/10.1016/j.gca.2006.07.036

Lagerström, M. E., Field, M. P., Séguret, M., Fischer, L., Hann, S., & Sherrell, R. M. (2013). Automated on-line flow-injection ICP-MS determination of trace metals (Mn, Fe, Co, Ni, Cu and Zn) in open ocean seawater: Application to the GEOTRACES program. *Marine Chemistry*, *155*, 71–80.

Landing, W. M., & Bruland, K. W. (1980). Manganese in the North Pacific. *Earth and Planetary Science Letters*, *49*(1), 45–56. https://doi.org/10.1016/0012-821X(80)90149-1

Landing, W. M., Haraldsson, C., & Paxeus, N. (1986). Vinyl polymer agglomerate based transition metal cation-chelating ion-exchange resin containing the 8-hydroxyquinoline functional group. *Analytical Chemistry*, *58*(14), 3031–3035. https://doi.org/10.1021/ac00127a029

Lane, E. S., Jang, K., Cullen, J. T., & Maldonado, M. T. (2008). The interaction between inorganic iron and cadmium uptake in the marine diatom Thalassiosira oceanica. *Limnology and Oceanography*, *53*(5), 1784–1789. https://doi.org/10.4319/lo.2008.53.5.1784

Lane, E. S., Semeniuk, D. M., Strzepek, R. F., Cullen, J. T., & Maldonado, M. T. (2009). Effects of iron limitation on intracellular cadmium of cultured phytoplankton: Implications for surface dissolved cadmium to phosphate ratios. *Marine Chemistry*, *115*(3), 155–162. https://doi.org/10.1016/j.marchem.2009.07.008

Lane, T. W., & Morel, F. M. M. (2000). A biological function for cadmium in marine diatoms. *Proceedings of the National Academy of Sciences*, *97*(9), 4627–4631. https://doi.org/10.1073/pnas.090091397

Lee, J.-M., Boyle, E. A., Echegoyen-Sanz, Y., Fitzsimmons, J. N., Zhang, R., & Kayser, R. A. (2011). Analysis of trace metals (Cu, Cd, Pb, and Fe) in seawater using single batch nitrilotriacetate resin extraction and isotope dilution inductively coupled plasma mass spectrometry. *Analytica Chimica Acta*, *686*(1–2), 93–101. https://doi.org/10.1016/j.aca.2010.11.052

Lee, J. G., Roberts, S. B., & Morel, F. M. M. (1995). Cadmium: A nutrient for the marine diatom Thalassiosira weissflogii. *Limnology and Oceanography*, *40*(6), 1056–1063. https://doi.org/10.4319/lo.1995.40.6.1056

Lee, J., & Morel, F. (1995). Replacement of zinc by cadmium in marine phytoplankton. *Marine Ecology Progress Series*, *127*, 305–309. https://doi.org/10.3354/meps127305

Lohan, M. C., Aguilar-Islas, A. M., Franks, R. P., & Bruland, K. W. (2005). Determination of iron and copper in seawater at pH 1.7 with a new commercially available chelating resin, NTA Superflow. *Analytica Chimica Acta*, *530*(1), 121–129. https://doi.org/10.1016/j.aca.2004.09.005

Löscher, B. M., van der Meer, J., de Baar, H. J. W., Saager, P. M., & de Jong, J. T. M. (1997). The global Cd/phosphate relationship in deep ocean waters and the need for accuracy. *Marine Chemistry*, *59*(1–2), 87–93. https://doi.org/10.1016/S0304-4203(97)00067-4

Mann, E. L., Ahlgren, N., Moffett, J. W., & Chisholm, S. W. (2002). Copper toxicity and cyanobacteria ecology in the Sargasso Sea. *Limnology and Oceanography*, *47*(4), 976–988. https://doi.org/10.4319/lo.2002.47.4.0976

Marchitto, T. M., & Broecker, W. S. (2006). Deep water mass geometry in the glacial Atlantic Ocean: A review of constraints from the paleonutrient proxy Cd/Ca. *Geochemistry, Geophysics, Geosystems*, *7*(12). https://doi.org/10.1029/2006GC001323

Mathis, J. T., Pickart, R. S., Hansell, D. A., Kadko, D., & Bates, N. R. (2007). Eddy transport of organic carbon and nutrients from the Chukchi Shelf: Impact on the upper halocline of the western Arctic Ocean. *Journal of Geophysical Research*, *112*(C5), C05011. https://doi.org/10.1029/2006JC003899

Mclaren, J. W., Mykytiuk, A. P., Willie, S. N., & Berman, S. S. (1985). Determination of Trace Metals in Seawater by Inductively Coupled Plasma Mass Spectrometry with Preconcentration on. *Analytical Chemistry*, (57), 2907–2911. https://doi.org/10.1021/ac00291a037

McLaughlin, F. A., Carmack, E. C., Macdonald, R. W., & Bishop, J. K. B. (1996). Physical and geochemical properties across the Atlantic/Pacific water mass front in the southern Canadian Basin. *Journal of Geophysical Research: Oceans*, *101*(C1), 1183–1197. https://doi.org/10.1029/95JC02634

McLaughlin, F., Carmack, E. C., Ingram, R. G., Williams, W., & Michel, C. (2004). Oceanography of the Northwest Passage. In A. R. Robinson & K. H. Brink (Eds.), *The Sea* (pp. 1211–1242). New York: Wiley.

McLaughlin, F., Shimada, K., Carmack, E., Itoh, M., & Nishino, S. (2005). The hydrography of the southern Canada Basin, 2002. *Polar Biology*, *28*(3), 182–189. https://doi.org/10.1007/s00300-004-0701-6

Measures, C. I., Landing, W. M., Brown, M. T., & Buck, C. S. (2008). A commercially available rosette system for trace metal-clean sampling. *Limnology and Oceanography: Methods*, *6*(9), 384–394. https://doi.org/10.4319/lom.2008.6.384

Michel, C., Ingram, R. G., & Harris, L. R. (2006). Variability in oceanographic and ecological processes in the Canadian Arctic Archipelago. *Progress in Oceanography*, *71*(2–4), 379–401. https://doi.org/10.1016/j.pocean.2006.09.006

Milne, A., Landing, W. M., Bizimis, M., & Morton, P. L. (2010). Determination of Mn, Fe, Co, Ni, Cu, Zn, Cd and Pb in seawater using high resolution magnetic sector inductively coupled mass spectrometry (HR-ICP-MS). *Analytica Chimica Acta*, *665*(2), 200–207. https://doi.org/10.1016/j.aca.2010.03.027

Moore, J. K., Doney, S. C., & Lindsay, K. (2004). Upper ocean ecosystem dynamics and iron cycling in a global three-dimensional model. *Global Biogeochemical Cycles*, *18*(4). https://doi.org/10.1029/2004GB002220

Moore, R. (1981). Oceanographic distributions of zinc, cadmium, copper and aluminium in waters of the central arctic. *Geochimica et Cosmochimica Acta*, *45*(12), 2475–2482. https://doi.org/10.1016/0016-7037(81)90099-5

Morel, F. M. M., & Price, N. M. (2003). The Biogeochemical Cycles of Trace Metals in the Oceans. *Science*, *300*(5621).

Morel, F. M. M., Reinfelder, J. R., Roberts, S. B., Chamberlain, C. P., Lee, J. G., & Yee, D. (1994). Zinc and carbon co-limitation of marine phytoplankton. *Nature*, *369*(6483), 740–742. https://doi.org/10.1038/369740a0

Peers, G., & Price, N. M. (2006). Copper-containing plastocyanin used for electron transport by an oceanic diatom. *Nature*, *441*(7091), 341–344. https://doi.org/10.1038/nature04630

Price, N. M., & Morel, F. M. M. (1990). Cadmium and cobalt substitution for zinc in a marine diatom. *Nature*, *344*(6267), 658–660. https://doi.org/10.1038/344658a0

Price, N. M., & Morel, F. M. M. (1994). Trace metal nutrition and toxicity in phytoplankton. In L. Rai, J. Gaur, & C. Soeder (Eds.), *Algae and Water Pollution* (Advances i, pp. 79–97). Stuttgart: E Schweizebbart'sche Verlagsbuchhandlung.

Prinsenberg, S. J., & Bennett, E. B. (1987). Mixing and transports in Barrow Strait, the central part of the Northwest passage. *Continental Shelf Research*, *7*(8), 913–935. https://doi.org/10.1016/0278-4343(87)90006-9

Pritzkow, W., Wunderli, S., Vogl, J., & Fortunato, G. (2007). The isotope abundances and the atomic weight of cadmium by a metrological approach. *International Journal of Mass Spectrometry*, *261*(1), 74–85. https://doi.org/10.1016/j.ijms.2006.07.026

Quay, P., Cullen, J., Landing, W., & Morton, P. (2015). Processes controlling the distributions of Cd and PO_4 in the ocean. *Global Biogeochemical Cycles*, *29*(6), 830–841. https://doi.org/10.1002/2014GB004998

Quay, P., & Wu, J. (2015). Impact of end-member mixing on depth distributions of δ13C, cadmium and nutrients in the N. Atlantic Ocean. *Deep Sea Research Part II: Topical Studies in Oceanography*, *116*, 107–116. https://doi.org/10.1016/j.dsr2.2014.11.009

Quéroué, F., Townsend, A., van der Merwe, P., Lannuzel, D., Sarthou, G., Bucciarelli, E., & Bowie, A. (2014). Advances in the offline trace metal extraction of Mn, Co, Ni, Cu, Cd, and Pb from open ocean seawater samples with determination by sector field ICP-MS analysis. *Analytical Methods*, *6*(9), 2837. https://doi.org/10.1039/c3ay41312h

Rehkämper, M., Wombacher, F., Horner, T. J., & Xue, Z. (2012). Natural and Anthropogenic Cd Isotope Variations. In *Handbook of Environmental Isotope Geochemistry* (pp. 125–154). Berlin, Heidelberg: Springer Berlin Heidelberg. https://doi.org/10.1007/978-3-642-10637-8_8

Ripperger, S., Rehkamper, M., Porcelli, D., & Halliday, A. N. (2007). Cadmium isotope fractionation in seawater — A signature of biological activity. *Earth and Planetary Science Letters*, *261*(3–4), 670–684. https://doi.org/10.1016/J.EPSL.2007.07.034

Rosenthal, Y., Boyle, E. A., & Labeyrie, L. (1997). Last Glacial Maximum paleochemistry and deepwater circulation in the Southern Ocean: Evidence from foraminiferal cadmium. *Paleoceanography*, *12*(6), 787–796. https://doi.org/10.1029/97PA02508

Roshan, S., & Wu, J. (2015). Cadmium regeneration within the North Atlantic. *Global Biogeochemical Cycles*, *29*(12), 2082–2094. https://doi.org/10.1002/2015GB005215

Rudnick, R. L., & Gao, S. (2014). 4.1 – Composition of the Continental Crust. In *Treatise on Geochemistry* (pp. 1–51). https://doi.org/10.1016/B978-0-08-095975-7.00301-6

Saager, P. M., & de Baar, H. J. W. (1993). Limitations to the quantitative application of Cd as a paleoceanographic tracer, based on results of a multi0box model (MENU) and statistical considerations. *Global and Planetary Change*, *8*, 69–92.

Saager, P. M., De Baar, H. J. W., & Howland, R. J. (1992). Cd, Zn, Ni and Cu in the Indian Ocean. *Deep Sea Research Part A. Oceanographic Research Papers*, *39*(1), 9–35. https://doi.org/10.1016/0198-0149(92)90017-N

Saito, M. A., & Schneider, D. L. (2006). Examination of precipitation chemistry and improvements in precision using the $Mg(OH)_2$ preconcentration inductively coupled plasma mass spectrometry (ICP-MS) method for high-throughput analysis of open-ocean Fe and Mn in seawater. *Analytica Chimica Acta*, *565*(2), 222–233. https://doi.org/10.1016/j.aca.2006.02.028

Shannon, R. D. (1976). Revised effective ionic radii and systematic studies of interatomic distances in halides and chalcogenides. *Acta Crystallographica Section A*, *32*(5), 751–767. https://doi.org/10.1107/S0567739476001551

Slater, J. C. (1964). Atomic Radii in Crystals. *The Journal of Chemical Physics*, *41*(10), 3199–3204. https://doi.org/10.1063/1.1725697

Sohrin, Y., Urushihara, S., Nakatsuka, S., Kono, T., Higo, E., Minami, T., Norisuye, K., & Umetani, S. (2008). Multielemental Determination of GEOTRACES Key Trace Metals in Seawater by ICPMS after Preconcentration Using an Ethylenediaminetriacetic Acid Chelating Resin. *Analytical Chemistry*, *80*(16), 6267–6273. https://doi.org/10.1021/ac800500f

Sunda, W. G., & Huntsman, S. A. (1995). Iron uptake and growth limitation in oceanic and coastal phytoplankton. *Marine Chemistry*, *50*(1–4), 189–206. https://doi.org/10.1016/0304-4203(95)00035-P

Sunda, W. G., & Huntsman, S. A. (1998). Control of Cd Concentrations in a Coastal Diatom by Interactions among Free Ionic Cd, Zn, and Mn in Seawater. *Environmental Science & Technology*, *32*(19), 2961–2968. https://doi.org/10.1021/es980271y

Sunda, W. G., & Huntsman, S. A. (2000). Effect of Zn, Mn, and Fe on Cd accumulation in phytoplankton: Implications for oceanic Cd cycling. *Limnology and Oceanography*, *45*(7), 1501–1516. https://doi.org/10.4319/lo.2000.45.7.1501

Sunda, W. G., & Huntsman, S. A. (2005). Effect of CO_2 supply and demand on zinc uptake and growth limitation in a coastal diatom. *Limnology and Oceanography*, *50*(4), 1181–1192. https://doi.org/10.4319/lo.2005.50.4.1181

Sverdrup, H. U., Johnson, M. W., & Fleming, R. H. (1942). *The Oceans: Their Physics, Chemistry, and General Biology*. New York: Prentice-Hall.

Tagliabue, A., Bowie, A. R., Boyd, P. W., Buck, K. N., Johnson, K. S., & Saito, M. A. (2017). The integral role of iron in ocean biogeochemistry. *Nature*, *543*(7643), 51–59. https://doi.org/10.1038/nature21058

Tan, F. C., & Strain, P. M. (1980). The distribution of sea ice meltwater in the eastern Canadian Arctic. *Journal of Geophysical Research*, *85*(C4), 1925. https://doi.org/10.1029/JC085iC04p01925

Tang, C. C. ., Ross, C. K., Yao, T., Petrie, B., DeTracey, B. M., & Dunlap, E. (2004). The circulation, water masses and sea-ice of Baffin Bay. *Progress in Oceanography*, *63*(4), 183–228. https://doi.org/10.1016/j.pocean.2004.09.005

Tanner, S. D., Baranov, V. I., & Bandura, D. R. (2002). Reaction cells and collision cells for ICP-MS: a tutorial review. *Spectrochimica Acta Part B: Atomic Spectroscopy*, *57*(9), 1361–1452. https://doi.org/10.1016/S0584-8547(02)00069-1

Tremblay, G., Belzile, C., Gosselin, M., Poulin, M., Roy, S., & Tremblay, J.-E. (2009). Late summer phytoplankton distribution along a 3500 km transect in Canadian Arctic waters: strong numerical dominance by picoeukaryotes. *Aquatic Microbial Ecology*, *54*, 55–70. https://doi.org/10.3354/ame01257

Trenberth, K. E., Jones, P. D., Ambenje, P., Bojariu, R., Easterling, D., Klein Tank, A., Parker, D., Rahimzadeh, F., Renwick, J. A., Rusticucci, M., Soden, B., & Zhai, P. (2007). Observations: Surface and Atmospheric Climate Change. In S. Solomon, D. Win, M. Manning, Z. Chen, M. Marquis, K. B. Averyt, M. Tignor & H. L. Miller (Eds.), *Climate Change 2007: The Physical Science Basis. Contribution of Working Group I to the Fourth Assessment Report of the Intergovernmental Panel on Climate Change*. Cambridge, United Kingdom and New York, NY, USA: Cambridge University Press.

Varela, D. E., Willers, V., & Crawford, D. W. (2011). Effect of zinc availability on growth, morphology, and nutrient incorporation in a coastal an an oceanic diatom. *Journal of Phycology*, *47*(2), 302–312. https://doi.org/10.1111/j.1529-8817.2010.00948.x

Vaughan, D. G., Comiso, J. C., Allison, I., Carrasco, J., Kaser, G., Kwok, R., Mote, P., Murray, T., Paul, F., Ren, J., Rignot, E., Solomina, O., Steffen, K., & Zhang, T. (2013). Observations: Cryosphere. In T. F. Stocker, D. Qin, G.-K. Plattner, M. Tignor, S. K. Allen, J. Boschung, A. Nauels, Y. Xia, V. Bex, & P. M. Midgley (Eds.), *Climate Change 2013: The Physical Science Basis. Contribution of Working Group I to the Fifth Assessment Report of the Intergovernmental Panel on Climate Change*. Cambridge, United Kingdom and New York, NY, USA: Cambridge University Press.

Wang, Q., Myers, P. G., Hu, X., & Bush, A. B. G. (2012). Flow Constraints on Pathways through the Canadian Arctic Archipelago. *Atmosphere-Ocean*, *50*(3), 373–385. https://doi.org/10.1080/07055900.2012.704348

Wieser, M. E., & Coplen, T. B. (2010). Atomic weights of the elements 2009 (IUPAC Technical Report). *Pure and Applied Chemistry*, *83*(2). https://doi.org/10.1351/PAC-REP-10-09-14

Wu, J., & Boyle, E. A. (1997). Low blank preconcentration technique for the determination of lead, copper, and cadmium in small-volume seawater samples by isotope dilution ICPMS. *Analytical Chemistry*, *69*(13), 2464–70. https://doi.org/10.1021/ac961204u

Wu, J., & Roshan, S. (2015). Cadmium in the North Atlantic: Implication for global cadmium–phosphorus relationship. *Deep Sea Research Part II: Topical Studies in Oceanography*, *116*, 226–239. https://doi.org/10.1016/j.dsr2.2014.11.007

Xie, R. C., Galer, S. J. G., Abouchami, W., Rijkenberg, M. J. A., De Jong, J., de Baar, H. J. W., & Andreae, M. O. (2015). The cadmium–phosphate relationship in the western South Atlantic — The importance of mode and intermediate waters on the global systematics. *Marine Chemistry*, *177*, 110–123. https://doi.org/10.1016/j.marchem.2015.06.011

Xu, Y., Feng, L., Jeffrey, P. D., Shi, Y., & Morel, F. M. M. (2008). Structure and metal exchange in the cadmium carbonic anhydrase of marine diatoms. *Nature*, *452*(7183), 56–61. https://doi.org/10.1038/nature06636

Xu, Y., Shi, D., Aristilde, L., & Morel, F. M. M. (2012). The effect of pH on the uptake of zinc and cadmium in marine phytoplankton: Possible role of weak complexes. *Limnology and Oceanography*, *57*(1), 293–304. https://doi.org/10.4319/lo.2012.57.1.0000

Xue, H., & Sigg, L. (1998). Cadmium speciation and complexation by natural organic ligands in fresh water. *Analytica Chimica Acta*, *363*(2–3), 249–259. https://doi.org/10.1016/S0003-2670(98)00081-6

Xue, Z., Rehkamper, M., Horner, T. J., Abouchami, W., Middag, R., van de Flierd, T., & de Baar, H. J. W. (2013). Cadmium isotope variations in the Southern Ocean. *Earth and Planetary Science Letters*, *382*, 161–172. https://doi.org/10.1016/J.EPSL.2013.09.014

Yamamoto-Kawai, M., Carmack, E., & McLaughlin, F. (2006). Nitrogen balance and Arctic throughflow. *Nature*, *443*(7107), 43–43. https://doi.org/10.1038/443043a

Yang, S.-C., Lee, D.-C., & Ho, T.-Y. (2012). The isotopic composition of Cadmium in the water column of the South China Sea. *Geochimica et Cosmochimica Acta*, *98*, 66–77. https://doi.org/10.1016/J.GCA.2012.09.022

Yeats, P. A. (1988). Manganese, nickel, zinc and cadmium distributions at the Fram 3 and Cesar ice camps in the Arctic Ocean. *Oceanologica Acta*, *11*(4), 383–388.

Yeats, P. A., & Westerlund, S. (1991). Trace metal distributions at an Arctic Ocean ice island. *Marine Chemistry*, *33*(3), 261–277. https://doi.org/10.1016/0304-4203(91)90071-4

00000aab0f26&acdnat=1501791363_49387c9bb233c6d36ffe42e205a23549

Yeats, P. A., Westerlund, S., & Flegal, A. R. (1995). Cadmium, copper and nickel distributions at four stations in the eastern central and south Atlantic. *Marine Chemistry*, *49*(4), 283–293. https://doi.org/10.1016/0304-4203(95)00018-M

Zhu, Y., & Itoh, A. (2016). Direct Determination of Cadmium in Seawater by Standard Addition ICP-QMS/QMS with an ORC. *Analytical Sciences*, *32*(12), 1301–1305. https://doi.org/10.2116/analsci.32.1301

Zirino, A., & Yamamoto, S. (1972). A pH-dependent model for the chemical speciation of copper, cadmium, zinc, and lead in seawater. *Limnology and Oceanography*, *17*(5), 661–671. https://doi.org/10.4319/lo.1972.17.5.0661

Appendix A
Cleaning Protocols

Trace metal analysis is contamination-prone; hence it is necessary to adhere to strict cleaning protocols. The following protocols were developed by the trace-metal community for the GEOTRACES program.

A.1 Sample bottle cleaning protocol

500mL LDPE bottles (Nalgene) were used for sample collection and storage, and underwent a rigorous cleaning procedure, outlined below.

1) The bottles were soaked in alkaline detergent for a minimum of one week.
2) The bottles were rinsed four times with reverse osmosis (RO) water.
3) The bottles were rinsed three times with ultra-pure deionized water (MQW) in a laminar-flow hood, in a Class-100 clean room.
4) The bottles were carefully over-filled with 6 M HCl (reagent grade) to form a concave meniscus and capped, ensuring that the threads and caps were leached during cleaning. Bottles were stored in acid for a minimum of one month.
5) The bottles were rinsed four times with MQW in a laminar-flow hood, in a Class-100 clean room.
6) The bottles were filled with 1 M HCl (environmental grade) and double-bagged. Bottles were filled a minimum of one month prior to cruise, and were transported on the cruise filled with 1 M HCl.

A.2 *seaFAST*-pico elution tubes cleaning protocol

Polypropylene metal-free centrifuge tubes (VWR) were used to store the eluted samples. The tubes are certified to be free of trace metals to <1ppb, however given the low expected concentrations of metals in our samples we opted to pre-clean using the following protocol.

1) Prior to the first use, tubes were soaked in detergent for a minimum of one week.
2) The tubes were rinsed four times with RO water.
3) The tubes were rinsed three times with MQW in a laminar-flow hood, in a Class-100 clean room.
4) The tubes were filled with 1 M HCl (environmental grade) for a minimum of one week.
5) The tubes were rinsed four times with MQW in a laminar-flow hood in a Class-100 clean room.
6) The tubes were air-dried in a laminar-flow hood in a Class-100 clean room. Once dry, tubes were capped and stored double-bagged until required.

Appendix B
Data Tables with dissolved Mn, Fe, Ni, Cu, Zn, Cd and Pb from the Canadian Arctic

Table B.1 Dissolved Mn, Fe, Ni, Cu, Zn, Cd and Pb from the Canada Basin (stations CB1, CB2, CB3, and CB4). Where contamination is suspected, samples are highlighted in red. Data is expected to be submitted to the GEOTRACES International Data Assembly Centre by December 2017.

Station	Latitude	Longitude	depth	dMn	dMn error	dFe	dFe error	dNi	dNi error	dCu	dCu error	dZn	dZn error	dCd	dCd error	dPb	dPb error
				nM	nM	nM	nM	nM	nM	nM	nM	nM	nM	pM	pM	pM	pM
CB1	75.33	-120.77	11	10.78	0.14	0.67	0.01	6.85	0.07	4.12	0.05	1.07	0.02	295	4	4.0	0.2
CB1	75.33	-120.77	15	8.00	0.11	0.53	0.01	6.85	0.11	4.01	0.05	0.94	0.01	295	3	12.0	0.4
CB1	75.33	-120.77	43	4.09	0.07	0.73	0.01	6.95	0.11	3.72	0.05	1.70	0.02	409	4	15.8	0.1
CB1	75.33	-120.77	59	1.61	0.02	0.86	0.01	6.93	0.12	3.63	0.05	2.55	0.04	528	10	13.0	0.3
CB1	75.33	-120.77	74	1.35	0.02	1.15	0.02	7.52	0.11	3.96	0.07	3.09	0.07	602	9	6.7	0.3
CB1	75.13	-120.89	148	0.90	0.01	0.96	0.01	5.73	0.07	2.98	0.04	3.49	0.03	505	8	7.2	0.4
CB1	75.13	-120.89	198	0.48	0.01	0.69	0.01	4.81	0.11	2.39	0.04	3.39	0.07	420	7	2.1	0.0
CB1	75.13	-120.89	248	0.68	0.01	0.97	0.01	4.30	0.07	2.12	0.04	3.31	0.07	353	9	6.7	0.3
CB1	75.13	-120.89	328	0.61	0.01	1.26	0.02	3.99	0.06	2.11	0.02	2.87	0.05	309	7	12.1	0.4
CB1	75.13	-120.89	348	0.55	0.01	0.76	0.01	3.80	0.08	2.02	0.05	2.96	0.04	291	6	4.6	0.3
CB1	75.13	-120.89	397	0.46	0.01	0.68	0.01	3.76	0.02	2.15	0.03	2.97	0.03	278	5	3.4	0.2
CB2	75.81	-129.22	10	5.07	0.07	0.52	0.01	6.95	0.11	4.31	0.07	1.82	0.01	295	5	5.0	0.2
CB2	75.80	-129.25	25	3.99	0.06	0.23	0.00	6.84	0.12	4.42	0.07	0.81	0.01	304	8	45.7	0.9
CB2	75.80	-129.25	40	1.61	0.02	0.37	0.00	6.75	0.10	3.91	0.04	1.87	0.04	513	10	2.3	0.2
CB2	75.81	-129.22	57	1.69	0.02	0.43	0.01	6.79	0.10	3.91	0.06	2.39	0.03	512	10	4.2	0.1
CB2	75.81	-129.22	64	1.46	0.02	0.48	0.01	6.84	0.10	3.82	0.06	2.29	0.03	563	7	9.7	0.3
CB2	75.80	-129.25	99	1.44	0.02	0.51	0.01	7.13	0.12	3.88	0.08	3.03	0.05	642	8	2.0	0.1
CB2	75.81	-129.22	139	1.98	0.03	0.54	0.01	7.48	0.10	3.68	0.06	3.95	0.05	706	10	5.1	0.2

Station	Latitude	Longitude	depth	dMn	dMn error	dFe	dFe error	dNi	dNi error	dCu	dCu error	dZn	dZn error	dCd	dCd error	dPb	dPb error
				nM	nM	nM	nM	nM	nM	nM	nM	nM	nM	pM	pM	pM	pM
CB2	75.81	-129.22	199	1.25	0.02	0.48	0.01	5.07	0.10	2.60	0.05	2.66	0.04	377	9	1.6	0.1
CB2	75.80	-129.25	297	0.44	0.01	1.06	0.01	3.74	0.07	1.68	0.03	2.35	0.03	260	4	4.0	0.1
CB2	75.80	-129.25	396	0.31	0.00	0.39	0.00	3.39	0.07	1.39	0.03	1.57	0.03	214	3	5.1	0.2
CB2	75.80	-129.25	792	0.37	0.01	0.50	0.00	3.51	0.10	1.43	0.03	1.59	0.02	201	3	5.0	0.2
CB2	75.80	-129.25	989	0.33	0.00	0.46	0.01	3.55	0.07	1.43	0.02	1.68	0.03	209	4	3.2	0.1
CB2	75.80	-129.25	1188	0.36	0.01	0.66	0.01	3.96	0.08	1.48	0.02	2.17	0.03	205	5	2.4	0.1
CB3	76.98	-140.04	10	7.13	0.16	0.48	0.01	6.84	0.17	4.33	0.11	1.18	0.03	271	6	4.9	0.3
CB3	76.98	-140.04	25	4.23	0.07	0.62	0.01	7.04	0.15	4.39	0.08	1.01	0.03	300	5	3.1	0.1
CB3	76.99	-140.03	40	2.95	0.05	0.34	0.01	6.82	0.10	4.17	0.05	0.99	0.01	352	4	3.3	0.2
CB3	76.98	-140.04	57	1.78	0.04	0.41	0.01	6.81	0.11	4.04	0.07	1.27	0.02	433	8	8.9	0.2
CB3	76.98	-140.04	57	1.85	0.02	0.38	0.01	6.68	0.11	4.07	0.07	1.26	0.02	417	6	8.1	0.4
CB3	76.99	-140.03	99	1.33	0.03	0.62	0.01	7.16	0.13	3.96	0.06	2.96	0.05	616	10	2.4	0.2
CB3	76.99	-140.03	119	1.53	0.02	0.64	0.01	7.34	0.14	3.81	0.08	3.20	0.06	647	11	1.6	0.1
CB3	76.99	-140.07	148	2.03	0.04	0.59	0.01	7.84	0.11	3.91	0.06	3.77	0.06	740	11	1.0	0.1
CB3	76.98	-140.04	178	1.87	0.02	0.56	0.01	7.65	0.11	3.82	0.05	3.89	0.05	728	11	3.1	0.1
CB3	76.98	-140.04	198	1.75	0.03	0.52	0.00	6.73	0.14	3.56	0.07	3.71	0.05	589	11	2.0	0.2
CB3	76.99	-140.07	247	0.96	0.01	0.40	0.00	4.30	0.08	2.04	0.03	1.92	0.04	291	7	1.7	0.1
CB3	76.99	-140.03	297	0.71	0.01	0.62	0.01	4.22	0.06	2.03	0.03	1.76	0.03	236	5	3.2	0.1
CB3	76.99	-140.03	475	0.37	0.00	0.28	0.01	3.55	0.08	1.42	0.03	1.37	0.04	204	5	4.1	0.1
CB3	76.99	-140.07	594	0.41	0.01	0.37	0.00	3.67	0.05	1.52	0.02	1.93	0.02	207	4	1.6	0.1
CB3	76.99	-140.03	792	0.39	0.01	0.28	0.00	3.60	0.06	1.40	0.03	1.45	0.04	206	7	4.9	0.3
CB3	76.99	-140.03	989	0.35	0.01	0.28	0.00	3.54	0.10	1.39	0.02	1.52	0.03	206	5	3.2	0.2
CB3	76.99	-140.07	1187	0.29	0.01	0.27	0.00	3.56	0.05	1.37	0.03	1.36	0.02	206	2	2.4	0.1
CB3	76.99	-140.03	1385	0.31	0.00	0.28	0.00	3.50	0.04	1.43	0.02	1.51	0.01	206	6	2.9	0.1

Station	Latitude	Longitude	depth	dMn	dMn error	dFe	dFe error	dNi	dNi error	dCu	dCu error	dZn	dZn error	dCd	dCd error	dPb	dPb error
				nM	nM	nM	nM	nM	nM	nM	nM	nM	nM	pM	pM	pM	pM
CB3	76.99	-140.07	1583	0.25	0.01	0.32	0.00	3.52	0.05	1.44	0.02	1.17	0.01	206	4	3.2	0.2
CB3	76.99	-140.07	1979	0.21	0.00	0.34	0.00	3.41	0.08	1.38	0.02	0.86	0.02	204	6	3.5	0.1
CB3	76.99	-140.07	2473	0.17	0.00	0.32	0.00	3.22	0.08	1.50	0.03	0.77	0.02	207	4	3.8	0.2
CB3	76.99	-140.07	2968	0.16	0.00	0.27	0.00	3.16	0.06	1.70	0.02	0.87	0.02	203	4	2.3	0.1
CB3	76.99	-140.07	3462	0.20	0.00	0.37	0.00	3.36	0.05	1.81	0.03	1.38	0.02	205	4	2.6	0.1
CB4	75.00	-150.00	10	5.86	0.10	3.62	0.07	6.66	0.13	4.54	0.05	1.08	0.01	262	7	8.3	0.4
CB4	75.00	-150.00	25	4.92	0.07	0.21	0.00	7.07	0.10	4.50	0.09	0.76	0.02	294	6	4.9	0.2
CB4	75.00	-150.00	26	5.73	0.09	0.34	0.01	7.14	0.08	4.52	0.05	0.72	0.02	277	6	5.5	0.2
CB4	75.00	-150.00	40	5.43	0.07	0.19	0.00	7.13	0.14	4.59	0.08	0.77	0.02	289	6	3.8	0.2
CB4	75.00	-150.00	70	1.89	0.04	0.27	0.00	6.74	0.12	4.14	0.08	0.84	0.03	346	9	7.6	0.2
CB4	75.00	-150.00	70	1.99	0.03	0.26	0.00	6.76	0.14	4.27	0.05	0.75	0.01	338	6	7.3	0.3
CB4	75.00	-150.00	99	1.25	0.02	0.51	0.01	6.89	0.13	4.07	0.07	2.33	0.04	548	12	8.9	0.4
CB4	75.00	-150.00	119	1.20	0.02	0.57	0.01	7.08	0.19	4.04	0.08	3.13	0.07	596	12	2.6	0.2
CB4	75.00	-150.00	148	1.46	0.02	0.55	0.01	7.28	0.12	3.94	0.05	3.15	0.05	643	5	1.3	0.1
CB4	75.00	-150.00	148	2.58	0.05	0.59	0.01	7.53	0.10	4.06	0.06	3.34	0.06	653	9	3.4	0.3
CB4	75.00	-150.00	218	1.70	0.03	0.57	0.01	7.40	0.12	3.94	0.07	3.89	0.06	667	16	2.9	0.1
CB4	75.00	-150.00	247	1.11	0.02	0.56	0.01	5.54	0.12	2.92	0.05	2.76	0.05	428	7	9.0	0.2
CB4	75.00	-150.00	297	0.67	0.01	0.60	0.01	4.29	0.06	2.07	0.04	2.14	0.05	284	6	5.4	0.1
CB4	75.00	-150.00	495	0.40	0.01	0.42	0.01	3.62	0.06	1.50	0.02	1.57	0.03	213	5	4.3	0.1
CB4	75.00	-150.00	594	0.45	0.01	0.53	0.01	3.67	0.05	1.50	0.03	1.54	0.02	207	6	1.3	0.1
CB4	75.00	-150.00	792	0.45	0.01	0.49	0.01	3.57	0.07	1.47	0.02	1.52	0.02	205	3	5.2	0.2
CB4	75.00	-150.00	989	0.57	0.01	0.45	0.01	3.61	0.08	1.46	0.02	1.70	0.04	204	4	3.0	0.2
CB4	75.00	-150.00	1220	0.35	0.01	0.41	0.00	3.56	0.10	1.49	0.03	1.48	0.03	205	6	2.8	0.1
CB4	75.00	-150.00	1386	0.32	0.01	0.39	0.01	3.57	0.05	1.55	0.03	1.51	0.03	208	3	3.2	0.1

Station	Latitude	Longitude	depth	dMn	dMn error	dFe	dFe error	dNi	dNi error	dCu	dCu error	dZn	dZn error	dCd	dCd error	dPb	dPb error
				nM	nM	nM	nM	nM	nM	nM	nM	nM	nM	pM	pM	pM	pM
CB4	75.00	-150.00	1583	0.27	0.00	0.38	0.00	3.47	0.05	1.38	0.02	1.19	0.02	206	4	3.5	0.1
CB4	75.00	-150.00	1980	0.22	0.00	0.36	0.00	3.36	0.06	1.35	0.02	0.89	0.01	206	3	4.0	0.1
CB4	75.00	-150.00	2473	0.17	0.00	0.30	0.01	3.23	0.07	1.39	0.02	0.75	0.01	196	5	4.1	0.1
CB4	75.00	-150.00	2968	0.17	0.00	0.34	0.01	3.13	0.07	1.51	0.03	0.79	0.03	204	5	1.8	0.2
CB4	75.00	-150.00	3461	0.17	0.00	0.22	0.00	3.26	0.04	1.54	0.02	0.95	0.01	204	2	4.6	0.2
CB4	75.00	-150.00	3462	0.21	0.00	0.19	0.00	3.17	0.04	1.92	0.03	0.88	0.03	204	3	2.6	0.2

Table B.2 Dissolved Mn, Fe, Ni, Cu, Zn, Cd and Pb from the Canadian Arctic Archipelago (stations CAA1, CAA2, CAA3, CAA4, CAA5, CAA6, CAA7, CAA8, and CAA9). Where contamination is suspected, samples are highlighted in red. Data is expected to be submitted to the GEOTRACES International Data Assembly Centre by December 2017.

Station	Latitude	Longitude	depth	dMn	dMn error	dFe	dFe error	dNi	dNi error	dCu	dCu error	dZn	dZn error	dCd	dCd error	dPb	dPb error
			m	nM	nM	nM	nM	nM	nM	nM	nM	nM	nM	pM	pM	pM	pM
CAA1	74.52	-80.56	10	5.38	0.08	0.84	0.01	5.36	0.11	3.52	0.05	0.56	0.04	216.5	4.9	9.6	0.2
CAA1	74.52	-80.56	29	4.95	0.10	1.17	0.02	4.62	0.13	3.36	0.09	0.64	0.01	175.3	7.6	12.9	0.5
CAA1	74.52	-80.56	44	4.85	0.08	1.97	0.03	5.79	0.14	3.49	0.05	1.89	0.03	327.9	10.0	12.6	0.2
CAA1	74.52	-80.56	59	4.77	0.08	2.66	0.04	6.11	0.07	3.67	0.08	2.49	0.03	362.0	5.5	15.7	0.5
CAA1	74.52	-80.56	80	4.55	0.05	2.48	0.04	6.28	0.12	3.60	0.05	1.90	0.05	399.7	6.2	12.4	0.2
CAA1	74.52	-80.56	100	4.02	0.08	2.65	0.05	6.27	0.15	3.45	0.07	2.38	0.05	432.1	10.5	12.6	0.5
CAA1	74.52	-80.57	120	3.66	0.06	2.38	0.04	6.11	0.07	3.35	0.05	2.29	0.02	435.4	7.5	8.2	0.4
CAA1	74.52	-80.57	149	3.39	0.05	2.42	0.03	6.03	0.12	3.19	0.04	2.27	0.01	434.5	10.8	5.7	0.1
CAA1	74.52	-80.57	199	3.50	0.07	3.14	0.06	5.43	0.12	2.81	0.05	2.09	0.05	398.6	6.6	6.4	0.3
CAA1	74.52	-80.57	298	3.35	0.06	3.82	0.03	4.91	0.07	2.42	0.05	2.19	0.04	374.3	8.7	5.6	0.1
CAA1	74.52	-80.57	398	3.67	0.05	3.55	0.02	4.62	0.05	2.22	0.03	2.73	0.04	349.2	6.5	2.8	0.1

Station	Latitude	Longitude	depth	dMn	dMn error	dFe	dFe error	dNi	dNi error	dCu	dCu error	dZn	dZn error	dCd	dCd error	dPb	dPb error
			m	nM	nM	nM	nM	nM	nM	nM	nM	nM	nM	pM	pM	pM	pM
CAA1	74.52	-80.57	597	3.16	0.06	7.69	0.11	4.63	0.13	2.28	0.05	2.36	0.07	335.5	6.1	5.2	0.3
CAA2	74.32	-80.50	11	4.09	0.07	0.37	0.01	5.30	0.15	3.31	0.08	0.25	0.01	189.5	7.1	5.1	0.3
CAA2	74.32	-80.50	29	3.63	0.07	0.54	0.01	5.71	0.10	3.23	0.05	0.91	0.01	288.1	6.1	4.7	0.1
CAA2	74.32	-80.50	42	3.19	0.06	0.88	0.00	5.69	0.15	3.21	0.06	1.23	0.02	315.1	7.1	4.9	0.2
CAA2	74.32	-80.50	60	2.56	0.06	0.94	0.02	5.15	0.12	2.77	0.05	1.18	0.02	298.8	12.2	5.8	0.3
CAA2	74.32	-80.50	79	2.63	0.07	0.91	0.02	5.03	0.12	2.72	0.08	1.16	0.03	278.5	3.7	8.2	0.2
CAA2	74.32	-80.50	99	2.56	0.05	0.86	0.02	5.04	0.11	2.69	0.07	1.83	0.05	277.5	7.6	14.7	0.4
CAA2	74.32	-80.50	120	2.23	0.05	0.96	0.02	4.94	0.13	2.65	0.06	1.12	0.03	307.8	8.2	8.5	0.3
CAA2	74.32	-80.50	149	1.38	0.03	1.07	0.02	4.80	0.13	2.44	0.05	1.57	0.04	346.5	3.8	11.0	0.4
CAA2	74.32	-80.50	199	1.15	0.02	1.41	0.01	4.85	0.09	2.41	0.03	2.02	0.03	361.1	8.9	4.0	0.1
CAA2	74.32	-80.50	298	1.29	0.03	1.65	0.01	4.61	0.09	2.13	0.04	2.18	0.04	352.3	5.4	5.9	0.1
CAA2	74.32	-80.50	399	1.70	0.04	2.55	0.01	4.51	0.07	2.07	0.04	2.29	0.05	337.0	4.4	5.0	0.1
CAA2	74.32	-80.50	597	8.66	0.12	7.38	0.08	4.68	0.10	2.18	0.04	2.49	0.04	360.8	8.3	5.6	0.2
CAA3	73.81	-80.41	9	5.49	0.13	1.10	0.02	4.84	0.09	3.54	0.07	0.34	0.01	147.8	4.7	7.3	0.3
CAA3	73.81	-80.41	18	5.11	0.13	0.85	0.02	4.78	0.11	3.45	0.09	0.44	0.01	156.2	5.4	8.8	0.4
CAA3	73.81	-80.41	29	4.79	0.10	0.71	0.01	5.93	0.11	3.32	0.07	0.73	0.02	250.6	9.4	8.3	0.3
CAA3	73.81	-80.41	40	4.16	0.08	0.74	0.01	7.22	0.19	3.48	0.08	1.43	0.02	388.1	6.0	9.3	0.2
CAA3	73.81	-80.41	60	3.99	0.09	0.79	0.01	7.42	0.14	3.39	0.07	1.96	0.04	480.7	12.7	4.9	0.3
CAA3	73.81	-80.41	80	3.08	0.06	1.19	0.02	6.72	0.15	3.40	0.07	2.67	0.05	501.6	11.9	4.1	0.2
CAA3	73.81	-80.41	100	2.89	0.06	1.60	0.03	6.40	0.13	3.29	0.07	2.79	0.06	496.0	14.0	3.8	0.3
CAA3	73.82	-80.49	119	3.03	0.08	1.70	0.03	6.44	0.18	3.29	0.07	2.88	0.05	485.3	13.1	3.9	0.2
CAA3	73.82	-80.49	149	2.35	0.05	1.29	0.02	5.59	0.11	3.01	0.05	1.77	0.04	358.8	5.2	2.6	0.1
CAA3	73.82	-80.49	198	1.80	0.04	1.38	0.03	5.44	0.10	2.80	0.04	2.27	0.05	394.9	6.7	2.9	0.2
CAA3	73.82	-80.49	298	0.83	0.02	0.98	0.02	4.58	0.10	2.21	0.04	1.86	0.04	354.3	5.7	9.1	0.5

Station	Latitude	Longitude	depth	dMn	dMn error	dFe	dFe error	dNi	dNi error	dCu	dCu error	dZn	dZn error	dCd	dCd error	dPb	dPb error
			m	nM	nM	nM	nM	nM	nM	nM	nM	nM	nM	pM	pM	pM	pM
CAA3	73.82	-80.49	398	1.21	0.03	1.42	0.03	4.41	0.11	2.05	0.05	2.07	0.04	327.0	3.1	4.5	0.1
CAA3	73.82	-80.49	598	1.75	0.04	2.42	0.04	4.51	0.14	2.11	0.03	2.47	0.08	342.8	9.4	3.7	0.1
CAA4	74.12	-91.51	9	6.22	0.05	0.68	0.02	5.97	0.28	4.14	0.49	0.84	0.06	285.0	8.4	5.1	0.3
CAA4	74.12	-91.51	33	5.05	0.08	0.42	0.02	5.91	0.59	3.80	0.73	0.74	0.07	256.5	8.4	4.5	0.4
CAA4	74.12	-91.51	47	4.60	0.09	0.44	0.01	6.10	0.12	3.74	0.05	0.92	0.01	250.0	7.7	6.7	0.3
CAA4	74.12	-91.51	59	3.59	0.08	0.87	0.01	5.81	0.40	3.89	0.43	1.39	0.08	355.8	7.0	7.8	0.8
CAA4	74.12	-91.51	79	3.16	0.05	2.03	0.04	6.68	0.14	3.75	0.08	2.52	0.06	483.6	11.6	9.0	0.3
CAA4	74.12	-91.51	95	2.97	0.09	2.03	0.04	5.97	0.40	3.73	0.54	2.87	0.16	520.7	12.0	3.5	0.4
CAA4	74.12	-91.51	116	2.57	0.05	1.78	0.07	6.35	0.18	4.03	0.41	2.96	0.12	554.9	14.5	6.1	0.6
CAA4	74.12	-91.51	149	3.13	0.09	2.20	0.05	6.14	0.48	3.65	0.57	3.33	0.07	557.0	12.4	7.0	0.6
CAA5	74.54	-90.81	11	5.58	0.08	1.26	0.04	4.23	0.60	3.73	0.24	0.59	0.04	162.0	6.8	7.0	0.7
CAA5	74.54	-90.81	21	5.60	0.14	1.34	0.04	4.15	0.44	3.57	0.26	0.51	0.04	161.5	5.3	11.8	0.8
CAA5	74.54	-90.81	45	4.94	0.08	0.98	0.01	6.29	0.56	3.46	0.35	1.32	0.09	383.8	5.6	6.3	0.3
CAA5	74.54	-90.81	70	3.93	0.07	1.64	0.04	6.00	0.56	3.52	0.29	2.56	0.08	523.6	11.0	6.2	0.5
CAA5	74.54	-90.81	78	4.02	0.07	1.96	0.04	5.85	0.15	3.54	0.19	2.81	0.10	517.4	13.4	8.8	0.6
CAA5	74.54	-90.81	100	5.52	0.10	4.61	0.07	4.92	0.49	4.49	0.50	13.27	0.36	234.2	11.8	83.4	1.4
CAA5	74.54	-90.80	119	4.10	0.11	2.40	0.03	5.56	0.34	3.09	0.35	2.76	0.13	517.7	7.6	4.1	0.5
CAA5	74.54	-90.80	139	4.44	0.11	2.65	0.07	5.24	0.17	2.95	0.31	2.41	0.12	471.1	7.5	4.4	0.8
CAA5	74.54	-90.80	158	2.61	0.03	2.23	0.05	4.87	0.22	3.05	0.17	2.08	0.10	402.6	5.0	6.5	0.2
CAA5	74.54	-90.80	188	4.86	0.12	3.73	0.06	5.10	0.38	2.90	0.26	2.01	0.15	422.6	12.9	5.9	0.4
CAA5	74.54	-90.80	218	4.70	0.13	3.80	0.10	4.79	0.31	2.74	0.36	2.26	0.09	424.1	15.5	4.3	0.5
CAA5	74.54	-90.80	219	5.70	0.13	4.42	0.09	5.50	0.36	2.72	0.17	2.29	0.08	432.3	4.8	5.8	0.5
CAA6	74.75	-97.46	9	4.93	0.08	0.95	0.01	4.22	0.08	3.36	0.04	0.62	0.01	169.4	2.8	9.3	0.4
CAA6	74.75	-97.46	33	4.33	0.07	1.07	0.01	2.44	0.05	2.96	0.05	0.48	0.02	71.5	1.4	7.2	0.3

Station	Latitude	Longitude	depth	dMn	dMn error	dFe	dFe error	dNi	dNi error	dCu	dCu error	dZn	dZn error	dCd	dCd error	dPb	dPb error
			m	nM	nM	nM	nM	nM	nM	nM	nM	nM	nM	pM	pM	pM	pM
CAA6	74.75	-97.46	74	4.70	0.07	2.72	0.03	6.00	0.13	3.20	0.05	2.18	0.02	409.1	8.5	10.0	0.3
CAA6	74.75	-97.46	99	4.88	0.08	3.26	0.05	6.24	0.13	3.24	0.05	2.25	0.02	420.7	5.3	10.1	0.5
CAA6	74.75	-97.46	150	5.50	0.08	4.98	0.07	6.21	0.08	3.26	0.05	2.43	0.03	430.9	10.0	11.0	0.5
CAA6	74.75	-97.46	175	5.52	0.09	5.08	0.08	6.17	0.11	3.28	0.06	2.49	0.03	434.4	8.0	6.7	0.2
CAA6	74.75	-97.46	189	5.66	0.08	5.23	0.08	6.14	0.17	3.28	0.04	2.56	0.04	445.2	8.1	8.2	0.3
CAA6	74.75	-97.46	239	5.89	0.10	5.51	0.10	6.01	0.12	3.19	0.06	2.81	0.04	455.9	9.6	11.1	0.3
CAA7	73.67	-96.52	10	5.81	0.10	0.83	0.01	6.18	0.11	3.73	0.06	0.78	0.01	295.5	5.8	3.7	0.1
CAA7	73.67	-96.52	30	4.41	0.06	1.36	0.01	6.26	0.08	3.59	0.05	1.66	0.03	404.9	5.6	3.4	0.2
CAA7	73.67	-96.52	50	3.27	0.06	1.60	0.02	6.75	0.14	3.71	0.08	2.55	0.05	483.4	10.8	4.4	0.3
CAA7	73.67	-96.52	75	2.43	0.03	1.41	0.00	6.44	0.08	3.41	0.06	2.85	0.05	522.9	7.4	5.6	0.1
CAA7	73.67	-96.52	104	2.45	0.05	1.36	0.02	6.71	0.12	3.50	0.06	3.38	0.08	553.5	16.6	9.5	0.4
CAA7	73.67	-96.52	120	2.06	0.04	1.26	0.01	6.94	0.17	3.56	0.05	4.03	0.06	597.8	16.5	3.6	0.1
CAA7	73.67	-96.52	160	4.10	0.07	1.69	0.03	6.99	0.16	3.54	0.07	3.63	0.09	571.0	9.8	5.6	0.2
CAA7	73.67	-96.52	188	5.90	0.09	2.67	0.04	6.36	0.15	3.23	0.06	3.26	0.06	525.9	12.1	3.2	0.2
CAA8	74.14	-108.84	10	8.22	0.13	0.39	0.01	7.24	0.18	3.97	0.08	1.14	0.03	330	8	1.9	0.1
CAA8	74.14	-108.84	45	2.58	0.04	0.66	0.01	6.79	0.09	3.72	0.06	2.07	0.03	495	9	25.8	0.4
CAA8	74.14	-108.84	48	2.74	0.05	0.63	0.01	6.83	0.12	3.72	0.09	2.04	0.03	489	12	17.5	0.2
CAA8	74.14	-108.84	89	1.53	0.02	1.17	0.02	7.35	0.09	3.76	0.06	4.39	0.05	656	6	8.1	0.2
CAA8	74.14	-108.84	119	1.15	0.03	1.05	0.02	6.77	0.17	3.41	0.07	3.72	0.10	627	22	3.9	0.1
CAA8	74.14	-108.84	148	0.81	0.02	0.80	0.02	5.55	0.14	2.78	0.06	3.48	0.07	493	11	2.3	0.1
CAA8	74.14	-108.84	198	0.86	0.02	0.80	0.02	4.99	0.11	2.48	0.04	3.36	0.05	431	7	4.2	0.1
CAA8	74.14	-108.84	247	0.62	0.01	0.60	0.01	4.47	0.09	2.34	0.03	3.35	0.06	396	9	3.0	0.1
CAA8	74.14	-108.84	297	0.50	0.01	0.52	0.01	4.16	0.09	2.13	0.06	3.13	0.06	346	12	7.5	0.4
CAA8	74.14	-108.84	346	0.47	0.01	0.50	0.01	3.95	0.07	2.08	0.04	3.20	0.06	321	6	5.4	0.3

Station	Latitude	Longitude	depth	dMn	dMn error	dFe	dFe error	dNi	dNi error	dCu	dCu error	dZn	dZn error	dCd	dCd error	dPb	dPb error
			m	nM	nM	nM	nM	nM	nM	nM	nM	nM	nM	pM	pM	pM	pM
CAA8	74.14	-108.84	445	0.44	0.01	0.48	0.01	3.98	0.08	2.59	0.05	3.96	0.06	348	10	11.9	0.5
CAA9	76.33	-96.75	11	9.75	0.20	2.03	0.04	5.33	0.09	3.70	0.08	1.03	0.03	221	5	3.6	0.3
CAA9	76.33	-96.75	17	8.26	0.17	1.59	0.03	5.38	0.13	3.58	0.07	1.04	0.01	237	4	14.3	0.3
CAA9	76.33	-96.75	49	3.93	0.09	1.17	0.03	5.84	0.11	3.16	0.08	1.85	0.04	385	7	9.8	0.4
CAA9	76.33	-96.75	69	3.33	0.06	1.17	0.02	5.85	0.12	3.11	0.08	2.24	0.03	410	3	4.8	0.1
CAA9	76.33	-96.75	89	3.34	0.06	1.35	0.02	6.11	0.12	2.95	0.06	3.36	0.09	430	7	5.0	0.1
CAA9	76.33	-96.76	119	4.02	0.07	1.94	0.04	5.70	0.14	2.70	0.05	2.54	0.06	447	4	3.5	0.2
CAA9	76.33	-96.76	148	3.93	0.09	1.83	0.03	5.74	0.12	2.69	0.05	2.64	0.05	452	13	3.2	0.1
CAA9	76.33	-96.76	199	4.66	0.09	2.50	0.04	5.66	0.10	2.67	0.04	2.63	0.07	459	8	5.5	0.3
CAA9	76.33	-96.76	247	3.60	0.05	2.06	0.03	5.53	0.08	2.59	0.04	2.58	0.05	448	15	4.0	0.2
CAA9	76.33	-96.76	297	3.54	0.07	2.08	0.04	5.52	0.14	2.62	0.06	2.64	0.06	446	12	3.5	0.2

Table B.3 Dissolved Mn, Fe, Ni, Cu, Zn, Cd and Pb from the Baffin Bay and the Labrador Sea (Stations BB1, BB2, BB3, K1, and LS2). Where contamination is suspected, samples are highlighted in red. Data is expected to be submitted to the GEOTRACES International Data Assembly Centre by December 2017.

Station	Latitude	Longitude	depth	dMn	dMn error	dFe	dFe error	dNi	dNi error	dCu	dCu error	dZn	dZn error	dCd	dCd error	dPb	dPb error
			m	nM	nM	nM	nM	nM	nM	nM	nM	nM	nM	pM	pM	pM	pM
BB1	66.86	-59.07	11	3.06	0.07	0.53	0.01	5.50	0.11	3.42	0.08	0.38	0.01	205.3	4.9	9.7	0.4
BB1	66.86	-59.07	21	2.55	0.07	0.76	0.02	5.66	0.17	3.45	0.09	1.07	0.03	324.5	9.4	15.5	0.5
BB1	66.86	-59.07	46	1.55	0.04	0.91	0.01	5.60	0.12	3.47	0.06	1.15	0.02	300.1	6.2	11.3	0.4
BB1	66.86	-59.07	99	1.21	0.04	0.79	0.01	5.22	0.10	3.08	0.07	1.53	0.03	280.5	6.8	7.7	0.4
BB1	66.86	-59.07	149	0.97	0.02	0.52	0.01	4.83	0.08	2.64	0.05	1.25	0.03	269.8	6.9	7.1	0.2
BB1	66.86	-59.07	200	0.59	0.01	0.70	0.01	4.65	0.08	2.48	0.05	1.86	0.05	324.4	9.7	6.0	0.1
BB1	66.86	-59.06	299	1.12	0.01	1.47	0.03	4.10	0.03	1.98	0.05	1.73	0.03	231.6	4.6	20.0	0.7

Station	Latitude	Longitude	depth	dMn	dMn error	dFe	dFe error	dNi	dNi error	dCu	dCu error	dZn	dZn error	dCd	dCd error	dPb	dPb error
			m	nM	nM	nM	nM	nM	nM	nM	nM	nM	nM	pM	pM	pM	pM
BB1	66.86	-59.06	399	0.72	0.01	1.13	0.02	4.36	0.12	1.90	0.05	1.87	0.04	309.2	4.4	11.9	0.6
BB1	66.86	-59.06	500	0.62	0.01	1.04	0.01	4.46	0.03	1.92	0.06	2.77	0.05	347.8	8.6	27.3	0.2
BB1	66.86	-59.06	599	0.62	0.02	1.01	0.02	4.19	0.12	1.92	0.05	2.47	0.06	345.3	11.3	19.4	0.7
BB1	66.86	-59.06	700	0.68	0.01	1.13	0.02	4.28	0.07	1.95	0.04	2.52	0.05	355.8	5.5	21.3	0.9
BB1	66.86	-59.06	800	0.76	0.01	1.41	0.02	4.96	0.11	2.21	0.04	3.21	0.05	388.1	7.9	8.8	0.3
BB1	66.86	-59.06	1001	0.82	0.02	1.47	0.02	5.14	0.10	2.42	0.05	4.49	0.06	414.7	12.2	9.8	0.2
BB2	72.75	-66.99	10	3.63	0.07	0.37	0.00	6.41	0.08	3.22	0.05	0.65	0.01	175.0	4.2	5.6	0.3
BB2	72.75	-66.99	29	3.82	0.06	0.59	0.01	6.12	0.08	3.18	0.04	0.64	0.01	254.7	1.4	6.3	0.2
BB2	72.75	-66.99	49	2.52	0.05	0.78	0.01	5.97	0.08	3.23	0.07	1.35	0.03	338.9	5.8	4.6	0.2
BB2	72.75	-66.99	99	1.14	0.01	0.66	0.01	5.38	0.07	3.11	0.04	1.28	0.02	298.2	5.6	6.7	0.3
BB2	72.75	-66.99	149	0.90	0.01	0.53	0.01	5.30	0.07	2.91	0.04	1.63	0.02	298.6	4.7	11.2	0.3
BB2	72.75	-66.99	199	0.62	0.01	0.68	0.01	5.00	0.12	2.55	0.05	2.32	0.04	315.5	4.9	13.6	0.6
BB2	72.75	-66.99	299	0.42	0.01	0.78	0.01	4.59	0.11	2.10	0.04	2.20	0.03	355.4	2.7	13.4	0.3
BB2	72.75	-66.99	398	0.45	0.00	0.86	0.01	4.54	0.06	1.96	0.02	2.33	0.04	346.8	6.9	16.8	0.4
BB2	72.75	-66.99	498	0.47	0.01	0.88	0.02	4.47	0.13	1.90	0.04	2.55	0.05	343.9	12.2	5.6	0.2
BB2	72.75	-66.99	597	0.45	0.01	0.87	0.02	4.47	0.12	1.89	0.04	2.58	0.03	349.2	7.6	8.8	0.3
BB2	72.75	-66.99	695	0.42	0.01	0.92	0.01	4.61	0.04	2.05	0.03	2.91	0.03	364.2	8.2	9.1	0.2
BB2	72.75	-66.99	800	0.39	0.01	0.93	0.01	4.71	0.04	2.06	0.04	2.92	0.04	371.9	2.7	10.1	0.1
BB2	72.75	-66.99	996	0.30	0.00	0.96	0.01	4.89	0.09	2.27	0.05	2.91	0.06	386.2	10.6	2.9	0.2
BB2	72.75	-66.99	1195	0.29	0.00	0.96	0.02	4.98	0.08	2.46	0.04	3.11	0.03	400.8	4.2	3.5	0.2
BB2	72.75	-66.99	1397	0.27	0.00	0.86	0.01	5.08	0.09	2.96	0.06	3.44	0.04	421.9	9.9	2.9	0.2
BB2	72.75	-66.99	1599	0.27	0.00	0.79	0.01	5.12	0.08	3.40	0.06	3.99	0.03	425.9	7.1	5.5	0.2
BB2	72.75	-66.99	1900	0.28	0.01	0.79	0.02	5.21	0.09	4.08	0.09	5.32	0.06	423.7	5.4	5.1	0.2
BB2	72.75	-66.99	2098	0.65	0.01	0.56	0.01	5.49	0.07	5.09	0.07	4.43	0.03	441.5	5.4	6.1	0.2

Station	Latitude	Longitude	depth	dMn	dMn error	dFe	dFe error	dNi	dNi error	dCu	dCu error	dZn	dZn error	dCd	dCd error	dPb	dPb error
			m	nM	nM	nM	nM	nM	nM	nM	nM	nM	nM	pM	pM	pM	pM
BB2	72.75	-66.99	2300	0.78	0.01	0.74	0.01	5.51	0.10	5.30	0.08	4.65	0.06	436.4	10.5	3.3	0.2
BB3	71.41	-68.60	10	3.73	0.10	0.34	0.00	5.25	0.08	3.32	0.06	0.32	0.01	212.4	5.5	4.7	0.2
BB3	71.41	-68.60	30	3.15	0.09	0.38	0.01	5.80	0.18	3.06	0.09	1.28	0.04	345.7	10.4	6.1	0.3
BB3	71.41	-68.60	50	3.31	0.09	0.77	0.01	5.76	0.08	3.15	0.07	1.76	0.04	401.5	6.6	6.9	0.3
BB3	71.41	-68.60	99	2.01	0.04	1.05	0.02	5.37	0.12	3.07	0.05	1.61	0.02	338.3	3.3	3.5	0.1
BB3	71.41	-68.60	147	1.30	0.03	0.90	0.02	5.13	0.32	2.92	0.08	1.61	0.04	317.0	12.8	4.5	0.2
BB3	71.41	-68.60	199	0.89	0.02	0.66	0.01	4.79	0.11	2.72	0.07	1.37	0.04	293.4	8.6	4.7	0.2
BB3	71.41	-68.60	297	0.59	0.02	0.98	0.02	4.87	0.38	2.72	0.29	2.32	0.09	361.8	10.5	4.4	0.6
BB3	71.41	-68.60	394	0.58	0.02	1.02	0.03	4.54	0.41	2.35	0.31	2.15	0.12	357.1	9.2	4.8	0.6
BB3	71.41	-68.60	485	0.58	0.01	1.04	0.03	4.27	0.18	2.39	0.44	2.51	0.08	358.6	9.3	9.7	0.9
BB3	71.41	-68.60	594	0.55	0.02	0.98	0.04	4.61	0.50	1.98	0.38	2.15	0.11	359.0	6.9	13.0	1.2
BB3	71.41	-68.60	693	0.56	0.02	1.02	0.03	4.37	0.46	2.20	0.18	2.54	0.12	362.4	13.4	26.7	1.4
BB3	71.41	-68.60	792	0.81	0.04	1.27	0.03	4.21	0.20	1.86	0.17	2.53	0.05	377.6	23.4	6.2	0.4
BB3	71.41	-68.60	990	4.20	0.05	2.13	0.02	4.91	0.05	2.35	0.04	3.18	0.04	384.8	3.1	3.3	0.1
K1	56.17	-53.37	9	0.90	0.01	0.31	0.01	3.49	0.10	1.66	0.05	0.26	0.00	24.7	1.4	16.4	0.5
K1	56.17	-53.37	29	0.47	0.01	0.07	0.00	3.08	0.10	1.07	0.03	0.28	0.01	53.9	1.7	31.4	0.9
K1	56.17	-53.37	50	0.54	0.01	0.09	0.00	3.34	0.08	1.33	0.03	0.50	0.01	107.0	4.0	25.7	0.5
K1	56.17	-53.37	99	0.75	0.02	0.30	0.00	3.57	0.08	1.34	0.03	0.91	0.02	229.0	9.2	30.2	0.8
K1	56.17	-53.37	148	0.77	0.02	0.52	0.01	3.67	0.07	1.32	0.03	2.10	0.05	255.3	9.3	79.8	1.9
K1	56.17	-53.37	198	0.75	0.02	0.70	0.01	3.72	0.11	1.31	0.04	5.35	0.12	263.2	6.8	77.3	2.0
K1	56.17	-53.37	302	0.68	0.02	0.69	0.01	3.63	0.08	1.27	0.03	1.26	0.02	254.8	6.1	74.1	2.0
K1	56.17	-53.37	400	0.65	0.01	1.00	0.47	3.70	0.07	1.29	0.02	1.34	0.03	253.1	5.3	94.2	2.4
K1	56.17	-53.37	500	0.58	0.02	0.69	0.01	3.67	0.11	1.29	0.03	2.37	0.04	255.0	8.7	43.7	1.6
K1	56.17	-53.37	602	0.60	0.02	0.69	0.01	3.65	0.08	1.31	0.04	1.80	0.03	248.6	9.5	45.6	1.5

Station	Latitude	Longitude	depth	dMn	dMn error	dFe	dFe error	dNi	dNi error	dCu	dCu error	dZn	dZn error	dCd	dCd error	dPb	dPb error
			m	nM	nM	nM	nM	nM	nM	nM	nM	nM	nM	pM	pM	pM	pM
K1	56.17	-53.37	700	0.57	0.02	0.72	0.01	3.68	0.07	1.45	0.04	2.78	0.08	249.5	6.6	88.1	2.0
K1	56.17	-53.37	799	0.60	0.01	0.70	0.01	3.78	0.07	1.75	0.04	4.44	0.09	259.6	6.8	85.1	2.3
K1	56.19	-53.41	1003	0.56	0.02	0.68	0.01	3.67	0.10	1.37	0.04	1.29	0.03	252.3	7.2	27.8	0.9
K1	56.19	-53.41	1202	0.51	0.01	0.69	0.02	3.65	0.10	1.28	0.03	1.33	0.04	251.3	7.5	43.1	1.7
K1	56.19	-53.41	1403	0.51	0.02	0.77	0.03	3.73	0.70	1.51	0.25	1.64	0.07	255.8	6.2	30.9	0.8
K1	56.19	-53.41	1604	0.42	0.01	0.81	0.03	3.66	0.48	1.55	0.27	1.63	0.10	263.4	5.3	30.7	1.3
K1	56.19	-53.41	2006	0.37	0.01	0.86	0.01	4.04	0.44	1.61	0.30	6.53	0.27	263.5	6.3	68.7	1.1
K1	56.19	-53.41	2259	0.35	0.02	0.81	0.02	3.67	0.49	1.40	0.22	3.94	0.10	258.9	12.4	76.0	1.8
K1	56.19	-53.41	2310	0.36	0.01	0.85	0.02	3.50	0.39	1.71	0.12	1.53	0.08	250.0	5.8	57.5	2.0
K1	56.19	-53.41	2462	0.34	0.01	0.84	0.03	3.66	0.32	1.44	0.22	1.72	0.10	248.1	9.2	71.4	3.0
K1	56.19	-53.41	2615	0.33	0.01	0.78	0.02	3.47	0.37	1.64	0.32	3.56	0.09	248.4	7.7	47.4	1.6
K1	56.19	-53.41	2764	0.35	0.01	0.77	0.02	3.62	0.27	1.51	0.26	2.09	0.10	253.3	5.0	29.7	1.6
K1	56.19	-53.41	3018	0.35	0.02	0.77	0.01	3.64	0.29	2.09	0.42	1.94	0.06	238.9	4.4	43.1	1.5
K1	56.19	-53.41	3019	0.40	0.02	0.77	0.02	3.38	0.26	2.06	0.32	3.53	0.12	239.0	5.0	51.4	1.0
LS2	60.65	-56.76	11	0.91	0.02	0.26	0.00	4.17	0.11	1.98	0.04	1.34	0.03	17.3	1.0	24.6	0.5
LS2	60.65	-56.76	30	1.12	0.02	0.36	0.00	3.82	0.08	1.71	0.01	0.58	0.01	67.1	2.7	28.5	0.9
LS2	60.65	-56.76	101	1.06	0.02	0.78	0.01	3.90	0.10	1.52	0.03	1.12	0.02	254.9	7.3	34.7	1.4
LS2	60.65	-56.76	150	0.92	0.02	0.78	0.01	3.96	0.09	1.53	0.04	1.26	0.02	254.1	3.6	34.7	0.8
LS2	60.65	-56.76	199	1.05	0.02	0.86	0.01	4.49	0.07	1.91	0.03	5.08	0.07	118.7	4.8	107.7	3.0
LS2	60.51	-56.56	297	0.66	0.03	0.70	0.03	3.61	0.43	1.47	0.32	1.16	0.06	252.2	12.3	24.2	1.2
LS2	60.51	-56.56	400	0.58	0.01	0.82	0.03	3.71	0.27	1.66	0.35	1.55	0.11	261.9	13.6	26.3	1.6
LS2	60.51	-56.56	498	0.54	0.02	0.71	0.01	3.83	0.22	1.47	0.27	1.18	0.03	264.9	6.3	28.3	1.1
LS2	60.51	-56.56	599	0.53	0.02	0.75	0.01	3.74	0.39	1.57	0.44	2.53	0.09	265.1	3.2	38.5	1.2
LS2	60.51	-56.56	699	0.49	0.02	0.75	0.02	3.68	0.24	1.51	0.27	1.14	0.06	253.9	5.7	40.3	3.5

Station	Latitude	Longitude	depth	dMn	dMn error	dFe	dFe error	dNi	dNi error	dCu	dCu error	dZn	dZn error	dCd	dCd error	dPb	dPb error
			m	nM	nM	nM	nM	nM	nM	nM	nM	nM	nM	pM	pM	pM	pM
LS2	60.51	-56.56	800	0.49	0.02	0.74	0.03	3.78	0.37	1.33	0.25	1.65	0.06	258.3	11.9	43.3	1.2
LS2	60.51	-56.56	1003	0.48	0.02	0.75	0.02	3.70	0.39	1.61	0.50	1.67	0.11	278.8	7.3	38.7	1.7
LS2	60.51	-56.56	1204	0.90	0.03	1.08	0.01	4.16	0.45	1.87	0.21	5.15	0.15	149.4	7.2	52.2	1.8
LS2	60.49	-56.57	1402	0.39	0.01	0.86	0.01	3.93	0.06	1.43	0.02	1.53	0.03	263.6	5.7	28.7	0.7
LS2	60.49	-56.57	1604	0.38	0.01	0.85	0.01	3.95	0.04	1.38	0.02	1.65	0.02	261.0	3.4	37.5	0.4
LS2	60.49	-56.57	2006	0.37	0.00	0.89	0.01	3.91	0.05	1.59	0.02	2.70	0.04	257.7	4.4	27.4	0.6
LS2	60.49	-56.57	2208	0.51	0.01	1.00	0.01	3.82	0.07	1.45	0.02	2.57	0.03	259.3	6.3	48.3	0.9
LS2	60.49	-56.57	2411	0.37	0.01	0.86	0.01	3.97	0.09	1.53	0.03	3.69	0.06	256.5	4.7	42.9	0.9
LS2	60.49	-56.57	2511	0.34	0.01	0.76	0.01	3.93	0.09	1.54	0.04	1.66	0.04	246.9	4.7	57.0	0.9
LS2	60.49	-56.57	2613	0.34	0.01	0.80	0.01	3.91	0.07	1.55	0.03	2.49	0.04	253.0	5.2	28.1	0.8
LS2	60.49	-56.57	2715	0.35	0.02	1.13	0.61	3.94	0.07	1.55	0.03	1.73	0.03	249.2	6.7	21.6	0.5
LS2	60.49	-56.57	2816	0.42	0.01	0.79	0.01	3.82	0.06	1.61	0.02	1.69	0.03	253.5	3.1	18.1	0.4